HEDL-TME 77-86
UC-79

CALIBRATION OF A FUEL-TO-CLADDING GAP CONDUCTANCE MODEL FOR FAST REACTOR FUEL PINS

Hanford Engineering Development Laboratory

HANFORD ENGINEERING DEVELOPMENT LABORATORY
Operated by Westinghouse Hanford Company
A Subsidiary of Westinghouse Electric Corporation
Prepared for the U.S. Department of Energy
under Contract No. EY-76-C-14-2170
P.O. Box 1970 Richland, WA 99352

NOTICE

Printed in the United States of America
Available from
National Technical Information Service
U.S. Department of Commerce
5285 Port Royal Road
Springfield, Virginia 22161
Price: Printed Copy $7.25 Microfiche $2.25

HEDL-TME 77-86
UC-79

CALIBRATION OF A FUEL-TO-CLADDING GAP CONDUCTANCE MODEL FOR FAST REACTOR FUEL PINS

Hanford Engineering Development Laboratory
R.B. Baker
May 1978

HANFORD ENGINEERING DEVELOPMENT LABORATORY
Operated by Westinghouse Hanford Company
A Subsidiary of Westinghouse Electric Corporation
Prepared for the U.S. Department of Energy
under Contract No. EY-76-C-14-2170
P.O. Box 1970 Richland, WA 99352

HEDL-TME 77-86
UC-79

CALIBRATION OF A FUEL-TO-CLADDING GAP CONDUCTANCE MODEL FOR FAST REACTOR FUEL PINS

R. B. Baker

ABSTRACT

This report presents refined methods for calculation of fuel temperatures in PuO_2-UO_2 fuel in Fast Breeder Reactor (FBR), fuel pins. Of primary concern is the calculation of the temperature changes across the fuel-to-cladding gap of pins with fuel burnups that range from 60 to 10,900 MWd/MTM (0.006 to 1.12 at.%). Described, in particular, are:

1) *A proposed set of heat transfer formulations and corresponding material properties for modeling radial heat transfer through the fuel and cladding.*

2) *The calibration of a fuel-to-cladding gap conductance model, as part of a thermal performance computer code (SIEX-M1) which incorporates the proposed heat transfer expressions, using integral thermal performance data from two unique in-reactor experiments.*

The test data used are from the HEDL P-19 and P-20 experiments which were irradiated in the Experimental Breeder Reactor Number Two (EBR-II), for the Hanford Engineering Development Laboratory (HEDL).

ACKNOWLEDGEMENTS

The author gratefully acknowledges the encouragement, guidance, and suggestions of Dr. R. D. Leggett, and Dr. R. E. Collingham (Joint Center for Graduate Study, Richland, Washington) in the development of this analysis. Further, I would like to acknowledge the technical advice of Mr. D. S. Dutt and suggestions of Mr. G. L. Fox which were most beneficial. The assistance of Mrs. B. B. Pravato, in locating references and compiling data and computer analyses results, and of Miss R. E. Horton and Miss K. C. Christenson, in their typing of the many drafts of this and related reports, is also gratefully acknowledged.

This research was based on work done at the Hanford Engineering Development Laboratory, operated by the Westinghouse Hanford Company under contract to the United States Department of Energy.

CONTENTS

		Page
	FIGURES	viii
	TABLES	iv
I.	INTRODUCTION	1
II.	SUMMARY	8
III.	SUMMARY OF HEDL P-19 AND P-20 INTEGRAL POWER-TO-MELT DATA	10
	A. SUMMARY HEDL P-19 TEST	10
	B. SUMMARY HEDL P-20 TEST	12
	C. DERIVED AND NORMALIZED POWER-TO-MELT DATA FROM HEDL P-19 AND P-20 TESTS	15
IV.	SUMMARY OF THE MATHEMATICAL REPRESENTATIONS FOR THE RADIAL HEAT PATH	24
	A. SUMMARY OF SIEX	24
	B. REVISIONS FOR SIEX-M1	25
	C. FUEL-TO-CLADDING THERMAL GAP CONDUCTANCE MODEL	27
V.	CALIBRATION OF CONSTANTS IN THE GAP CONDUCTANCE MODEL	32
	A. GAS GAP CONSTANT B	32
	B. CONTACT CONSTANTS A_2 AND D FROM CLOSED GAP DATA	33
	C. DISCUSSION	37
VI.	CONCLUSIONS	47
	REFERENCES	48

APPENDICES

A -	RADIAL HEAT TRANSFER PATH IN THE FUEL PIN	A-1
B -	REVIEW OF SELECTED MATERIAL PROPERTIES	B-1
C -	REVIEW OF FUEL BEHAVIOR RELATED TO GAP CONDUCTANCE	C-1
D -	NOMENCLATURE	D-1

FIGURES

		Page
1.	Locations of Temperature Drops Through Fuel Pin.	3
2.	Typical Temperature Distribution Across a Fuel Pin Operating at a Power Sufficient to Cause Fuel Melting at the Edge of the Central Void.	4
3.	Peak Power History for a Nominal HEDL P-20 Pin.	16
4.	Normalized Q'_m Values for Fresh Fuel.	22
5.	Normalized Q'_m Values for Fuel with Significant Burnup.	23
6.	Calculated Values of Constant B from Test Data.	36
7.	Comparison of Predicted and Inferred Temperature Drops Across the Fuel-to-Cladding Gaps.	38
8.	Comparison of Normalized Q'_m Data and Predictions for "Fresh" Fuel.	39
9.	Comparison of Normalized Q'_m Data and Predictions for Pre-irradiated Fuel.	40
10.	Behavior of Calibrated Gap Conductance Model Predictions with Burnup at Q'_m.	43
11.	SIEX-M1 Predictions for FFTF Fuel Pins.	44

TABLES

		Page
I.	Summary of Fabrication Parameters for Each P-19 Pin.	11
II.	Scope of the HEDL P-20 Thermal Performance Test.	13
III.	Summary of Fabrication Parameters for Pins in Each Phase of P-20.	14
IV.	Summary of P-20 Irradiation Conditions.	17
V.	Fuel Melting Results for the Phase III HEDL P-20 Test Pins.	18
VI.	Estimates of Restructuring at Axial Extents of Melting.	19
VII.	Peak Pin Powers and Axial Extents of Melting for HEDL P-19 Pins.	20
VIII.	Calculated Values of Gap Conductance Parameters for Data Points.	34
IX.	Contributions to the Total Gap Conductance Predicted by the Calibrated Model.	42

I. INTRODUCTION

Thermal performance predictions for Fast Breeder Reactor (FBR) fuel pins typically are made to determine:

1. The heat rate which would cause incipient fuel melting, Q'_m. Typically, two cases are encountered:

   a) Those where there are prototypic Q'_m test data that can be applied, with little adjustment, to the pins of interest.

   b) Those where there are no prototypic Q'_m data and the only way to obtain Q'_m predictions for these pins is through calculations techniques.

2. The operating temperatures in the fuel under normal conditions, significantly below melting, for development of fuel behavior models (such as fission gas release, fuel restructuring, fuel swelling, etc.).

Two irradiation tests have been completed that address the thermal performance in mixed-oxide (PuO_2-UO_2) FBR fuel: HEDL P-19 and HEDL P-20. Reference 1 summarizes the direct derivation of "integral" Q'_m values from these test data. The present report discusses the use of these data to calibrate the thermal gap conductance model of an FBR fuel pin thermal performance computer code, an updated version of SIEX.[2] This calibrated code can be used to make predictions of fuel temperatures and Q'_m, based on a consistent set of thermal models calibrated to actual thermal performance data, thus reducing the uncertainty of the predictions to a minimum. The following summarizes some of the test background and analysis concepts that are germane to the study and calibration described herein.

A current design requirement for the Fast Flux Test Facility (FFTF) is for a low probability of fuel melting even with the reactor operating at 115%

of its normal power level. The uncertainty in the calculation of Q'_m is thus translated directly in the reactor design to the specific power levels that are allowed in the fuel pins under normal operating conditions.

The calculation of fuel centerline temperatures and Q'_m in the fuel pin is complex. The calculation of radial temperature drops from the coolant to the fuel melt boundary can be expressed by:

$$(1) \qquad \int_{T_I}^{T_m} dT = \Delta T_{Fl} + \Delta T_C + \Delta T_G + \Delta T_F + \Delta T_{RF}$$

where: T_m = Melting temperature of fuel,
T_I = Sodium coolant temperature,
ΔT_{Fl} = Temperature drop between coolant and cladding,
ΔT_C = Temperature drop through cladding,
ΔT_G = Temperature drop through fuel-to-cladding gap,
ΔT_F = Temperature drop through unrestructured fuel region, and
ΔT_{RF} = Temperature drop through restructured fuel regions.

Figures 1 and 2 illustrate the physical conditions being modeled, and Figure 2 provides a typical temperature distribution across the radius of a fuel pin. Note the large temperature drop over the small distance at the gap: typically 25% of the total temperature drop for "fresh" fuel (fuel with no prior irradiation) similar to that in Figure 1. There are two methods of characterizing this heat transfer system with respect to fuel melting in a pin. The right side of Equation (1) can be used to characterize the temperature drop in each region from the coolant to the fuel center, or the left side can be used to define the integral effect based on prototypic test data from a power-to-melt experiment.

Using the right side of Equation (1) to calculate fuel temperatures at linear heat rates high enough to cause melting results in a large uncertainty. The individual temperature drops in the fuel-to-cladding gap and the fuel

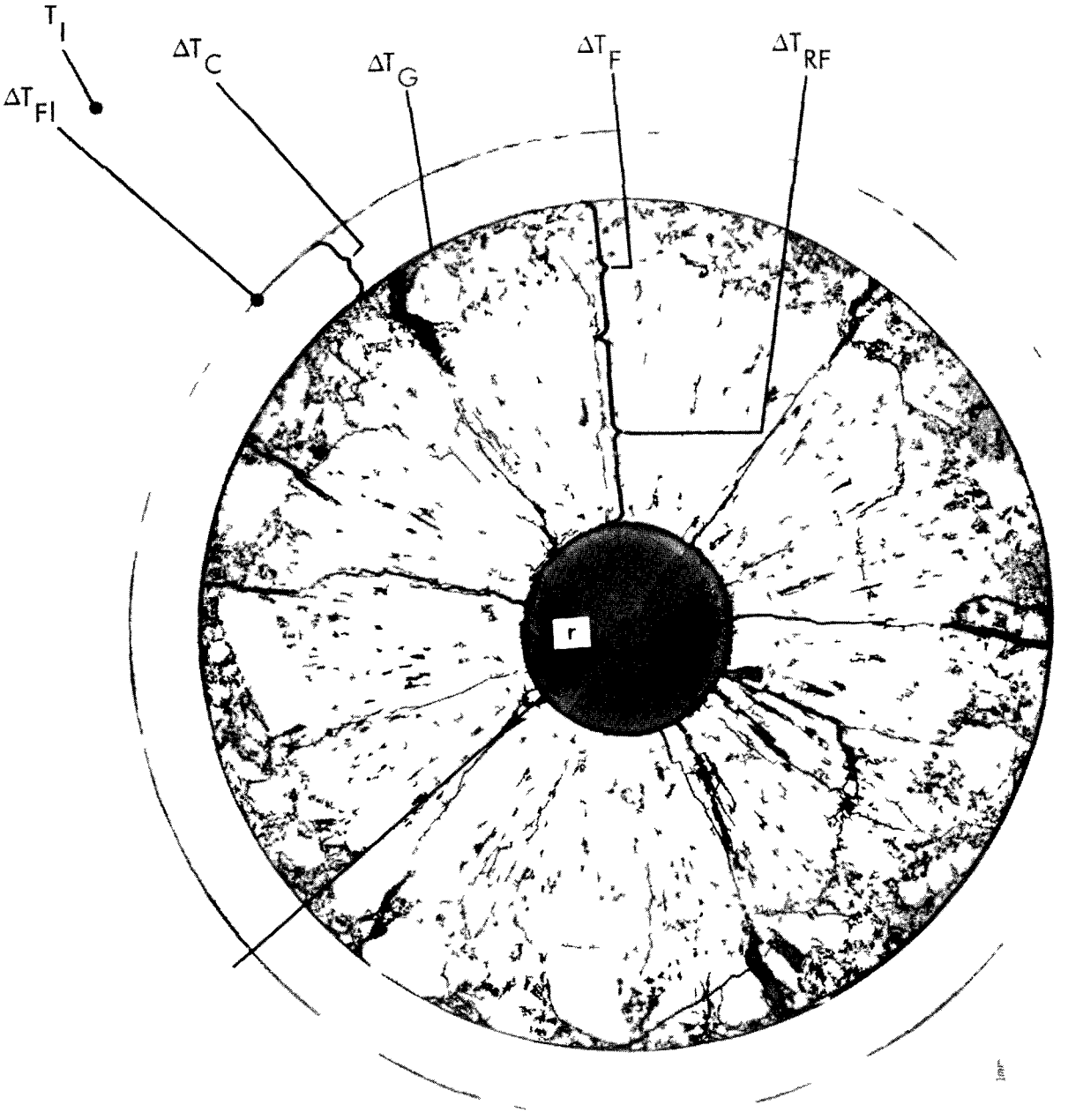

HEDL 7707-27.1

FIGURE 1. Locations of Temperature Drops Through Fuel Pin.

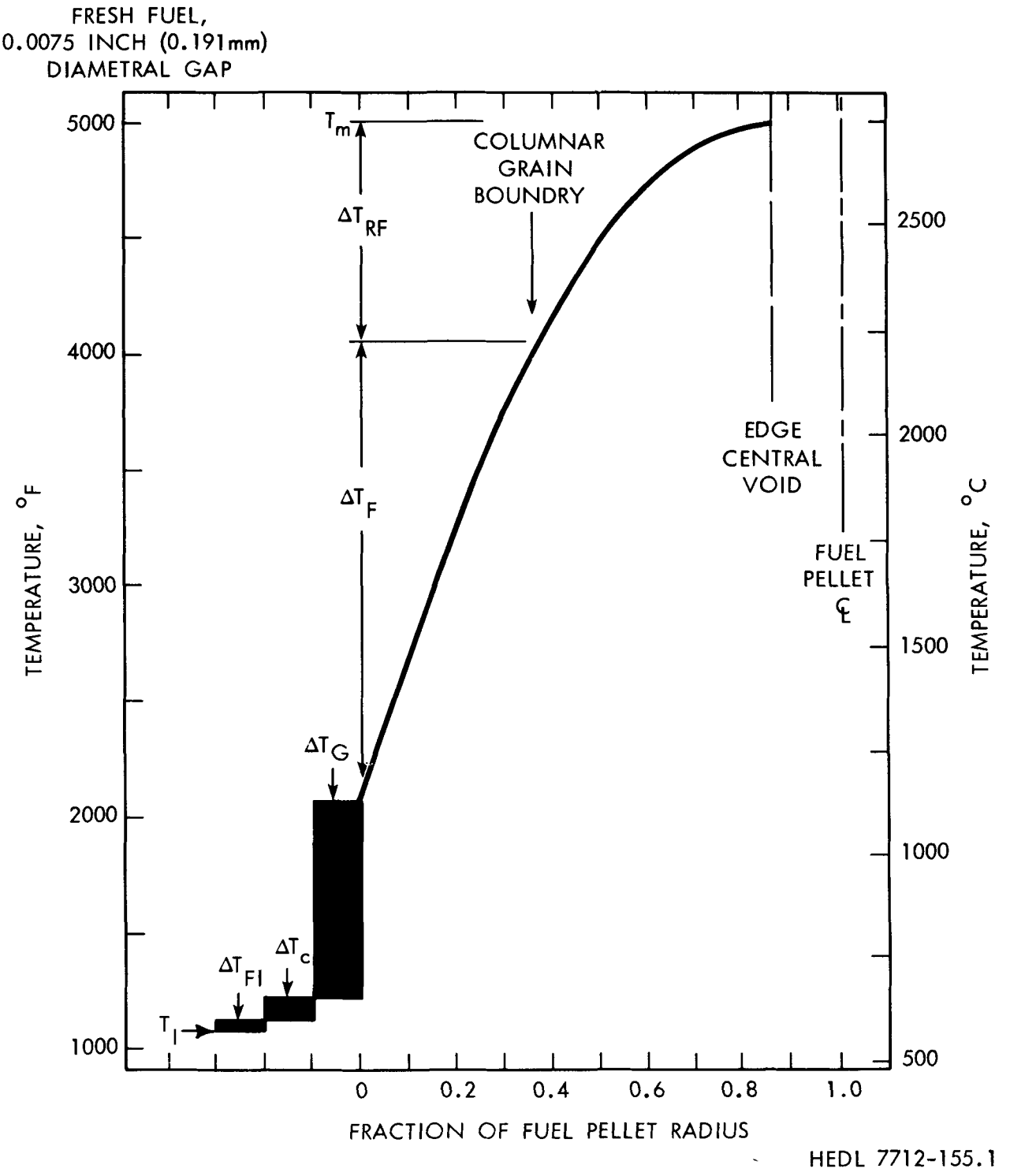

FIGURE 2. Typical Temperature Distribution Across a Fuel Pin Operating at a Power Sufficient to Cause Fuel Melting at the Edge of the Central Void.

have significant uncertainty due their complexity, the present "state-of-the-art" of understanding, and the limited data base. For example, calculation of the temperature drop across the gap depends on the gap size, the gas composition in the gap, interface pressure, gas pressure, and the surface conditions of the fuel and cladding. The effective thermal conductivity of the mixed-oxide fuel depends on temperature, density, size and shape of porosity, the oxygen-to-metal-ratio (O/M), and perhaps several other parameters such as fuel-cracking patterns and fission products. Uncertainty for conductivity of PuO_2-UO_2 fuel above 1700°C is large because very little data are available. Further, to calculate fuel temperatures, the size of the columnar grain region and central void and the density of the columnar grain region must be calculated since these have a significant effect on fuel temperatures (in a high power fuel the centerline temperature can be reduced as much as 600°F or 315°C due to restructuring). Development of the columnar grain region and central void is generally understood qualitatively, but their prediction involves significant uncertainty.

The large uncertainties associated with calculating individual temperature drops, the right side of Equation (1), led to the development of integral heat-rate-to-incipient-fuel melting, Q'_m, ("power-to-melt") tests, such as P-19 and P-20. These tests were, in effect, used to evaluate the left side of Equation (1). These experiments, based on prototypic parameters, resulted in Q'_m values which can be applied to reactor design with a minimum of additional calculation. Uncertainty was reduced to characterizing local linear heat rates in the test fuel. Thus, these experimental results represent the best values for satisfying the usual reactor design criterion of a low probability of fuel melting.

The fuel pins and operating conditions of the P-19 and P-20 experiments[1] were as prototypic of FFTF design as possible. The primary variables were fabricated fuel-to-cladding gap size and fuel burnup to 10,900 MWd/MTM. While the integral method of analysis is best for direct design applications, the need remains for the predictions of Q'_m where there are no test data or of

fuel temperatures at heat rates less than Q'_m. Thus, calibrated, thermal performance, computer codes which calculate values for, or model, the right side of Equation (1) have been and are being developed.

The P-19 and P-20 experiment results were used exclusively in the code calibration analysis done in this study because these represented a unique set of data in the fast reactor program. Only one other test, General Electric F-20, was designed to provide these type data. Complete results of the F-20 test[3] remain to be published but are expected to extend the data ranges of the parameters in P-19 and P-20 tests. The use of the isotherm for fuel melting in these test fuels represents the best available data to date for calibrating fuel thermal performance models. Other methods for measuring fuel temperatures introduce something extra, i.e., thermocouples or melt wires, into the fuel which may affect the results. Further, experiments using these other methods in fast reactor fuel have been used very little in the U.S. testing program.

This report describes the calibration of the gap conductance model in a revised version of the SIEX[2] thermal performance code using the P-19 and P-20 data, as derived in Reference 1. The gap conductance model was chosen to be calibrated because it had the largest uncertainty associated with it in the calculation of fuel temperatures.

The appendices include a summary of the heat transfer formulations selected to be used in the revised code, SIEX-M1, and a critical review of the related material properties. As is seen by Equation (1), any gap conductance model calibrated using integral Q'_m data is meaningful only if the complete heat transfer path is clearly specified since assumptions made for each of the regions are not unique. Using the integral fuel melting data and the "best" heat transfer formulations should result in a gap conductance model and heat transfer system with a minimum of uncertainty in predicted fuel temperature drops through each region and in the system as a whole.

The SIEX[2] code was chosen for calibration because of its successful and extensive use at HEDL[4] for fast reactor fuel thermal performance

predictions. It offers quick running times and can be correlated to large data bases. Other codes in the U.S., GAPCON,[5] FMODEL,[6] LIFE,[7] and UNCLE,[8] use methods similar to those used in versions of SIEX for calculating gap conductance though detailed assumptions may vary.

The development of this gap conductance model and review of calculational assumptions are part of an effort to develop methods of calculating fuel temperatures and assist in fuel design. The SIEX code and its updated versions are the tools being used to obtain these goals.

II. SUMMARY

This study developed a thermal model representing the radial heat transfer system of an FBR fuel pin. A set of heat transfer formulations was defined and developed, consistent with the present "state-of-the-art" using unique integral heat-rate-to-incipient-fuel melting, Q'_m, data from the HEDL P-19 and P-20 experiments[1].

Particular emphasis was placed on the complex heat transfer system at the fuel-cladding gap because of the large temperature drop involved, the lack of direct data, and the number of parameters it was dependent on. For the calibration of the gap conductance model, calculation of the fuel-to-cladding "hot" gap size was critical. The hot gap was modeled as realistically as possible by using:

1. A residual "cold" gap model correlated to measurements from 77 ceramographic samples from the P-19 and P-20 tests. This model sought to account for permanent deformation of the fuel due to cracking, fission product buildup, and fuel-cladding interaction.

2. A fuel thermal expansion model based on observations from the P-19 and P-20 tests. Fuel expansion was calculated by the summation of radial expansion rather than the radial average.

The development of this second interpretation allowed the residual gap measurements to be used. This had not been possible in prior SIEX calibration work because measurements could not be rationalized with Q'_m behavior. These models and the refined heat transfer formulations were programmed into the revised SIEX[2] thermal performance code, SIEX-M1.

Using versions of SIEX-M1, which allowed direct calculation of Q'_m values and adjustment of the calibration constants, data from the P-19 and P-20 experiments on Q'_m were used to develop the three calibration constants in the gap conductance model. The resulting model was found to predict the

total data set, which ranged in diametral gap size from 0.003 to 0.0100 inch (0.076 to 0.025 mm) and burnup from 60 to 10,900 MWd/MTM (0.006 to 1.12 at.%), very well. Using this calibrated code, predictions of Q'_m for a standard FFTF driver fuel pin, with 10% Xe tag, were made as a function of gap size and burnup.

The combination of the refined heat transfer model and calibration to Q'_m data from fueled tests in a fast reactor enviroment, is believed to result in the most realistic gap conductance and temperature prediction system presently available for FBR fuel pins.

III. SUMMARY OF HEDL P-19 AND P-20 Q'_m DATA

Derivation of data on the power required to cause incipient fuel melting, based on combined analysis of the HEDL P-19 and P-20 tests, is described in detail in Reference 1. Initial results of these tests were documented[10,11,12,13] separately for each test prior to this final combined analysis. The following briefly summarizes the scope and results of these two tests.

A. SUMMARY OF HEDL P-19 TEST

The experiment HEDL P-19 was conducted in EBR-II to determine the effect of the original fabricated diametral fuel-to-cladding gap, size from 0.0034 to 0.010 inches (0.086 to 0.254 mm), on the linear-heat-rate (Q'_m) required to cause incipient fuel melting in mixed-oxide (25% PuO_2-75% UO_2) fuel pins under rapid startup conditions. P-19 was a nineteen pin (encapsulated) subassembly consisting of eight 0.230 inch (5.84 mm) OD pins, eight 0.250 inch (6.35 mm) OD pins, and three pre-irradiated pins. All pins were backfilled with pure helium. The fresh pins were clad with 316 SS (20% CW) and were fabricated, where test parameters allowed, to RDT Standards for Liquid Metal Fast Breeder Reactor (LMFBR) fuel. Appendix A of Reference 13 summarizes detailed fabrication data for the P-19 test pins; Table I shows data of direct interest to this analysis.

The P-19 test was conducted to simulate a fast startup to steady state full power. After a one-hour hold period, power was increased rapidly an additional 15%. This level was held ten minutes; then the reactor was scrammed to quench-in the fuel structure. All 0.230 inch (5.84 mm) OD pins with fuel-to-cladding gaps equal to or less than 0.0055 inch (0.14 mm) had no fuel melting. The remaining 0.230 inch (5.84 mm) OD pins and all the 0.250 inch (6.35 mm) OD pins experienced partial centerline fuel melting.

Pin powers and fuel temperatures peaked near the fuel column midplane and were lowest near the top and bottom of the column. These operating conditions resulted in the fuel in most cases melting only near the center of the fuel column. Q'_m values were determined from these pins by:

TABLE I

SUMMARY OF FABRICATION PARAMETERS FOR EACH HEDL P-19 PIN

Pin Identification[a]	Nominal Diametral Fuel-to-Cladding Gap, mil (mm)	Average Fuel Pellet Density (% TD[c])	Average Cladding OD, inches (mm)
P-19-2	7.8 (0.198)	90.75	0.230 (5.84)
P-19-3R	10.0 (0.254)	92.40	0.250 (6.35)
P-19-5	5.7 (0.145)	90.75	0.230 (5.84)
P-19-6	3.9 (0.099)	90.75	0.230 (5.84)
P-19-7R	6.2 (0.158)	92.40	0.250 (6.35)
P-19-8	9.6 (0.244)	90.75	0.230 (5.84)
P-19-13	7.8 (0.198)	90.75	0.230 (5.84)
P-19-20	9.7 (0.246)	90.75	0.230 (5.84)
P-19-24R	10.0 (0.254)	92.40	0.250 (6.35)
P-19-25R	8.0 (0.203)	92.40	0.250 (6.35)
P-19-26R	6.6 (0.152)	92.40	0.250 (6.35)
P-19-27R	4.0 (0.102)	92.40	0.250 (6.35)
P-19-28[b]	3.4 (0.086)	92.40	0.250 (6.35)
P-19-30[b]	7.0 (0.178)	92.40	0.250 (6.35)
P-19-33[b]	4.9 (0.125)	90.75	0.230 (5.84)
P-19-35[b]	7.2 (0.183)	90.75	0.230 (5.84)
P-19/PNL-1-11	6.0 (0.152)	89.45	0.240 (6.12)
P-19/PNL-2-16	6.1 (0.155)	90.56	0.238 (6.05)
P-19/PNL-2-18	5.9 (0.150)	90.05	0.238 (6.05)

[a] All pins backfilled with helium, and all fuel was high-pressure preslugged except for that in P-19/PNL-1-11, P-19/PNL-2-16, and P-19/PNL-2-18.

[b] Pellet surfaces in the as-sintered condition. All other pins contained ground pellets.

[c] TD = Theoretical Density ($\sim$ 10.9 gm/cc) of the fuel.

1. Locating (using radiography and ceramography) the axial extents of fuel melting toward the top and bottom of each fuel column, and

2. Calculating the local power at the position of each axial extent of melting.

The power at this point was the Q'_m under local coolant and fabrication conditions.

B. SUMMARY OF HEDL P-20 TEST

The primary purpose of the HEDL P-20 test was to determine the effect of fuel burnup, up to 1.1 at.% (about 10,900 MWd/MTM), on power-to-melt, Q'_m, over a range of fuel-to-cladding gap sizes. Table II summarizes the experiment variables and general fabrication parameters. Table III summarizes specific pin data.

Pins with 0.0035, 0.0055, or 0.0075 inch (0.0899, 0.140 or 0.191 mm) fuel-to-cladding diametral gap sizes were included in the test. These pins were backfilled with pure helium to permit a direct comparison of the results with the HEDL P-19 results. Several pins with 0.0075 inch (0.191 mm) fuel-to-cladding gap sizes backfilled with 82% He-18% Xe were included to assess the effect of "tag" gas on thermal performance. (FFTF driver and FBR fuel pins will be filled, "tagged", with a 90% He-10% (Xe + Kr) mixture with unique ratios of Xe and Kr isotopes for a given subassembly to allow identifying "leakers" in the event of a cladding breach.) In addition, pins were included with fuel columns made up of different diameter pellets (to evaluate axial smoothing of Q'_m) and with fuel fabricated by low-pressure preslugging[14] (to determine the impact on Q'_m of varying the type of porosity). Other pins in the test were unirradiated spares from the P-19 test (to provide the internal calibration of the P-20 test to the P-19 test) and a pin from the PNL-2[15] subassembly (to help assess Q'_m at high burnup).

TABLE II

SCOPE OF THE HEDL P-20 THERMAL PERFORMANCE TEST

General Parameters

Cladding

316 20% CW stainless steel

0.230 inch (5.84 mm) OD x 0.015 inch (0.38 mm) wall thickness

Fuel

75% UO_2-25% PuO_2

Preslugged (high pressure) same as P-19

O/M - 1.96

Pellet density ∿91% [similar to P-19, 0.230 inch (5.84 mm) OD pins]

He bonded to cladding

13.5 inch (34.3 cm) fuel column length

Subassembly

19 encapsulated pins

Pins were in individual flow tubes

Main Variables

Fuel burnup, three increments to 10,900 MWd/MTM (1.1 at.%)

Fuel-to-cladding diametral gap:

- Phases I and II: 0.0035 to 0.0096 inch (0.089 to 0.24 mm)
- Phase III: 0.0035 inch (0.089 mm), 0.0055 inch (0.014 mm) and 0.0075 inch (0.19 mm)

Secondary Variables

Fill gas: pins with 18% Xe tag

Fuel fabricated structure: pins with low pressure preslugged fuel

HEDL P-19 fuel batch

Mixed fuel-to-cladding gaps in the same pin

One high burnup PNL-2 pin [304 SS cladding 0.250 inch (6.35 mm) OD x 0.016 inch (0.41 mm) wall]

TABLE III

SUMMARY OF FABRICATION PARAMETERS FOR PINS IN EACH PHASE OF HEDL P-20

Pin Identification[a]	Nominal Diametral Fuel-to-Cladding Gap, mils (mm)	Average Fuel Pellet Density (% TD)[c]	Plenum Fill Gas[d]	Phase[e] I	Phase[e] II	Phase[e] III
P-20-1	7.6 (0.193)	90.7	He	X		
P-20-2R	7.6 (0.193)	91.0	He	X		X
P-20-3	7.6 (0.193)	90.9	He	X	X	
P-20-4	7.6 (0.193)	90.6	He	X	X	X
P-20-5	7.6 (0.193)	90.8	He		X	
P-20-7	7.6 (0.193)	91.1	He			X
P-20-8	7.6 (0.193)	90.6	He		X	X
P-20-9	7.4 (0.187)	91.2	Xe + He	X		
P-20-10	7.6 (0.193)	91.2	Xe + He	X		X
P-20-11	7.5 (0.191)	91.1	Xe + He	X	X	
P-20-12	7.5 (0.191)	91.2	Xe + He		X	
P-20-13	7.4 (0.187)	91.1	Xe + He			X
P-20-15	7.7[b] (0.196)	91.4	He		X	
P-20-18	M 5.5[b] (0.140)	91.4	He	X		
P-20-19	M 5.4[b] (0.137)	91.3	He	X		X
P-20-20	M 5.6[b] (0.142)	91.3	He	X	X	
P-20-21	M 5.5[b] (0.140)	91.2	He		X	
P-20-22	M 5.6[b] (0.142)	91.4	He			X
P-20-24	5.6 (0.142)	90.8	He	X		
P-20-25R	5.6 (0.142)	91.2	He	X		X
P-20-26	5.5 (0.140)	91.1	He	X	X	
P-20-27	5.6 (0.142)	91.0	He	X	X	X
P-20-28	5.5 (0.140)	91.2	He		X	
P-20-29	5.6 (0.142)	91.3	He		X	X
P-20-30	5.5 (0.140)	91.0	He			X
P-20-32	3.6 (0.091)	90.6	He	X		
P-20-33	3.6 (0.091)	90.6	He	X		X
P-20-34R	3.5 (0.089)	91.1	He	X	X	
P-20-35	3.5 (0.089)	90.7	He	X	X	X
P-20-36	3.6 (0.091)	90.6	He		X	
P-20-37	3.5 (0.089)	90.6	He		X	X
P-20-39	7.6 (0.193)	91.5	He			X
P-20/19-1R	9.6 (0.244)	90.8	He		X	
P-20/19-14	3.8 (0.097)	90.8	He		X	
P-20/19-21	7.6 (0.193)	90.8	He			X
P-20/19-23	3.8 (0.097)	90.8	He	X		
P-20/19-34	7.2 (0.183)	90.8	He			X
P-20/PNL-2-5	6.0 (0.152)	91.7	He			X

[a] All fuel pins have 0.230 inch (5.48 mm) cladding OD's except the PNL-2-5 pin which has 0.250 inch (6.35 mm).

[b] M 5.5 = Mixed gap pin; mixed gap sizes over four inches length near axial midplane with indicated gap in remainder of fuel column.

[c] Fuel for pins P-20-15 and P-20-39 was fabricated with low-pressure preslugging techniques; all other P-20 fuel was made with high-pressure preslugging methods. TD = Theoretical Density (~ 10.9 gm/cc) of the fuel.

[d] He = 100% Helium; Xe + He = 18.3% Xenon + 81.7% Helium.

[e] Phase I, Subassembly #X169A; Phase II, Subassembly #X169; Phase III, Subassembly #X169B.

Detailed fabrication descriptions for the pins discussed in this report are given in Appendix C, Reference 13. These pins were the same design as the 0.230 inch (5.84 mm) OD pins used in the P-19 experiment. The mixed gap P-20 pins and the PNL 2-5 pins are not included in this study because analyses on them are still preliminary.

The P-20 test was conducted in three phases (see Figure 3). The purpose of Phases I and II was to accumulate fuel burnup under steady-state conditions on groups of well characterized pins, some of which would be used in Phase III. The peak fuel pin linear power in these phases was about 13.75 kW/ft (451 W/cm) or approximately 78% of the peak linear power during Phase III. After Phases I and II some pins were removed, and unirradiated (fresh) pins were added so that three burnup levels were achieved (see Table IV). Then Phase III was conducted using pins from each of the three burnup levels plus six "fresh" pins and one PNL-2 fuel pin.

The Phase III portion of the test was scheduled to be conducted with the same power-time history as in the P-19 test; however, several of the hold times during the rise to power for Phase III were longer than in the P-19 test. These were judged to be of no consequence to the test results because they occurred at fairly low powers. The Q'_m values were derived from axial extents of melting observed in the pins, similar to the P-19 analysis. Table V summarizes those pins that experienced fuel melting.

C. DERIVED AND NORMALIZED DATA FROM THE HEDL P-19 AND P-20 TESTS

The location of the axial extents of melting was based on the appearance of the neutron radiography and ceramography samples. Using these locations, the axial power profiles the Q'_m values under local conditions were calculated. Tables VI and VII summarize these data.

The Q'_m values under local conditions were normalized, as described in Reference 1, to a single set of basic FFTF parameters:

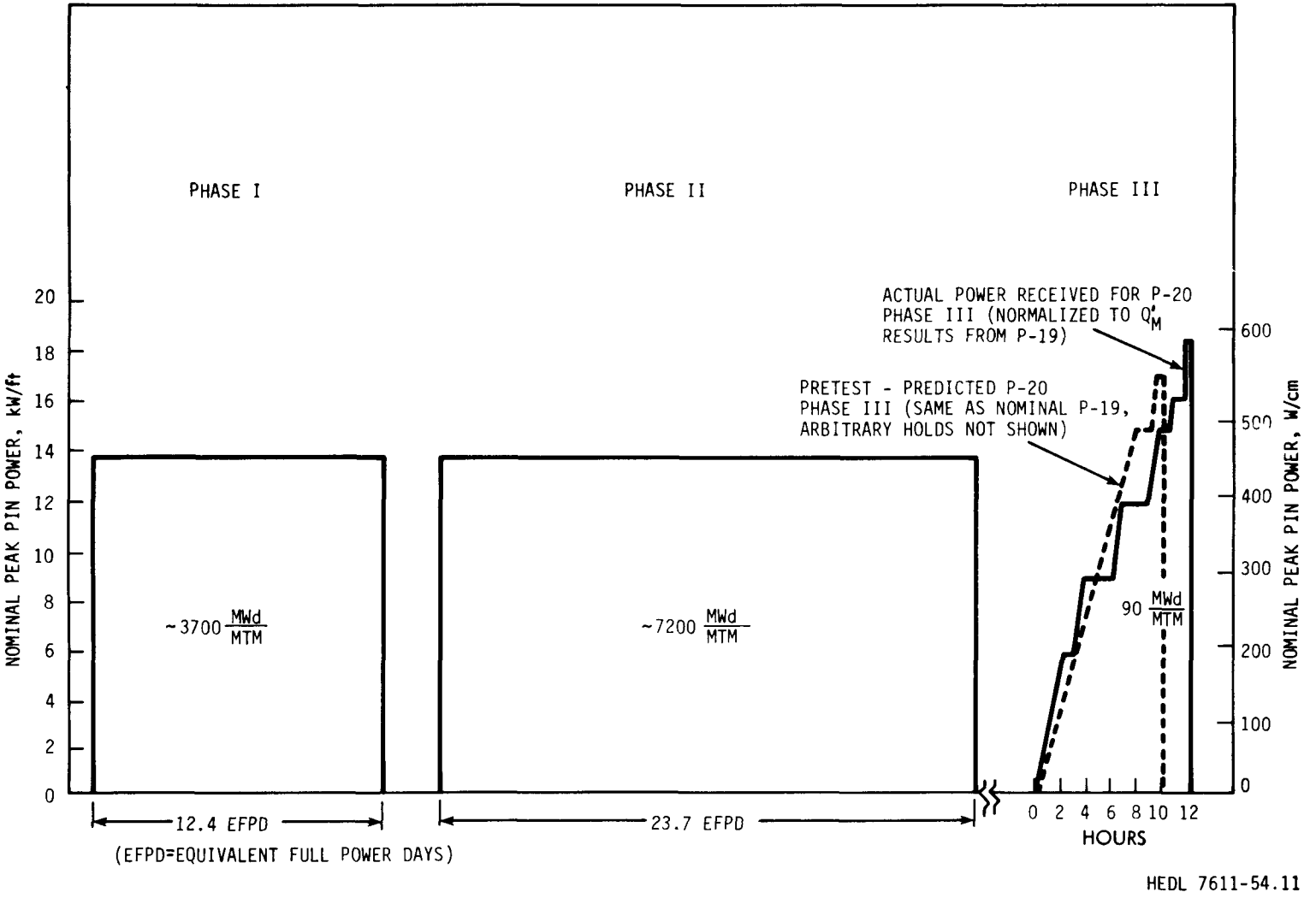

FIGURE 3. Peak Power History for a Nominal HEDL P-20 Pin.

TABLE IV

SUMMARY OF HEDL P-20 IRRADIATIONS CONDITIONS

	EBR-II		Equivalent Full Power Days	Approximate Accumulated Burnup MWd/MTM (at.%)	Reactor Full Power Cycles
	Run No.	Test Position			
Phase I	61A	3F2	12.4	3700 (0.38)	2
Phase II	59B	3F2	23.7	7200 (0.74)	6
Phase I + II	---	---	36.1	10900 (1.12)	8
Phase III	62E	1N1	0.26	90 (0.0093)	1

TABLE V

FUEL MELTING RESULTS FOR THE PHASE III HEDL P-20 TEST PINS

Preirradiated Burnup, MWd/MTM (at.%)	Total Pins	Pure He Pin Fill Gas					18% Xe-82% He Pin Fill Gas	Comments
		3.5 (0.089)[a]	5.5 (0.14)[a]	7.5 (0.19)[a]	Mixed	Other	7.5 (0.19)[a]	
~0	7	--	1	2[b]	1	2[c]	1	All pins had fuel melting
3700 (0.38)	5	1	1	1	1	--	1	Only the 3.5 mil (0.089 mm) gap pin had fuel melting
7200 (0.74)	3	1	1	1	--	--	--	No fuel melting
10900 (1.1)	3	1	1	1	--	--	--	No fuel melting
65000 (6.7)	1	--	--	--	--	1	--	PNL-2-5 had fuel melting

[a] As-built, nominal fuel-to-cladding diametral gap size, mil (mm).

[b] One pin contained low-pressure preslugged fuel.

[c] P-19 spare pins, 7.2 and 7.6 mil (0.18 and 0.19 mm) gaps.

TABLE VI

ESTIMATES OF RESTRUCTURING AT AXIAL EXTENTS OF MELTING

	Top Axial Extent of Melting			Bottom Axial Extent of Melting		
Pin Identity	Radius Central Void, inches, (mm)	Radius Columnar Grain, inches, (mm)	Calculated[b] Columnar Grain, Region Density (%TD[c])	Radius Central Void, inches, (mm)	Radius Columnar Grain, inches, (mm)	Calculated[b] Columnar grain, Region Density (%TD[c])
P-19-2	0.014 (0.36)	0.061 (1.55)	96.4	0.015 (0.38)	0.060 (1.52)	98.0
P-19-3R	0.016 (0.41)	0.073 (1.85)	96.9	0.016 (0.41)	0.073 (1.85)	97.2
P-19-7R	0.015 (0.38)	0.068 (1.73)	97.4	0.015 (0.38)	0.061 (1.55)	98.6
P-19-8	0.017 (0.43)	0.063 (1.60)	98.0	0.016 (0.41)	0.062 (1.58)	98.0
P-19-13	0.014 (0.36)	0.061 (1.55)	98.0	0.015 (0.38)	0.060 (1.52)	98.0
P-19-20	0.017 (0.43)	0.062 (1.58)	97.3	0.016 (0.41)	0.062 (1.58)	97.4
P-19-24R	0.008 (0.20)	0.067 (1.70)	93.1	0.008 (0.20)	0.067 (1.70)	92.9
P-19-25R	0.018 (0.46)	0.071 (1.80)	98.5	0.009 (0.23)	0.068 (1.73)	93.6
P-19-26R	0.017 (0.43)	0.066 (1.68)	98.2	0.015 (0.38)	0.060 (1.52)	98.6
P-19-27R	0.014 (0.36)	0.057 (1.45)	98.4	0.012 (0.31)	0.060 (1.52)	96.1
P-19-28	0.008 (0.20)	0.058 (1.47)	94.5	0.009 (0.23)	0.057 (1.45)	94.5
P-19-30	0.015 (0.38)	0.065 (1.65)	97.9	0.013 (0.33)	0.065 (1.65)	96.0
P-19-35	0.016 (0.41)	0.064 (1.63)	96.6	0.015 (0.38)	0.067 (1.70)	96.0
P-20-7	0.015 (0.38)	0.065 (1.65)	96.9	0.015[a] (0.38)	0.064 (1.63)	96.9
P-20-13	0.015 (0.38)	0.071 (1.80)	98.0	0.015 (0.38)	0.070 (1.78)	98.0
P-20-30	0.018 (0.46)	0.065 (1.65)	98.5	0.018[a] (0.46)	0.060 (1.52)	98.5
P-20-33	0.012 (0.31)	0.072 (1.83)	93.5	0.019 (0.48)	0.074 (1.88)	96.5
P-20-39	0.016 (0.41)	0.068 (1.73)	97.1	0.016[a] (0.41)	0.064 (1.63)	98.2
P-20/19-21	0.012 (0.31)	0.065 (1.65)	93.9	0.015 (0.38)	0.068 (1.73)	96.0
P-20/19-34	0.017 (0.43)	0.065 (1.65)	96.1	0.014 (0.36)	0.061 (1.55)	97.8

[a] The central void at the bottom section was obliterated by molten fuel relocation. In this case the central void size from the top of the pin was used (see Appendix A).

[b] Based on densification of columnar grain needed to form central void. Densities were limited to no higher than 98.5% TD based on observations of grain region.

[c] TD = Theoretical Density (~ 10.9 gm/cc) of the fuel.

TABLE VII

PEAK PIN POWERS AND AXIAL EXTENTS OF MELTING FOR HEDL P-19 PINS

Pin Identity	Peak Pin Power kW/ft, (W/cm)	Bottom Axial Extent of Melting			Top Axial Extent of Melting		
		Location[a]	Local Power[b] kW/ft, (W/cm)	Coolant Temp. °F (°C)	Location[a]	Local Power[b] kW/ft, (W/cm)	Coolant Temp. °F (°C)
P-19-2	16.6 (545)	2.84 (7.21)	15.8 (518)	726 (385.6)	9.78 (24.84)	15.4 (505)	799 (426.1)
P-19-3R	19.5 (640)	0.35 (0.89)	16.0 (525)	704 (373.3)	12.32 (31.29)	15.7 (515)	843 (450.6)
P-19-5	17.1 (561)	---	---	---	---	---	---
P-19-6	17.1 (561)	---	---	---	---	---	---
P-19-7R	20.3 (666)	1.61 (4.09)	18.0 (591)	718 (381.1)	11.27 (28.63)	17.3 (568)	839 (448.3)
P-19-8	16.4 (538)	2.49 (6.32)	15.5 (509)	723 (383.9)	10.48 (26.62)	14.8 (486)	805 (429.4)
P-19-13	16.6 (545)	3.33 (8.46)	16.1 (528)	732 (388.9)	9.41 (23.90)	15.7 (515)	796 (424.4)
P-19-20	16.5 (541)	3.87 (9.83)	16.0 (525)	737 (391.7)	10.64 (27.03)	14.8 (486)	807 (430.6)
P-19-24R	19.7 (646)	0.59 (1.50)	16.1 (528)	706 (374.4)	12.60 (32.00)	15.1 (495)	848 (453.3)
P-19-25R	20.1 (660)	0.83 (2.11)	16.8 (551)	709 (376.1)	12.01 (30.51)	16.1 (528)	846 (452.2)
P-19-26R	20.4 (669)	1.84 (4.67)	18.4 (604)	720 (382.2)	10.68 (28.13)	18.2 (597)	833 (445.0)
P-19-27R	20.4 (669)	2.33 (5.92)	18.8 (617)	727 (386.1)	10.18 (25.86)	18.5 (607)	828 (442.2)
P-19-28	20.7 (679)	2.35 (5.97)	18.9 (620)	727 (386.1)	10.70 (27.18)	18.0 (591)	835 (446.1)
P-19-30	20.0 (656)	1.11 (2.82)	17.2 (564)	712 (377.8)	11.35 (28.83)	17.1 (561)	838 (447.8)
P-19-33	16.8 (551)	---	---	---	---	---	---
P-19-35	16.5 (541)	3.26 (8.28)	16.0 (525)	731 (388.3)	8.84 (22.45)	16.0 (525)	790 (421.1)

[a] Distance from bottom of fuel column in inches (cm).

[b] Powers corrected for once molten fuel plugs if present in ceramography.

- 0.230 inch (5.84 mm) OD cladding geometry
- 90.4% TD fuel pellet density
- 1060°F (571°C) cladding ID temperature
- 1060°F pin gas plenum temperature.

This was done using a version of the SIEX-M1 thermal performance code.

Figure 4 summarizes the results for the "fresh" (60 to 90 MWd/MTM burnup) fuel pin data. The P-20 pin with xenon tag gas had centerline fuel melting from the top to the bottom of the fuel column; thus there were no valid axial extents of melting. The power, under local conditions, at the ends of this pin were taken as "upper bound" points of Q'_m (i.e., Q'_m was less than these powers). For those pins with no fuel melting, such as the small-gap P-19 pins with 0.230 inch (5.84 mm) cladding OD, the peak powers of each were taken to establish a "lower bound" of Q'_m for each pin (i.e., Q'_m is greater than the peak powers in these pins). The trend (observed from Figure 4) was for Q'_m to increase with decreasing fabricated fuel-to-cladding gap size up to a gap size of about 0.0045 inch (0.114 mm) and then to level off to a constant value.

Figure 5 shows the normalized results from the pins with the three higher levels of burnup from the HEDL P-20 test. Most of these data were from pins with no melting; thus, these are shown as lower bound Q'_m points. The improvement in normalized Q'_m for the 18%-xenon-tagged pin was more than 25% in going from the upper bound of the "fresh" pin Q'_m, Figure 4, to the lower bound of the Phase I pin irradiated to 3700 MWd/MTM. It was concluded that the effect of initial fabricated fuel-to-cladding gap size on the power-to-melt was no longer a dominant variable after a small amount of irradiation. The apparent reasons for this occurrence are discussed in detail in Reference 1; primarily it was caused by maturing of the fuel restructuring and rapid fuel-to-cladding gap closure.

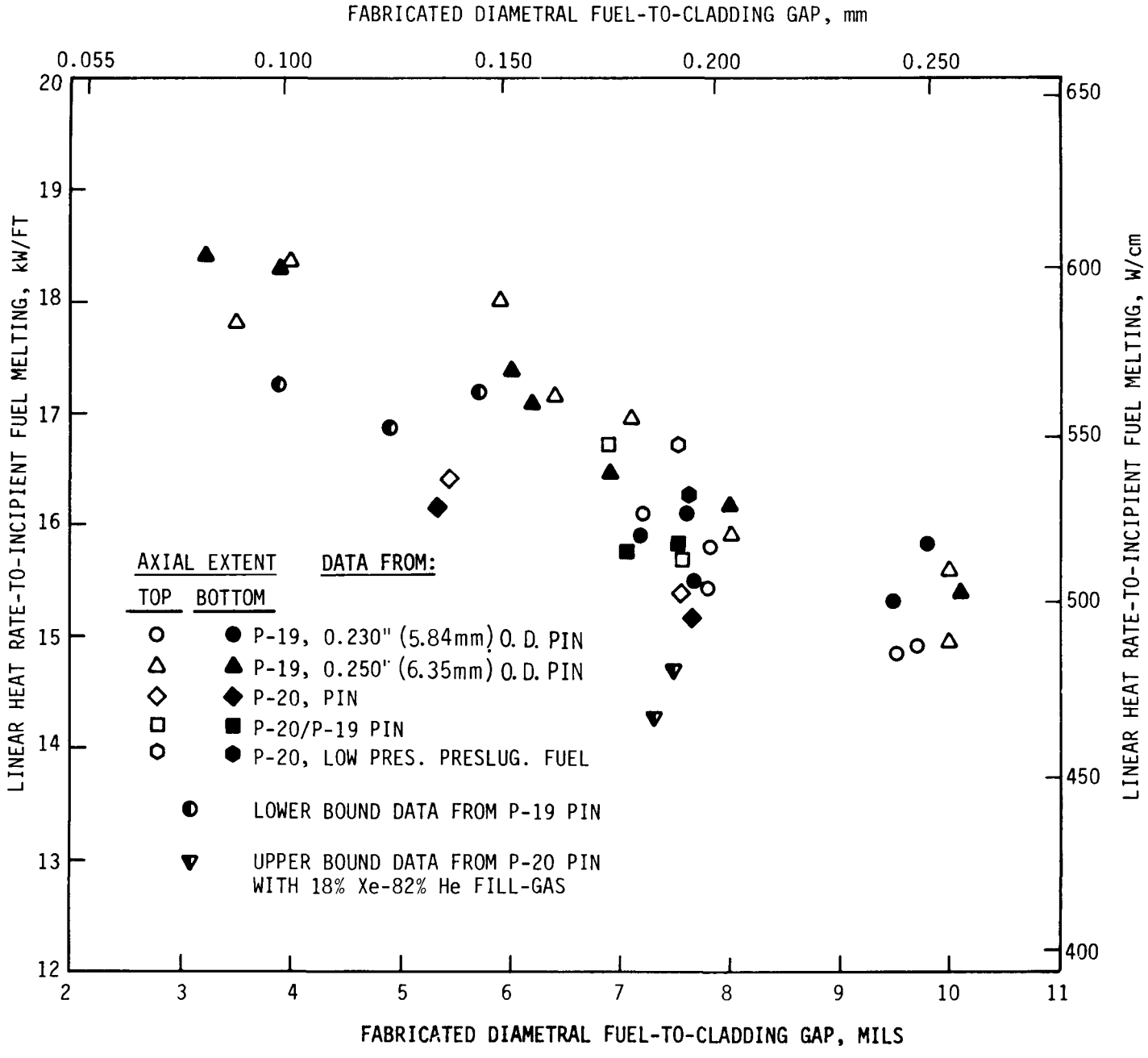

FIGURE 4. Normalized Q'_m Values for "Fresh" Fuel.

HEDL 7611-54.21

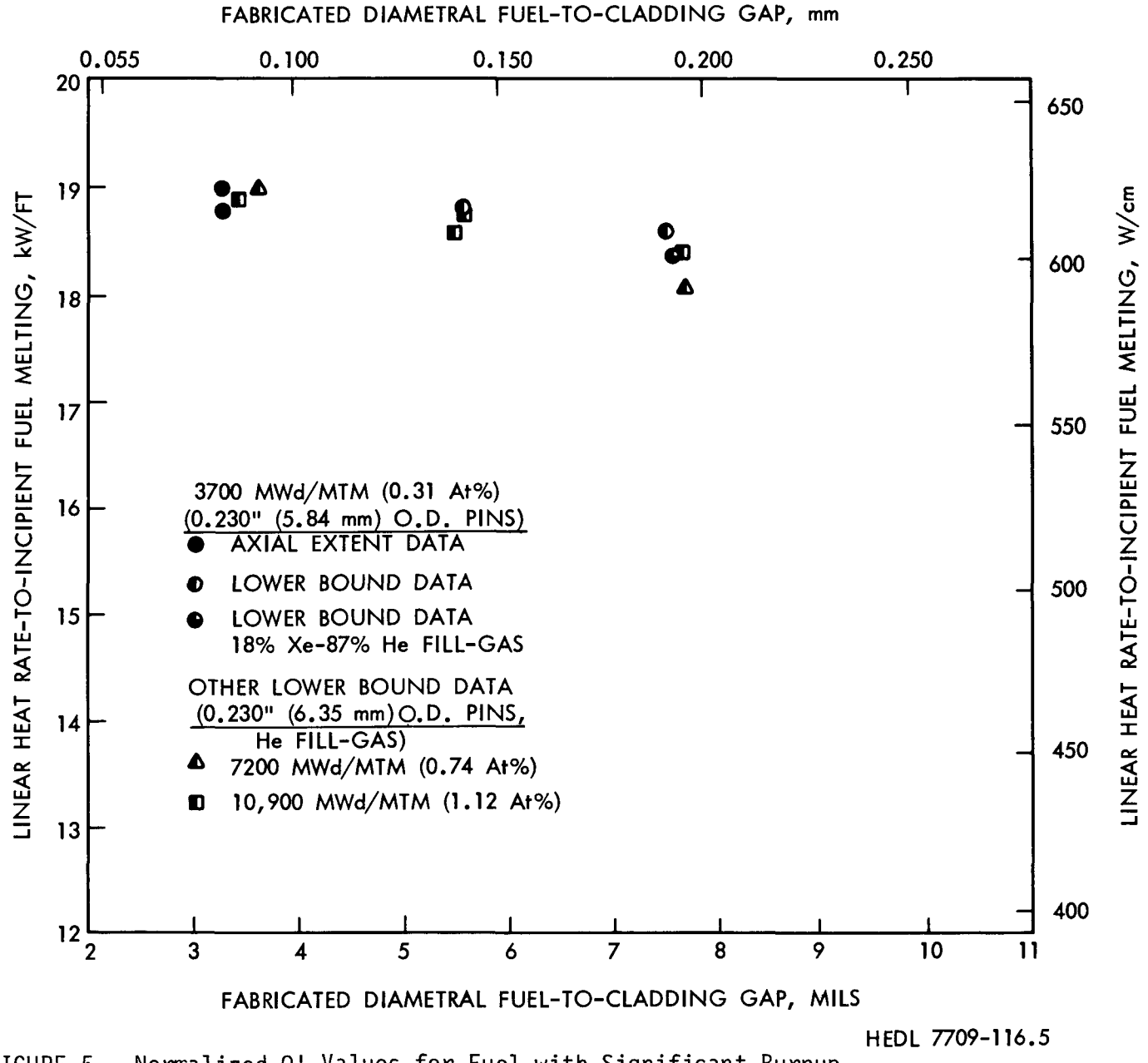

FIGURE 5. Normalized Q'_m Values for Fuel with Significant Burnup.

IV. SUMMARY OF THE MATHEMATICAL REPRESENTATIONS FOR THE RADIAL HEAT PATH

The SIEX[2] code was chosen as the starting point for the thermal calibration work using the HEDL P-19 and P-20 integral Q'_m data. SIEX has been used extensively at HEDL[16] for the past several years for prediction and analysis work on fast reactor fuel. In preparation for calibration of a gap conductance model, the heat transfer formulations of SIEX were reviewed in detail. Material properties and formulations related to the heat transfer across the fuel pin radii, especially those concerned with the gap conductance model, were updated where appropriate to make them consistent with the present state-of-the-art of the technology. These revisions were included in an updated version of SIEX designated "SIEX-M1". These expressions should result in the most accurate calculation of all temperature drops across the fuel pin radius. This was important since integral Q'_m data, based on the total temperature drop from the fuel centerline to the coolant, was used for the calibration. Thus the "correctness" of all these models had a direct bearing on the calibration of the gap conductance model to reflect the actual conditions that occurred in the gap.

The following sections describe the general revisions made to the SIEX formulations and give a brief description of the gap conductance model.

A. SUMMARY OF SIEX

SIEX is a code which calculates the thermal performance characteristics and dimensional changes (swelling and thermal expansion) of mixed-oxide fuel pins in a fast neutron environment. SIEX is comprised of a series of subroutines which model certain fast reactor fuels phenomena and was originally correlated to a significant amount of EBR-II irradiation test data. Program development and numerical techniques have been carried out in a way which provides a code with short running times and modular independence of models. This code has been shown to satisfy the need for a data analysis and design tool in the LMFBR program. The code is fully described in Reference 2 and is available through the Argonne National Computer Code Center (ANCCC).

B. REVISIONS FOR SIEX-M1

The methods of calculating the temperature drops along the radial heat path for SIEX-M1 are essentially unchanged from the original SIEX[2] code. These methods and equations are described in detail in Appendix A. Reviews showed that these formulations, including the fuel-to-cladding thermal conductance expressions, provided an accurate physical representation, within the present level of understanding, of the radial temperature drops. However, it was concluded that changes to several of the thermal material properties were warranted to make a better representation of the heat transfer system. In addition, a residual fuel-to-cladding gap model (the gap observed during destructive examinations), derived solely from the HEDL P-19 and P-20 data, was developed to produce the most realistic predictions of hot gap size.

Material Properties for SIEX-M1

Appendix B describes the material properties that were used in SIEX-M1. Several of these thermal properties were revised from those used in the SIEX code and Appendix B includes the reasons for the changes. Revised properties were used for:

- Accommodation coefficients and jump distance in the gap thermal conductance model,
- Thermal conductivity of the plenum gases Xe, Kr, N_2, Ar, and He and their mixture, and
- Fuel thermal conductivity.

Fuel Behavior Assumptions for SIEX-M1

Appendix C discusses some of the fuel behavior observed in the experimental fuel pins that may affect thermal performance. These included:

- Residual fuel-to-cladding gap (gap observed after irradiation),
- Thermal expansion,
- Fuel restructuring, and
- Fission and sorbed gas release.

Correlated general models for each of these were not made since only HEDL P-19 and P-20 data were analyzed, and the scope of these tests was limited to high-power, low-burnup data. Appendix C discusses some of the logic used in the calibration of models within SIEX. For this study, models for residual gap closure and fuel thermal expansion were developed based on the P-19 and P-20 data. For calibration of the gap conductance model, measured values were directly input for the remaining fuel behavior phenomena of gas release and restructuring.

The residual fuel-to-cladding gap model was important to the development of a gap conductance model. The calculation of thermal expansion of both the fuel and cladding and the residual gap (permanent gap closure) determined the calculated size (X_G) of the gap at operating temperatures. The residual fuel-to-cladding gap model was based on previous gap closure models and a detailed analysis of measurements of residual gap sizes taken from 77 transverse ceramography samples from P-19 and P-20 Phase III pins. This model is described in detail in Appendix C. The model was dependent on power, burnup, reactor cycles, and original gap size. It took the form:

$$(2) \quad G_p = G \{1 - \tau[1 - \exp(-\Theta_3 \cdot N_c)] - [\Theta_4 - \tau][1 - \exp(-\Theta_5 \cdot Bu)]\} + Q_2' \Theta_6/G$$

where: $\tau = \Theta_1 \cdot Q_1' \cdot (Q_1' - \Theta_2)$,

Q_1' = Time averaged local linear heat rate, kW/ft [W/cm] (for "fresh" fuel $Q_1' = Q_2'$),

Q_2' = Maximum local linear heat rate, kW/ft [W/cm],

Bu = Local burnup, MWd/kgM,

N_c = Number of full power cycles,

G_p = Postirradiation diametral gap, mil [cm], and

G = Fabricated diametral gap, mil [cm].

Θ's Fitting Coefficients	
$\Theta_1 = 0.00672$	$\Theta_4 = 0.890$
$\Theta_2 = 12.5$	$\Theta_5 = 7.11$
$\Theta_3 = 0.919$	$\Theta_6 = 0.239$

Θ's Fitting Coefficients (CGS Units)	
$\Theta_1 = 6.24 \times 10^{-6}$	$\Theta_4 = 0.890$
$\Theta_2 = 410$	$\Theta_5 = 7.11 \times 10^{-4}$
$\Theta_3 = 0.919$	$\Theta_6 = 4.70 \times 10^{-8}$

The mathematic fit of the model to the data had a root mean squared deviation of 0.66. The random variations observed in this type measurement were quite large; thus, the fit was considered good.

Fuel thermal expansion in SIEX-M1 was calculated by summing the thermal expansion over the fuel radius rather than the prior method, used in SIEX[2], of calculating the radial average expansion. It was assumed by this that the fuel had cracked and the pieces could expand freely. The revised method resulted in greater calculated expansion. This interpretation correlated two observations:

- The measured residual fuel-to-cladding gaps found in the fresh fuel pins, and

- The fabricated gap size at which the fresh fuel was observed to contact the cladding based on the behavior derived in Q'_m data.

During prior SIEX calibration[2] these two observations could not be resolved, and the measured residual gap data were not used.

C. FUEL-TO-CLADDING THERMAL GAP CONDUCTANCE MODEL

The gap conductance model, based on that proposed by Ross and Stoute,[9] used in SIEX was compared to other available models. It was concluded (Appendix A) that this model should be used in SIEX-M1. The primary reasons for its continued use were:

1. Theoretically "better" models were more complex in form and required parameter values not presently available for FBR fuel. Further, because of the very limited data base there was a question of whether the expressions actually modeled the phenomena better.

2. Past experience with this model form had shown it to provide reasonable predictions[16] when used in the SIEX code.

Appendix A describes the assumptions used in developing the selected gap conductance model. The gap conductance, H, was assumed to be the sum of the conductance caused by the three parallel mechanisms of heat transfer acting through the gap:

$$H = H_G + H_S + H_R$$

where: H_G = Thermal conductance due to heat transfer through the gas (Because of surface roughness, this term was applicable even after the fuel and cladding were in contact.),

H_S = Thermal conductance due to heat transfer through fuel-to-cladding (solid-to-solid) contact, and

H_R = Thermal conductance due to radiant heat transfer through the gas.

When the fuel and cladding were in contact there was still significant heat transfer through the gas. This occurred because only the asperities of the surface roughness actually contacted, leaving pockets of gas in between (see Appendix A Section 4).

Equation (A-23) of Appendix A summarizes the gap conductance model equation.[1] The expressions for the thermal conductance values could be summarized as follows:

(3) $$H = H_G + H_S + H_R$$

[1]As derived, the expression for gas conductance, H_G, was for the gas voids between contacting roughness asperities; however, for application to the total gap conductance model, this portion of the model, and its related constants, was applied to any "open" hot gap, including that present prior to fuel-cladding contact.

(3.a) $$H_G = \frac{k_G}{Be^{D \cdot P} + X_G + (g_F + g_C)}$$

where: k_G = Thermal conductivity of the gas mixture in the gap, $W/cm^2\text{-}°C$,

B = An empirical constant that included the effect of fuel and cladding surface roughness and "waviness", cm,

D = An empirical constant representing the reduction of surface roughness with increasing interface pressure, $cm^2/dynes$,

P = Apparent interface pressure between fuel and cladding, $dynes/cm^2$,

X_G = Distance between the fuel and cladding (hot gap), taken from the furthest extreme of one surface mean roughness to the other, cm, and

$g_F + g_C$ = The sum of the "jump" distances at the fuel and cladding surfaces, cm.

(3.b) $$H_S = \frac{A_2 k_m P}{y_c}$$

where: A_2 = An empirical constant that represented fuel and cladding surface roughness and waviness (in part modeled the inverse radius of the area at the contacting roughness peaks), cm^{-1},

k_m = Harmonic mean of the conductivities of the fuel and cladding $\left(k_m = \frac{2k_F k_C}{k_F + k_C}\right)$, $\left(\frac{W}{cm\text{-}°C}\right)$, and

y_c = Yield strength of the cladding, $dynes/cm^2$.

(3.c) $$H_R = \frac{r_F \sigma\left(T_F^2 + T_C^2\right)\left(T_F + T_C\right)}{r_C\left[\frac{1}{F} + \left(\frac{r_F}{r_C}\right)\left(\frac{1}{C} - 1\right)\right]}$$

where: r_F, r_C = The radius of the outside surface of the fuel and the inside surface of the cladding, respectively, cm,

T_F, T_C = The surface temperatures at r_F and r_C, respectively °C,

ε_F, ε_C = The emissivity of the surfaces at r_F and r_C, respectively, and

σ = Stefan-Boltzman constant, $W/cm^2\text{-}°K$.

The three constants in this gap conductance model equation, A_2, B, and D, were calibrated using the P-19 and P-20 Q'_m data. These constants included surface roughness of the cladding and fuel and the "waviness" of these surfaces. In addition, the constant A_2 (see Equation 4) included the effects of the ratio of the yield strength, y_c, of the softer wall material (the cladding) to its hardness, h. Roughness was included as a constant for A_2, B, and D since values for roughness were not measured for the surfaces of the test fuel and cladding; nor were they characterized for FBR fuel pins at the present time. Since the test fuel and cladding were prototypic of those used for FFTF fuel pins, values derived from the tests should be directly applicable to present FBR fuel.

These constants had the following form if surface roughness and hardness were identified:

$$A_2 = \frac{y_c}{A_1 \bar{R}^{-1/2} h} \tag{4}$$

$$Be^{D \cdot P} = C_1 \left(R_F + R_C\right) \tag{5}$$

where: h = Meyer's hardness of the cladding,

A_1 = Empirical constant, cm,

R_F, R_C = Arithmetic mean of surface roughness of fuel and cladding respectively, cm,

$$\bar{R} = \left(\frac{R_F^2 + R_C^2}{2}\right), \text{ cm, and}$$

C_1 = Empirical constant.

The constant A_1, in part, represented the average cross-sectioned radius of contacting roughness asperities. An effect due to surface waviness was also accounted for through this constant. The constant C_1 modeled the decrease in roughness and waviness when the fuel and cladding were in contact under pressure (see Appendix A). In Section V.C the constants A_1 and C_1 were used for comparison to out-of-reactor experimental results,[9] using assumed surface roughness values, after the other constants (A_2, B, and D) were calibrated using the test data.

V. CALIBRATION OF CONSTANTS IN THE GAP THERMAL CONDUCTANCE MODEL

The calibration of the fuel-to-cladding gap conductance model constants discussed in the previous section, using the Q'_m data from the HEDL P-19 and P-20 experiments, was the final step in developing the fuel-to-cladding gap conductance model. The measured local values of Q'_m discussed in Section III were used. Calculations for the analysis were made with modified versions of the SIEX-M1 code, which included the residual gap closure model of Equation (2).

The three constants (see Equation 3) of the gap conductance model could not be determined uniquely from the test data. For an open hot gap (heat transfer solely through gas) only the constant B was applicable. Once the fuel and cladding were in contact, all three constants were used in the calculation. For calibration, a value of B was correlated based on the data calculated to have an open hot gap. Of the remaining two constants, D was set based on judgment and past work by others, and A_2 was set based on the data calculated to have a "closed" hot gap.

Each pin's measured plenum gas composition, with respect to He, Kr, Xe, Ar, and N_2 (see Appendix C), after irradiation was used directly for calibration calculations. The measured columnar region radius, central void radius, and the implied columnar grain density near the axial extents of melting were also used directly in each instance. These measurements are discussed in general in Appendix C and are tabulated in Reference 1. For comparisons of normalized Q'_m to model predictions after the calibration was complete, typical or average values of gas release and restructuring were used.

A. GAS GAP CONSTANT B

When the fuel and cladding were not in contact, the interface pressure, P, was zero and the constant remaining in Equation (3) was B. The data from all the axial extents of melting were analyzed using a version of the SIEX-M1

code that calculated the value of B needed to match the observed melting conditions in each case. Those values of B corresponding to open hot gaps are included both in Table VIII and Figure 6.

Figure 6 shows there was a significant amount of scatter in these values of B; however, all the experimental and fuel model uncertainties were reflected in these values. No bias was observed for the different sized pins or between the HEDL P-20 and P-19 data. [One way to think of this plot is that the lower values of B were calculated when a smaller effective hot gap value, X_G, was needed to explain the gap conductance required to match the Q'_m conditions of the data (see Equation 3a).]

A slightly conservative, with respect to Q'_m, value of 1.65×10^{-3} cm was chosen for B. More weight was given to fitting the data where the hot gap was almost closed and to being conservative at larger gaps. There did appear to be a slight trend to the plot, the B values increasing with decreasing gap size; however, the constant value, chosen considering the uncertainties involved, was deemed sufficient for the characterization. The data from the P-20 pin with a 0.0055 inch (0.140 mm) diametral gap were not weighted as heavily as the other data. The differences between these data from one P-20 pin and the P-19 data at this same gap range are discussed in Reference 1. The actual reason for the different values remains to be explained. There were some indications that the differences may have been caused by small differences in surface roughness and waviness in the P-20 fuel pins compared to the P-19 fuel pins. These differences could affect the heat transfer as the fuel begins to contact the cladding.

B. CONTACT CONSTANTS A_2 AND D FROM CLOSED GAP DATA

Assuming the constant B to be fixed, the constants A_2 and D were evaluated with the data from pins with calculated closed fuel-to-cladding gaps (X_G = 0.0 in Equation 4) at operating temperatures. The data from the HEDL P-19 and P-20 experiments did not allow the separation of these constants; therefore, they were not solved uniquely. Laboratory experiments can

TABLE VIII

CALCULATED VALUES OF GAP CONDUCTANCE PARAMETERS FOR DATA POINTS

Pin Section		Fabricated Diametral Gap, mil (mm)	Hot Gap Radial, mil (mm)	Gas Conductivity W/cm-°C	Jump Distance cm	Interface Pressure$_2$ dynes/cm^2	H_G W/cm^2-°C	H_S W/cm^2-°C	H_R W/cm^2-°C	Constant B cm
P-19-20	D	9.8 (0.249)	2.19 (0.056)	3.81×10^{-3}	7.78×10^{-4}	0.0	0.549	0.0	0.024	0.583×10^{-3}
	None	9.7 (0.246)	1.87 (0.047)	3.65×10^{-3}	7.25×10^{-4}	0.0	0.644	0.0	0.021	-0.831×10^{-4}
P-19-8	D-2	9.5 (0.241)	2.09 (0.053)	3.85×10^{-3}	7.92×10^{-4}	0.0	0.515	0.0	0.025	0.137×10^{-2}
	A-3	9.5 (0.241)	1.83 (0.046)	3.75×10^{-3}	7.57×10^{-4}	0.0	0.539	0.0	0.023	0.155×10^{-2}
P-19-13	D	7.8 (0.198)	1.33 (0.034)	3.64×10^{-3}	7.01×10^{-4}	0.0	0.844	0.0	0.019	0.239×10^{-3}
	B	7.6 (0.193)	1.11 (0.028)	3.52×10^{-3}	6.65×10^{-4}	0.0	0.929	0.0	0.017	0.303×10^{-3}
P-19-2	E-2	7.8 (0.198)	1.32 (0.034)	3.79×10^{-3}	7.53×10^{-4}	0.0	0.623	0.0	0.023	0.198×10^{-2}
	A-3	7.7 (0.196)	1.14 (0.029)	3.67×10^{-3}	7.13×10^{-4}	0.0	0.669	0.0	0.020	0.187×10^{-2}
P-19-35	F-1	7.2 (0.183)	0.98 (0.025)	3.66×10^{-3}	7.21×10^{-4}	0.0	0.762	0.0	0.021	0.158×10^{-2}
	A-2	7.2 (0.183)	0.92 (0.023)	3.62×10^{-3}	7.09×10^{-4}	0.0	0.697	0.0	0.020	0.214×10^{-2}
P-19-3R	C	10.0 (0.254)	1.88 (0.048)	3.79×10^{-3}	9.29×10^{-4}	0.0	0.562	0.0	0.025	0.106×10^{-2}
	A	10.1 (0.257)	1.66 (0.042)	3.67×10^{-3}	8.14×10^{-4}	0.0	0.518	0.0	0.022	0.206×10^{-2}
P-19-24R	C-3	10.0 (0.254)	2.26 (0.057)	3.64×10^{-3}	8.70×10^{-4}	0.0	0.696	0.0	0.021	-0.137×10^{-2}
	A-2	10.1 (0.257)	1.87 (0.047)	3.41×10^{-3}	7.82×10^{-4}	0.0	0.826	0.0	0.016	-0.139×10^{-2}
P-19-25R	E-1	8.0 (0.203)	1.05 (0.027)	3.74×10^{-3}	9.04×10^{-4}	0.0	0.625	0.0	0.024	0.243×10^{-2}
	A-3	8.0 (0.203)	0.93 (0.024)	3.36×10^{-3}	7.60×10^{-4}	0.0	0.976	0.0	0.016	0.313×10^{-3}
P-19-30	E-2	7.1 (0.180)	0.59 (0.015)	3.57×10^{-3}	8.36×10^{-4}	0.0	0.965	0.0	0.019	0.135×10^{-2}
	A-2	6.9 (0.175)	0.42 (0.011)	3.39×10^{-3}	7.72×10^{-4}	0.0	0.954	0.0	0.016	0.173×10^{-2}
P-19-7R	D	6.4 (0.163)	0.36 (0.0091)	3.62×10^{-3}	8.09×10^{-4}	0.0	1.027	0.0	0.019	0.179×10^{-2}
	B	6.2 (0.157)	0.04 (0.0010)	3.44×10^{-3}	7.47×10^{-4}	0.0	1.104	0.0	0.016	0.228×10^{-2}
P-19-26R	G-2	5.9 (0.150)	0.01 (0.00025)	3.58×10^{-3}	7.94×10^{-4}	0.0	1.222	0.0	0.018	0.212×10^{-2}
	A-2	6.0 (0.152)	0.0 (0.0)	3.38×10^{-3}	7.25×10^{-4}	1.73×10^{8}	1.201	0.0	0.015	0.217×10^{-2}

TABLE VIII (Cont'd)

Pin Section	Fabricated Diametral Gap, mil (mm)	Hot Gap Radial, mil (mm)	Gas Conductivity W/cm-°C	Jump Distance cm	Interface Pressure, P_2 dynes/cm^2	H_G W/cm^2-°C	H_S W/cm^2-°C	H_R W/cm^2-°C	Constant B cm
P-19-27R H-1	4.0 (0.102)	0.0 (0.0)	3.41×10^{-3}	7.35×10^{-4}	5.77×10^{8}	1.420	0.728	0.015	0.187×10^{-2}
A-2	3.8 (0.099)	0.0 (0.0)	3.25×10^{-3}	6.83×10^{-4}	6.53×10^{8}	1.525	0.747	0.013	0.166×10^{-2}
P-19-28 H-2	3.5 (0.089)	0.0 (0.0)	3.40×10^{-3}	7.26×10^{-4}	5.03×10^{8}	1.537	0.642	0.015	0.164×10^{-2}
A-3	3.2 (0.081)	0.0 (0.0)	3.21×10^{-3}	6.61×10^{-4}	6.44×10^{8}	2.294	0.761	0.012	0.839×10^{-3}
P-20-7 H	7.5 (0.191)	1.39 (0.035)	3.90×10^{-3}	7.84×10^{-4}	0.0	0.636	0.0	0.027	0.183×10^{-2}
A-1	7.5 (0.191)	1.13 (0.029)	3.69×10^{-3}	7.15×10^{-4}	0.0	0.568	0.0	0.022	0.292×10^{-2}
P-20-13 J	7.3 (0.185)	1.51 (0.038)	2.50×10^{-3}	1.07×10^{-3}	0.0	0.520	0.0	0.029	-0.909×10^{-4}
A-1	7.5 (0.191)	1.17 (0.030)	2.29×10^{-3}	9.27×10^{-4}	0.0	0.545	0.0	0.022	0.297×10^{-3}
P-20-39 G	7.55 (0.192)	1.12 (0.028)	3.78×10^{-3}	8.92×10^{-4}	0.0	0.863	0.0	0.023	0.647×10^{-3}
B	7.65 (0.194)	0.93 (0.024)	3.64×10^{-3}	8.37×10^{-4}	0.0	0.719	0.0	0.021	0.187×10^{-2}
P20/P19-34 G	6.95 (0.177)	0.93 (0.024)	3.83×10^{-3}	7.23×10^{-4}	0.0	0.849	0.0	0.024	0.144×10^{-2}
B	7.05 (0.179)	0.86 (0.022)	3.60×10^{-3}	6.54×10^{-4}	0.0	0.760	0.0	0.019	0.188×10^{-2}
P20/P19-21 G	7.50 (0.191)	1.45 (0.037)	3.76×10^{-3}	7.14×10^{-4}	0.0	0.856	0.0	0.023	-0.412×10^{-5}
B	7.45 (0.189)	0.98 (0.025)	3.61×10^{-3}	6.67×10^{-4}	0.0	0.697	0.0	0.020	0.203×10^{-2}
P-20-30 H	5.45 (0.138)	0.48 (0.012)	3.83×10^{-3}	7.27×10^{-4}	0.0	0.838	0.0	0.024	0.264×10^{-2}
C-4	5.35 (0.136)	0.22 (0.006)	3.60×10^{-3}	6.54×10^{-4}	0.0	0.792	0.0	0.019	0.334×10^{-2}
P-20-33 F	3.55 (0.090)	0.0 (0.0)	1.90×10^{-3}	6.50×10^{-4}	5.51×10^{8}	1.146	0.665	0.018	0.113×10^{-2}
C-1	3.55 (0.090)	0.0 (0.0)	1.89×10^{-3}	6.43×10^{-4}	5.96×10^{8}	0.848	0.658	0.018	0.179×10^{-2}

W/cm^2-°C = 1762 Btu/ft^2-hr-°F.

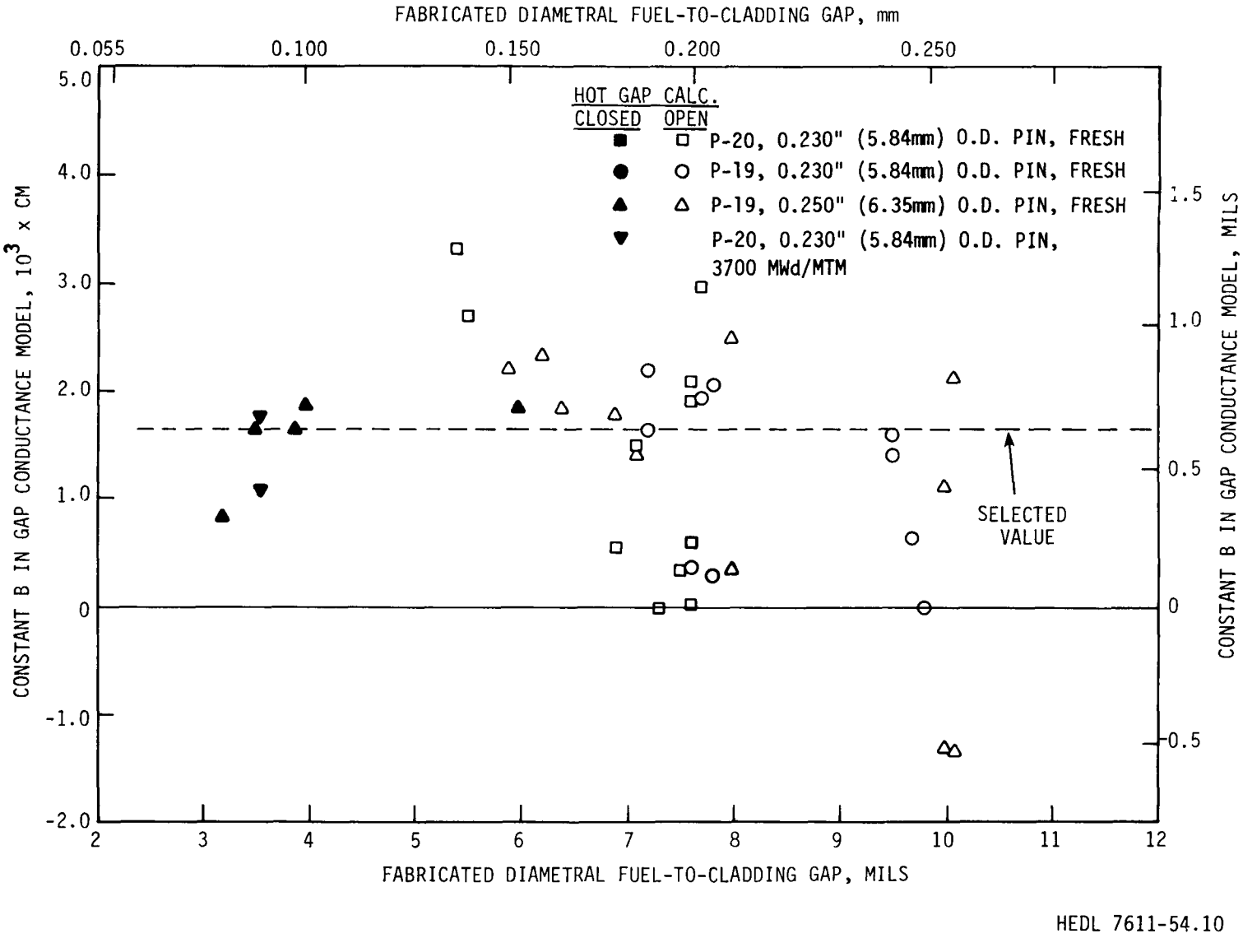

FIGURE 6. Calculated Values of Constant B from Test Data (Calculations for Closed Gap Data Assumed Constants A_2 = 100 and D = -.2 x 10^{-9}).

separate these constants by doing part of the tests in a vacuum, thus eliminating any heat transfer through the gas ($H_G = 0$), allowing a constant like A_2 to be calibrated. For this calibration work it was decided to set the constant D equal to -0.2×10^{-9} cm^2/dyne based on results of Ross and Stoute, past work by Dutt and Baker with SIEX (Reference 2), and the physical meaning of the constant. It was expected, since this constant sought to model the decrease in "waviness" and roughness of the softer surface material under surface to surface pressure, that the effect would be less than found for Zr-UO_2 pairs by Ross and Stoute. The yield point of the stainless steel (about 72 ksi at 950°F or 5.0×10^9 dynes/cm^2 at 510°C) is higher than that of Zircaloy (about 10 ksi at 950°F or $6.9 \times 10^{+8}$ dynes/cm^2 at 510°C).

The constant A_2, Equation (3.b), in the solid-to-solid heat conductance expression, was correlated based on the data with calculated closed hot gaps. The version of SIEX-M1 used to find values for B from the Q'_m data was used here also. The agreement of the calculated constant B for the closed hot gap cases to the value previously set, 1.65×10^{-3} cm, was iterated on while A_2 was adjusted until the best agreement was obtained. The final value of A_2 resulting from this analysis was 100 cm^{-1}. Figure 6 gives an indication of the final agreement of calculated B values using the calibrated constants: $A_2 = 100$ cm^{-1} and $D = -0.2 \times 10^{-9}$ cm^2/dyne.

C. DISCUSSION

Figure 7 shows the agreement of the temperature drops, across the fuel-to-cladding gaps, predicted by the calibrated model and those inferred from the local Q'_m test data. Predicted values were somewhat conservative (i.e., temperature drops predicted tended to be high) but in general agreed well with the observed calculated values. Figures 8 and 9 indicate the agreement of the normalized Q'_m data with the predictions using the calibrated gap conductance model was also, in general, very good.

The trend of predicted lower Q'_m values with increasing burnup, Figure 9, for pins with small fabricated fuel-to-cladding gaps (0.0035 inch or 0.089 mm

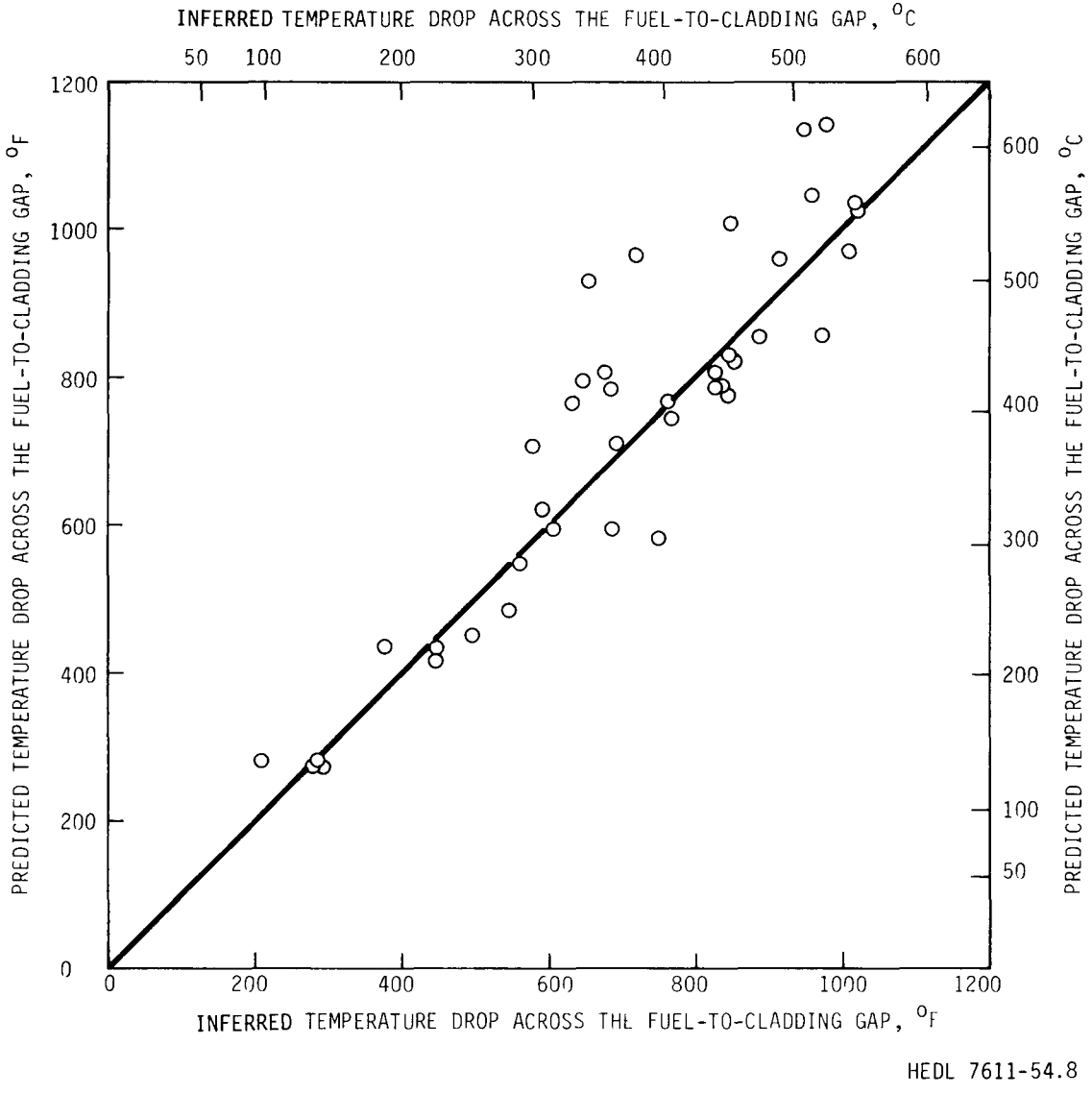

FIGURE 7. Comparison of Predicted and Inferred Temperature Drops Across the Fuel-to-Cladding Gaps.

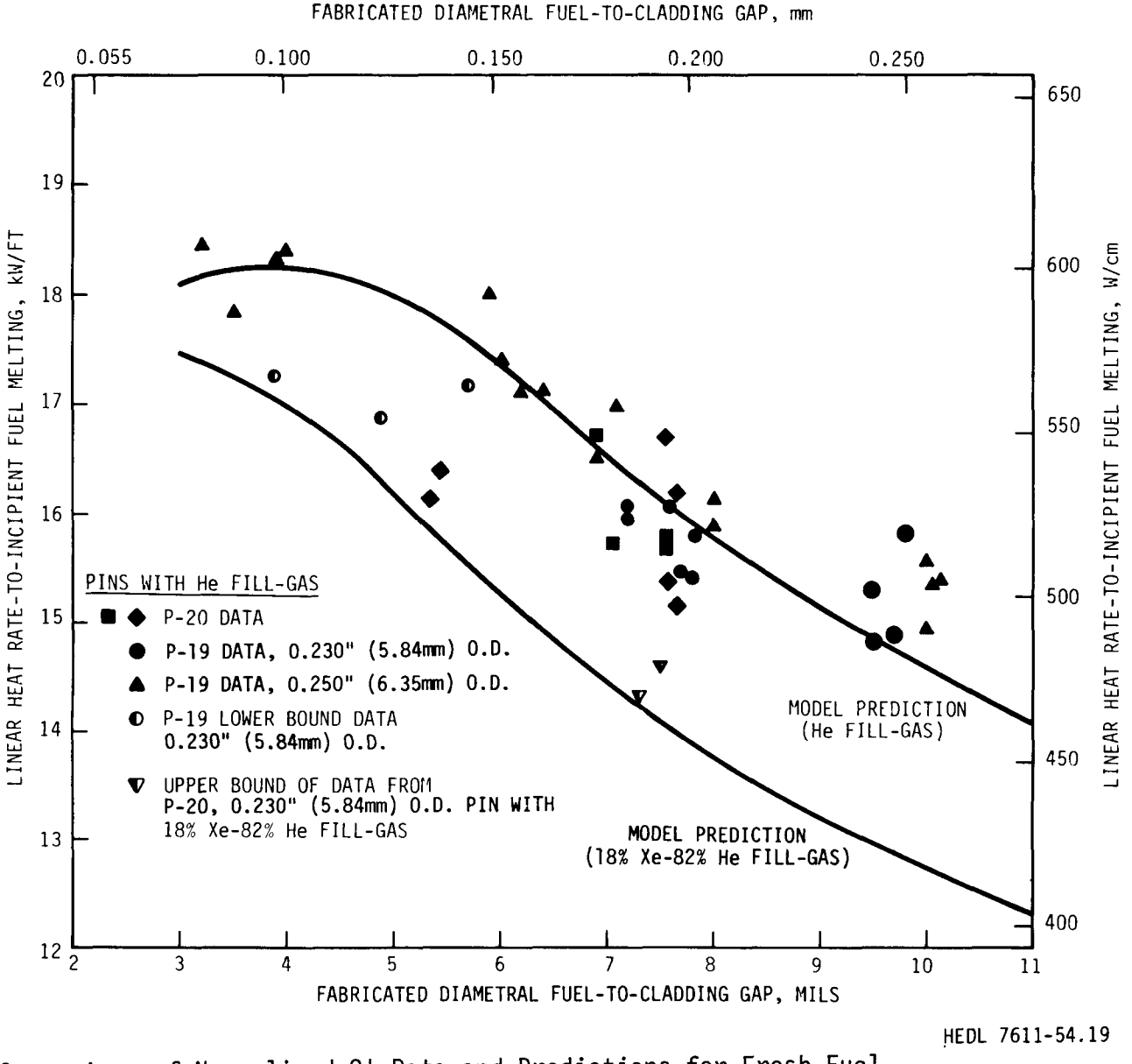

FIGURE 8. Comparison of Normalized Q'_m Data and Predictions for Fresh Fuel.

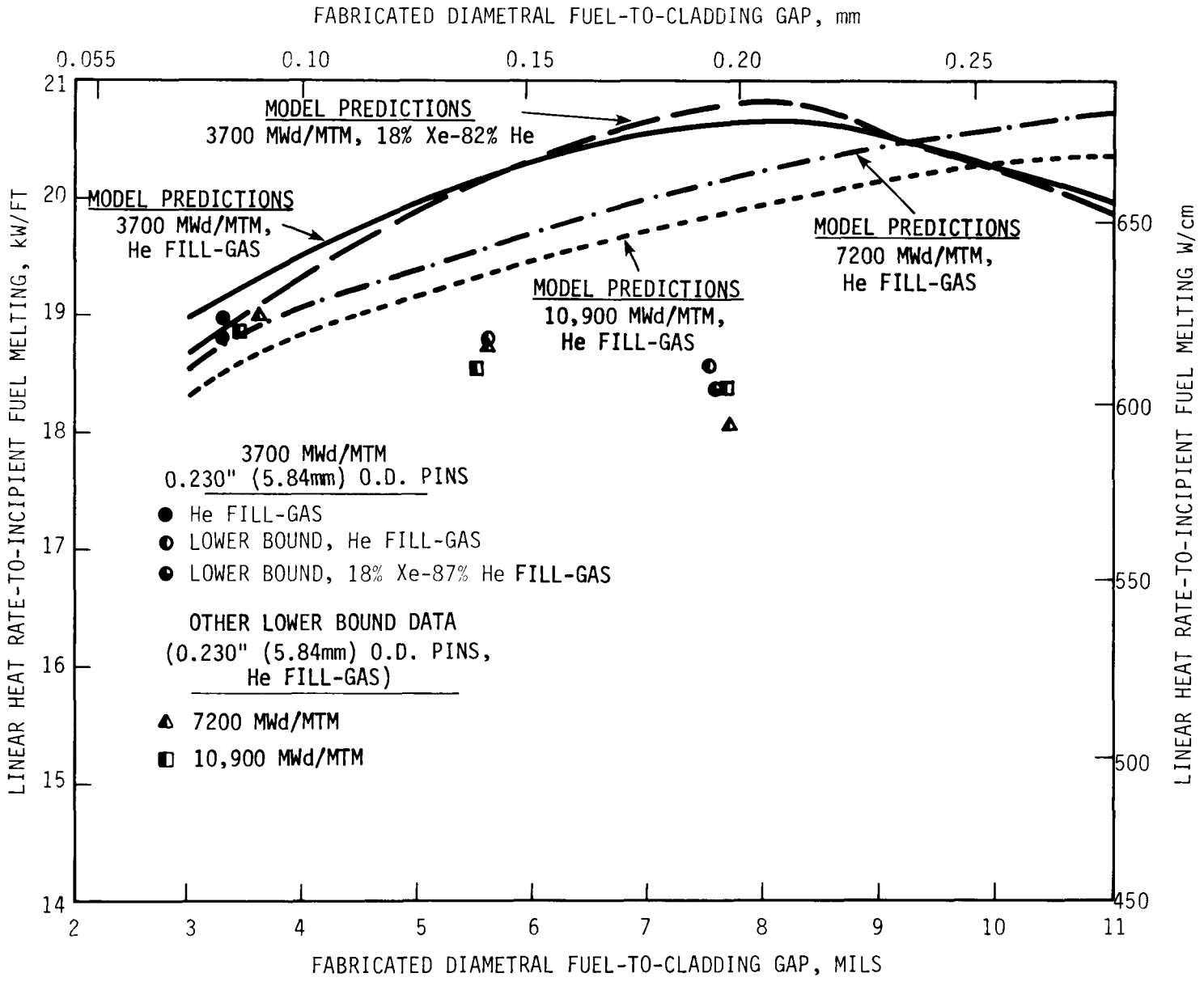

FIGURE 9. Comparison of Normalized Q'_m Data and Predictions for Pre-irradiated Fuel. HEDL 7611-54.24

diametral), was not necessarily reflected by the limited test data. While the disagreement of the predictions with what little data there was at that point was well within the test uncertainties, Q'_m may increase with burnup rather than decreasing as predicted. This could be caused by two burnup dependent phenomena not considered in this analysis: 1) the creep of the contacting roughness asperities (causing greater solid-to-solid heat transfer); and 2) the buildup of solid fission products between the contacting roughness asperities where heat was assumed transferred through the gas alone. The data from these HEDL P-19 and P-20 tests were insufficient to characterize this type behavior. Application of the calibrated gap conductance model to burnups higher than 10,900 MWd/MTM (1.1 at.%) will require further evaluation of these mechanisms to assure temperature drops across the gaps are not over-predicted, resulting in calculated values of Q'_m being too low. The original SIEX[2] code included an expression to account for this behavior. Very little applicable data exist for calibration of such terms.

Table IX gives some examples of the conductance values being summed in the model to give the total gap conductance predicted. The power in these cases was at Q'_m. Figure 10 indicates the predicted change in total gap conductance with fabricated gap at different burnup levels. The residual gap model was the primary influence on the curve shapes. Contact of the fuel and cladding occur at higher burnups as fabricated gap sizes increase.

Prediction of Q'_m, using the calibrated SIEX-M1 code, for a fresh FFTF fuel pin, with an original plenum gas composition of 10% Xe-90% He, is shown in Figure 11. Also shown in Figure 11 are the predicted Q'_m values for this pin after fuel burnups of 3700 MWd/MTM (0.38 at.%) and 10,900 MWd/MTM (1.1 at.%) have been accumulated. The predicted initial improvement in Q'_m with burnup for a pin with an original 0.0075 inch (0.191 mm) gap was about 35%.

Some comparison of the constants derived in this study with out-of-reactor laboratory results is warranted even though the roughness values for the surfaces of the test materials in the present study were not measured.

TABLE IX

CONTRIBUTIONS TO THE TOTAL GAP CONDUCTANCE PREDICTED BY THE CALIBRATED MODEL

Burnup MWd/MTM	Percent Xe In Fill Gas	Fabricated Diametral Fuel-to-Cladding Gap, mil (mm)	Calculated Hot Diametral Fuel-to-Cladding Gap, mil (mm)	H_G		H_S		H_R	
				$\frac{W}{cm^2-°C}$	$\left(\frac{Btu}{ft^2-hr-°F}\right)$	$\frac{W}{cm^2-°C}$	$\left(\frac{Btu}{ft^2-hr-°F}\right)$	$\frac{W}{cm^2-°C}$	$\left(\frac{Btu}{ft^2-hr-°F}\right)$
~ 0.0	0.0	4.0 (0.102)	0.0 (0.0)	1.599	2820	0.516	910	0.0137	24
0.0	0.0	5.5 (0.138)	0.2 (0.0051)	1.367	2410	0.0	0	0.0157	28
0.0	0.0	8.0 (0.203)	2.54 (0.065)	0.666	1170	0.0	0	0.0216	38
~ 0.0	18.0	4.0 (0.102)	0.0 (0.0)	0.903	1590	0.26	460	0.0166	29
0.0	18.0	5.5 (0.138)	0.76 (0.019)	0.661	1160	0.0	0	0.0218	38
0.0	18.0	8.0 (0.203)	3.24 (0.082)	0.372	655	0.0	0	0.0303	53
3700	0.0	4.0 (0.102)	0.0 (0.0)	0.866	1530	0.756	1330	0.0155	27
3700	0.0	5.5 (0.138)	0.0 (0.0)	0.870	1530	0.751	1320	0.0157	28
3700	0.0	8.0 (0.203)	0.0 (0.0)	0.864	1520	0.746	1310	0.0158	28
3700	18.0	4.0 (0.102)	0.0 (0.0)	0.680	1200	0.737	1300	0.0164	29
3700	18.0	5.5 (0.138)	0.0 (0.0)	0.688	1210	0.732	1290	0.0166	29
3700	18.0	8.0 (0.203)	0.0 (0.0)	0.688	1210	0.714	1260	0.0169	30
7200	0.0	4.0 (0.102)	0.0 (0.0)	0.618	1090	0.732	1290	0.0166	29
7200	0.0	5.5 (0.138)	0.0 (0.0)	0.671	1180	0.733	1290	0.0165	29
7200	0.0	8.0 (0.203)	0.0 (0.0)	0.691	1220	0.730	1290	0.0166	29
10900	0.0	4.0 (0.102)	0.0 (0.0)	0.504	890	0.716	1260	0.0173	30
10900	0.0	5.5 (0.138)	0.0 (0.0)	0.546	960	0.717	1260	0.0173	30
10900	0.0	8.0 (0.203)	0.0 (0.0)	0.570	1000	0.715	1260	0.0174	31

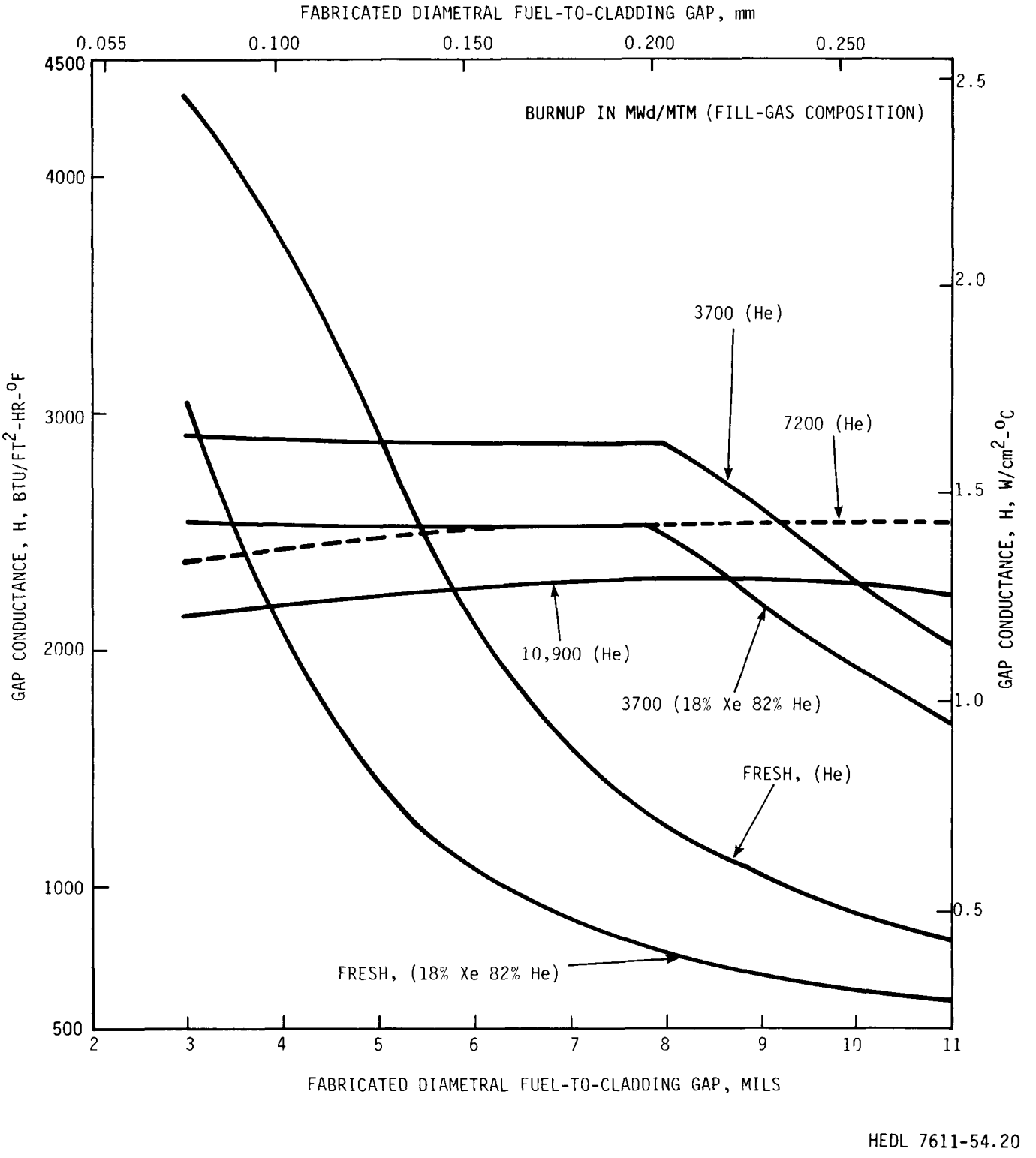

FIGURE 10. Behavior of Calibrated Gap Conductance Model Predictions with Burnup at Q'_m.

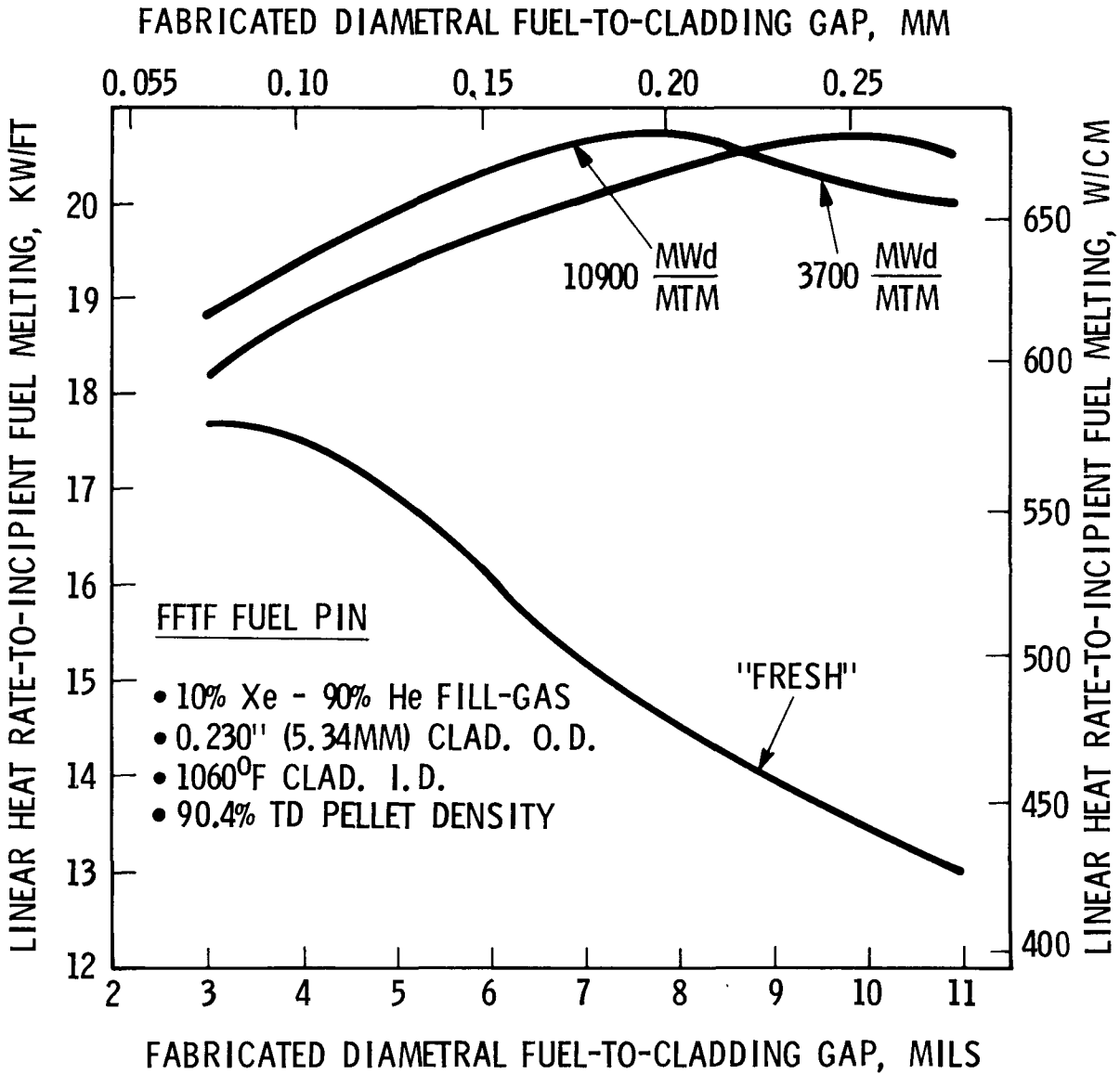

FIGURE 11. SIEX-M1 Predictions for FFTF Fuel Pins

HEDL 7803-268.7

Values from Ross and Stoute's[9] work are compared here to the results of this study using the roughness assumptions from Appendix B and assuming Meyers' hardness of the cladding is equal to one-third the yield strength[5]:

	This Study (PuO_2-UO_2 SS)	Ross and Stoute (UO_2-Zr Pairs)	dynes/cm^2
C_1 (= B[exp(D · P)]) = (Equation 5)	3.2	2.5	P = 9.8 x 10^7
	2.9	1.5	P = 4.9 x 10^8
A_1 = (Equation 4)	1.84	0.5	--

Horn[5] found, apparently fitting data from Ross and Stoute, a value for the constant D of -1.26 x 10^{-9} (P in dynes/cm^2) compared to this study's assumed value of -0.2 x 10^{-9}. As noted previously, selection of the lower values of D was reasonable because of the difference in materials involved. Because of the range of roughness that were possible, this comparison of the constants independent of roughness (i.e., A_1 and C_1) could vary significantly. As noted, all the fuel used in these tests were, however, fabricated with methods typical of those used in commercially-made FBR fuel and thus should be representative and directly applicable to them. (In the near future it is hoped that archive fuel samples from these tests can be characterized for roughness.)

Gap conductance values found in the present analyses of the P-19 and P-20 data compared favorably with the general values derived from the in-reactor tests described by Calza-Bini, et al.[17] Here UO_2-PuO_2 fuel pellets were irradiated in Zircaloy-2 cladding tubes which had inside diameters of 0.5189 inch (1.318 cm). A detailed comparison was not made with these tests. This would have been difficult because not only was a larger fuel size used but also; 1) they were irradiated in a thermal-flux-making fuel behavior, based on power, dependent on the radial flux depression, and 2) only one fuel-to-cladding gap size was included.

The combination of the refined heat transfer models and calibration to all the currently available in-reactor Q'_m data is believed to have resulted in the most realistic gap conductance and temperature prediction system presently available for FBR fuel pins.

VI. CONCLUSIONS

A refined thermal performance modeling system for FBR fuel has been proposed which should be consistent with the present state-of-the-art. A complete set of heat transfer formulations similar to the SIEX[2] code, were described (Appendix A) for temperature calculations from the coolant to the fuel centerline. The corresponding material properties to be used with these were also reviewed and updated as needed. It was concluded that the basic gap conductance model (Equation 2) used in past versions of SIEX was consistent with data and technology available for modeling present FBR fuel. This model was based on the form developed by Ross and Stoute[9].

The SIEX-M1 computer code was developed using this refined modeling system plus residual gap and differential thermal expansion models for the fuel and cladding which were consistent with test data from the P-19 and P-20 experiments. The three constants in the gap conductance model were calibrated using integral power-to-melt, Q'_m, data from these two thermal performance tests from which gap conductances were calculated. Gap conductance values from these data ranged from 1009 to 4025 Btu/ft^2-hr-°F (0.563 to 2.29 W/cm^2-°C) for the diametral fabricated gap range of 0.0098 to 0.0039 inch (0.249 to 0.102 mm). Calculated hot radial gaps for these data ranged from 0.0 to 0.0022 inch (0.0 to 0.056 mm). The resulting constants were:

$$A_2 = 100 \text{ cm}^{-1}$$
$$B = 1.65 \times 10^{-3} \text{ cm}$$
$$D = 0.2 \times 10^{-9} \text{ cm}^2/\text{dyne}$$

The agreement of the calibrated model predictions to the temperature drops found in the data was very good. This predictive heat transfer system, calibrated to <u>in-reactor</u> integral data and based on formulations and material properties consistent with present technology, is believed to be the best available for early-in-life (up to 10,900 MWd/MTM or 1.1 at.% burnup) thermal performance predictions of FBR mixed-oxide fuel.

REFERENCES

1. R. B. Baker, "Integral Heat Rate-to-Incipient Melting of PuO_2-UO_2 Fast Reactor Fuel," HEDL-TME 77-23, to be published.

2. D. S. Dutt and R. B. Baker, "A Correlated Code for the Prediction of Liquid Metal Fast Breeder Reactor (LMFBR) Fuel Thermal Performance," HEDL-TME 74-55, June 1975.

3. B. L. Harbourne and W. H. McCarthy, "Axial Fuel Redistribution by Vapor Transport in LMFBR Fuel Rods", Trans. Amer. Nucl. Soc., Volume 23, page 146, 1976.

4. Richard A. Dean, "Thermal Contact Conductance," Thesis for Masters Degree Program, University of Pittsburgh, 1963.

5. G. R. Horn and F. E. Panisko, "User's Guide for GAPCON: A Computer Program to Predict Fuel-to-Cladding Heat Transfer Coefficients in Oxide Fuel Pins," HEDL-TME 72-128, September 1972.

6. C. M. Cox, F. J. Homan, and R. L. Diamond, "LMFBR Fuel Cycle Progress Report," ORNL-TM-3759, February 1972.

7. V. F. Jankus and R. W. Weeks, "LIFE-II - A Computer Analysis of Fast-Reactor Fuel-Element Behavior as a Function of Reactor Operating History," First International Conference on Structural Mechanics in Reactor Technology, Berlin, Germany, September 20-24, 1971.

8. M. C. Billone, J. Rest, and R. B. Poeppel, "UNCLE - A Computer Code to Predict the Performance of Advanced Fuels in Breeder Reactors," Trans. Amer. Nucl. Soc. 19, p. 96 (1974).

9. A. M. Ross and R. D. Stoute, "Heat Transfer Coefficient Between UO_2 and Zircaloy-2," AECL-1552, June 1962.

10. R. D. Leggett, R. B. Baker, E. O. Ballard, G. R. Horn, and D. S. Dutt, "Linear Heat Rating for Incipient Fuel Melting in UO_2-PuO_2," Trans. Amer. Nucl. Soc., Volume 15, No. 2, p. 752, 1972.

11. R. D. Leggett, R. B. Baker, D. S. Dutt, and S. A. Chastain, "Influence of Burnup on Heat-Rating to Melting for UO_2-PuO_2 Fuel," Trans. Amer. Nucl. Soc., Volume 19, p. 137, October 1974.

12. "Interim Status Report on Thermal Performance of LMFBR Oxide Fuel HEDL P-19," Compiled by R. D. Leggett, HEDL-TME 71-92, June 1971.

13. R. B. Baker, R. D. Leggett, and D. S. Dutt, "Interim Report: Effect of Burnup on Heat-Rating-to-Incipient Fuel Melting HEDL P-20," HEDL-TME 75-63, undated.

14. W. E. Warden, "Process Development to Fabricate 90% Dense Fuel for Irradiation Testing," HEDL-TME 71-149, October 1971.

15. J. E. Hanson, "Experiment Description and Hazards Evaluation for the Pacific Northwest Laboratory Mixed Oxide (UO_2-PuO_2) Irradiation in EBR-II, Task A Subtask I Irradiations", BNWL-650, July 1968.

16. D. S. Dutt, R. B. Baker, J. W. Weber, and S. A. Chastain, "A Correlated Model for Prediction of the Performance of LMFBR Fuel," Trans. Amer. Nuc. Soc., Vol 22., p. 228, November 1975.

17. A. Calza-Bini, G. Cosoli, G. Filacchioni, M. Lanchi, "In-Pile Measurement of Fuel-Cladding Conductance for Pellet and Vipac Zircaloy-2 Sheathed Fuel Pin," Nuc. Tech. Vol. 25, January 1975.

APPENDIX A

CONTENTS

		Page
1.	SODIUM COOLANT TEMPERATURES AT AN AXIAL POSITION	A-3
2.	SODIUM-TO-CLADDING TEMPERATURE DROP	A-4
3.	CLADDING TEMPERATURE DROP	A-5
4.	HEAT TRANSFER ACROSS THE FUEL-TO-CLADDING GAP	A-5
	a. Solid-to-Solid Heat Transfer, H_S	A-7
	b. Heat Transfer Through Gas, H_G	A-15
	c. Thermal Conductance by Radiant Heat Transfer, H_r	A-17
	d. Heat Transfer Due to Convection, H_{Con}	A-18
	e. Total Fuel-to-Cladding Gap Conductance	A-19
5.	HEAT TRANSFER IN THE FUEL	A-19
	a. Fuel Temperature	A-20
	b. Fuel Restructuring	A-23
	REFERENCES	A-26

FIGURES

A-1.	Surface Texture (Vertical Axis Exaggerated).	A-8
A-2.	Surface Roughness Model Definitions.	A-11
A-3.	Fuel and Cladding Heat Transfer Geometry.	A-22
A-4.	Example of Transverse Fuel Ceramography.	A-24

RADIAL HEAT TRANSFER PATH IN THE FUEL PIN

Because of the length of the fuel columns in question (13.5 inches or 34.3 cm) compared to the radii (about 0.1 inch or 0.25 cm) and the fact that the axial power/temperature profiles have no abrupt discontinuities, it was assumed that all heat was transferred from the fuel pins in the radial direction. The exception to this, which was not considered in this study, was at the ends of the fuel column. Here there was axial heat transfer also, but the effects of this were seen only back into the fuel column about a distance of two fuel radii.

The extrapolation of the effect of fuel-to-cladding gap size on Q'_m beyond the actual test conditions, and the calibration of a fuel thermal performance code were very dependent on the heat transfer models and assumptions used. The following summarizes the models used in this study for the radial heat transfer path from the sodium coolant to the fuel center.

1. SODIUM COOLANT TEMPERATURES AT AN AXIAL POSITION

The temperature of the sodium coolant, T_I, at any axial location, x_i, along the pin was based on the reactor inlet temperature, T_{In}, (which was 700°F or 371°C for the test pins) and the integration of the heat deposited in the coolant flow channel from the pin up to the point of interest.

$$T_I = T_{In} + \frac{\int_0^{x_i} Q' dy}{M_F C_p} \qquad \text{(A-1)}$$

where: M_F = Coolant mass flow rate,
C_p = Specific heat of sodium, and
Q' = Linear rate or linear power.

Each HEDL P-19 and P-20 fuel pin had an individual flow tube; thus no coolant mixing needed to be considered. The mass flow rate, M_F, for these pins was calculated from the measured pressure drop across the reactor core at the time of the test and results of flow tests made on each subassembly prior to irradiation. The shape of the axial power profile was derived from measured burnup values taken along several fuel columns.

2. SODIUM-TO-CLADDING TEMPERATURE DROP

The temperature drop due to the fluid boundary layer formed next to the tube wall in flowing sodium was relatively small and could be characterized for thermal conductance purposes by a film coefficient, H_F, from an equation similar to that noted by Bird, et al.[A1] and credited to Martinelle[A2]:

$$H_F = \frac{k_{Na}}{D_e} Nu = \frac{k_{Na}}{D_e} \left[7.0 + 0.025\ (Re\ Pr)^{0.8}\right]$$

where: k_{Na} = Thermal conductivity of sodium,
D_e = Coolant equivalent diameter,
Nu = Nusselt number,
Re = Reynolds number, and
Pr = Prandtle number.

A typical value for an FBR pin is about 25,000 Btu/ft^2-hr-°F (14 W/cm^2-°C).

For a normal LMFBR pin, this temperature drop would be the only one between the coolant and the cladding outside diameter, however, the test pins were encapsulated using an outer stainless steel tube bonded to the fuel pin cladding with stagnant NaK (see Appendices A and C of Reference A3). Thus, additional thermal resistance was present. Using the thermal conductivity of the two capsule materials and the thicknesses of each, an equivalent film coefficient, H_{eq}, applied to the cladding OD, was calculated to simplify

analysis. This coefficient included the effects of the actual film and the capsule materials. Coefficients calculated for the pins with 0.230 inch (5.84 mm) and 0.250 inch (6.35 mm) OD cladding were 4770 Btu/ft^2-hr-°F (2.7 W/cm^2-°C) and 4860 Btu/ft^2-hr-°F (2.8 W/cm^2-°C) respectively. The difference was caused by a narrower NaK region for the larger pins. Thus, the temperature drop between the coolant and pin cladding wall, ΔT_{Fl}, was calculated using H_{eq} and the equation:

$$\Delta T_{Fl} = \frac{Q'_i}{H_{eq} \pi r_{C,OD}}. \qquad \text{(A-2)}$$

where: $r_{C,OD}$ = radius of the cladding OD.

3. CLADDING TEMPERATURE DROP

The thermal conductivity of the 316 SS wall of the cladding tube was taken from standard sources similar to those in Reference A4. A nominal value for cladding conductivity, k_C, was 11.4 Btu/ft-hr-°F (0.1972 W/cm-°C). The temperature drop, ΔT_C, across the cladding wall was simply:

$$\Delta T_C = \frac{Q'_i \left(r_{C,OD} - r_C\right)}{k_C \pi r_C} \qquad \text{(A-3)}$$

where: r_C = radius of the cladding ID.

4. HEAT TRANSFER ACROSS THE FUEL-TO-CLADDING GAP

Calculation of the heat transfer across the fuel-to-cladding gap was based primarily on expressions suggested by Ross and Stoute[A5], past work by Dutt[A6], and results of literature reviews and analyses made by the author. The modified Ross and Stoute models are briefly described in the documentation[A6] of the SIEX computer code. While work in this and related areas had

been progressing for many years, specific applicable data for verifying conclusively theoretical models proposed for the complex heat transfer mechanisms involved was limited. This was true for out-of-reactor values but especially true for information from fast reactors (where data was almost nonexistent).

Heat transfer through the fuel-to-cladding gap was assumed separated into four parallel mechanisms. These were:

1) Conductivity through the gas gap (indicated by subscript G),
2) Conductivity through the solid-to-solid contact (subscript S),
3) Radiant heat transfer (subscript R), and
4) Convective heat transfer (subscript Con). (This was found to be negligible, as noted by other authors.)

In the following sections, thermal conductance values for each of the mechanisms are developed and these summed together for the total gap conductance, H.

(A-4) $$H = H_S + H_G + H_R + H_{Con}$$

This follows directly from the total heat rate being equal to

(A-5) $$q = q_S + q_G + q_R + q_{Con},$$

and the empirical Fourier relation, or Newton's law of cooling, governing heat transfer which state:

(A-6) $$q = kA \frac{T_F - T_C}{X} = HA \left(T_F - T_C\right)$$

where: q = Heat flow rate,
A = Surface area,
$T_F - T_C$ = Temperature across the material,

X = Thickness of the material,

H = Unit thermal conductance or gap conductance, and

k = Thermal conductivity of the material.

Since $A(T_F - T_C)$ was constant for each mechanism, substitution of Equation (A-6) into (A-5) resulted in (A-4).

a. Solid-to-Solid Heat Transfer, H_S

A literature review of solid-to-solid heat transfer mechanisms was made to verify the model proposed by Ross and Stoute, which is presently used in the SIEX code. Consideration was given to models proposed by Dean [A7] Rapier, et al.[A8] Cetinkale and Fishenden,[A9] and Mikic, et al.[A10] In addition, recent survey reviews made by Jacobs and Todreas,[A11] and Lanning and Hann,[A12] comparing current models in use to results of out-of-reactor gap conductance studies made in-vacuum, were considered. Some general observations that could be made from this literature review were:

- As noted by Lanning and Hann,[A12] all models for the mechanism can be reduced to the general form:

$$H_S = Fk_m \left(\frac{P}{h}\right)^N \qquad \text{(A-7)}$$

where:

P = Apparent interface pressure,

h = Meyer's hardness of softer material (which is assumed directly related to yield strength of the material),

F = A function that is dependent on surface roughness and "waviness" (see Figure A-1),

N = Exponent (which may be pressure dependent), and

k_m = Harmonic mean $\left(\frac{2k_1k_2}{k_1 + k_2}\right)$ of the thermal conductivity of the surfaces.

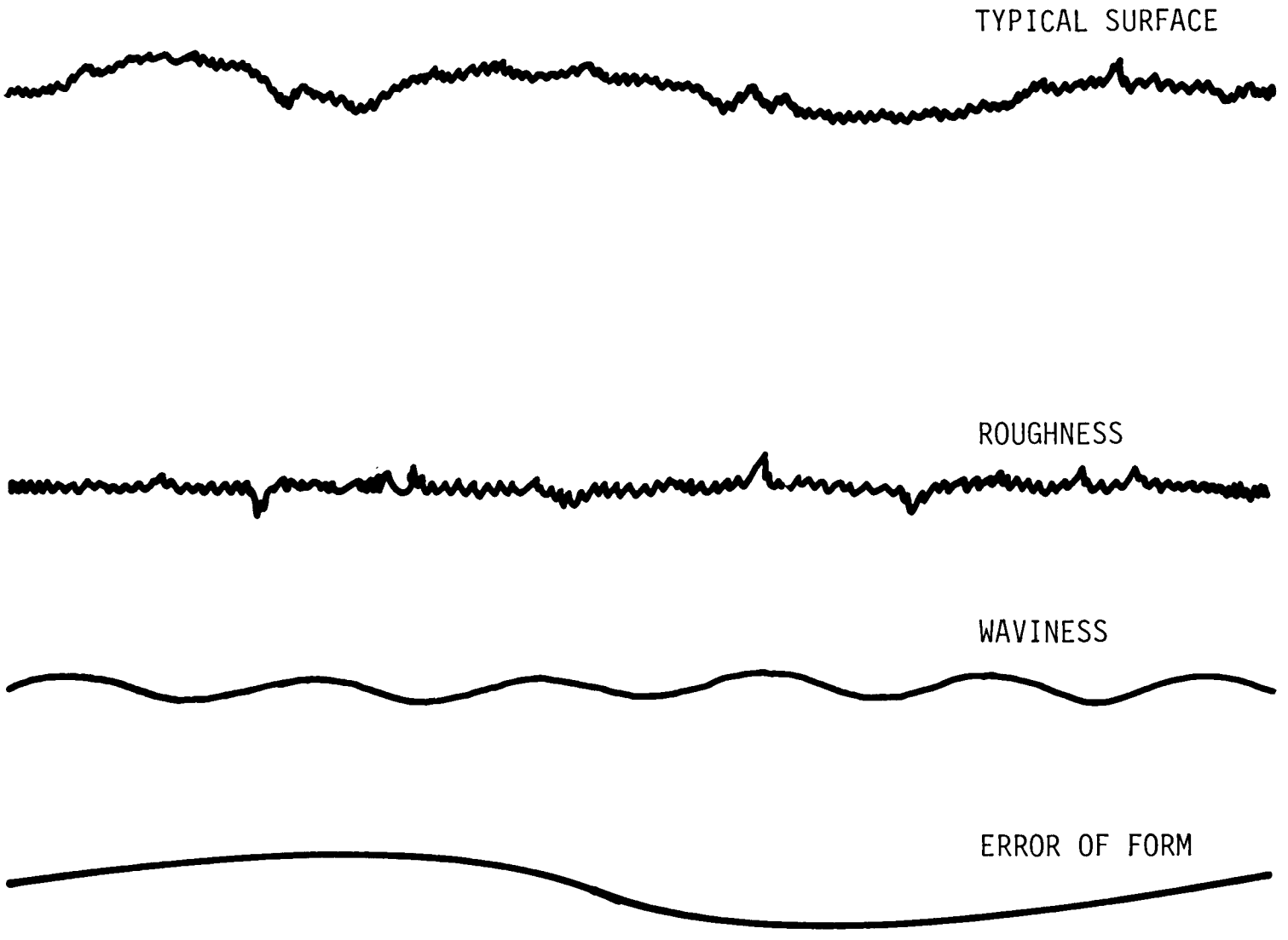

FIGURE A-1. Surface Texture (Vertical Axis Exaggerated).

HEDL 7611-54.4

However, there was considerable difference in the variables that F and N were assumed dependent on.

- While several proposed models could be considered theoretically better than the Ross and Stoute model they also included the need for data which was not readily available for fast reactor fuel pins. Specific examples of these were the need for: 1) a "transition pressure" at which the softer surface changed its behavior at contacting microscopic points from elastic to plastic; and 2) the slope of the roughness asperities. Data needed for several of these models was lacking from what few data studies had been made, thus making confirmation, compared to out-of-reactor results, difficult.

- The data base to check or calibrate to was very limited. Apparently there were only four significant studies which had generated data (References A5, A7, A8 and A13) sufficient for model development, and these were all performed out-of-reactor. All of these studies were run under considerably different test conditions. Only two in-reactor studies were found. One by Campbell and Haies[A14] confirmed, in principle, the existing model's (Ross and Stoute type) validity; however, it was, of necessity, of limited scope. The second, by Calza-Bini et al.,[A28] was also performed in a thermal flux reactor using several types of fuel in Zircaloy cladding in both instrumented and integral type tests. Gap conductances values were derived, and a Ross and Stoute type model was again found to correlate these data well.

It should be noted, similar to what Jacobs and Todreas pointed out, the thermal behavior of the contact surfaces which are very dependent on the behavior of the contacting roughness asperities of "a-spots" may be significantly affected by in-reactor operation where there is power cycling, high temperatures, and a neutron flux. The response of a metal-ceramic fuel interface under these conditions -- because of variation in pressure, solid fission product build-up, and possible creep mechanisms -- is not completely understood at this time. This was true even at the relatively low fuel burnup (less than 10,900 MWd/MTM) levels of data used in this study.

The Ross and Stoute model for solid-to-solid heat transfer was fairly simple compared to several of the models reviewed, and the required data for its evaluation were reasonably available or could be made available, at least for the out-of-reactor tests. A correlated version of this model had been used for the past three years in the SIEX thermal performance code at the Hanford Development Engineering Laboratory, HEDL, with good success in predicting thermal performace and fuel behavior for in-reactor fuel tests.(A3,A15) It was the conclusion of this review that there was no advantage to incorporating a different more complex model into the SIEX code. The model should be changed when a clearly defined advantage is demonstrated for both out-of-reactor and in-reactor predictions. The uncertainties at the time of this study appeared to overshadow the selection of another model as being better for application.

It should be noted that the Mikic model, as proposed by Jacobs and Todreas, appears to be the most promising as a future model. It does a better job of predicting the low pressure (100 psi) out-of-reactor data than the Ross and Stoute model, which under-predicts conductances. This is mainly because the Mikic-Jacobs model uses a "transition pressure" at which point the exponent N is changed from 0.5 to 1. The out-of-reactor value of this transition pressure is postulated to be approaching 1000 psi (6.90×10^7 dynes/cm^2) for metal-ceramic interface. For in-reactor values they note this may be too high; however, there is no data available to confirm this.

The following summarizes the derivation of the model suggested by Ross and Stoute. It is included for completeness and so the assumptions made are apparent. The correlation of the constant A_2 in the final model form will be derived from experimental results described in the text of this report.

Model of Surface Contact

When two surfaces are brought together only a small portion of the apparent geometric area of contact is actually in contact. Microscopic roughness is present on all surfaces (Figure A-1), and the contact surfaces

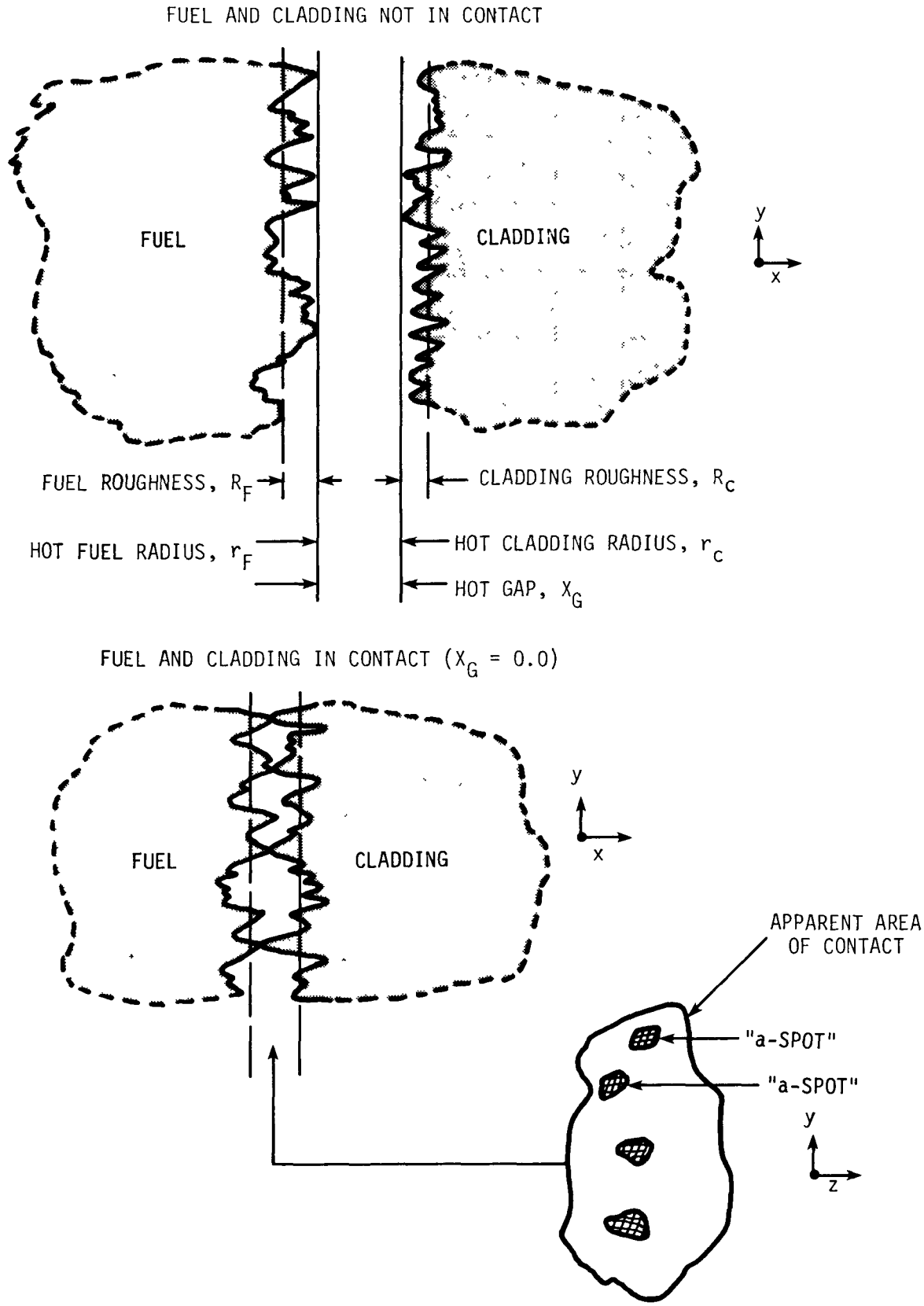

FIGURE A-2. Surface Roughness Model Definitions.

HEDL 7611-54.1

touch only on the points of asperities (Figure A-2). These points of contact are sometimes referred to as a-spots[A16] (in a particular nomenclature, "a" refers to the average size of a contact point or spot, πa^2; to avoid confusion, this definition of "a" is not used in this work), and the thermal resisitance through this area, when a lower thermal conductivity substance occupies the noncontacting areas, is often referred to as "constriction" resistance. Thus, even when the two surfaces are in contact under pressure, two modes of heat transfer are acting: 1) solid-to-solid through the a-spots; and 2) conductance, convection, and radiant heat transfer through the substance, occupying the area between the contacts spots. The solid-to-solid model will be reviewed here. It is assumed the conductance, convection, and radiant heat transfer in the non-contacting regions can be characterized by the models described in later sections.

Area of Real Contact

If two plane surfaces contact under a pressure P, and the a-spots are assumed circular and of equal size, the force balance on the surface is:

(A-8) Force on the apparent interface = Total force on asperitites or

$$P \cdot A = h\alpha^2 n A \pi$$

where: α = Radius of the contact spots, cm,
n = Number of contact spots per unit area,
A = Area of apparent contact between surfaces, cm^2,
h = Meyer's hardness, dynes/cm^2, and
P = Pressure, dynes/cm^2 (apparent).

This follows from the assumption that the radii of curvature of the contact spots are so small that they are plastically deformed by very low loads. Thus, the pressure on each spot will be equal to the Meyer's* hardness of the softer material when all the contact spots are plastically deforming.

*The indentation resistance of a material expressed in force per unit area. In this case, it is equal to $h = L_r/r^2$, where r is the radius of the mouth of an indentation formed by pressing an infinitely hard ball of radius r into the material with a load L_r. This should be proportional to the yield stress.

Holm[A16] experimentally found the mean force on each contact spot only attains values equivalent to between 0.5 and 0.7 x ($h\Pi\alpha^2$). In studies made with cylindrical indentors, Moore[A17] found that the identities of the asperities were retained though complete plastic deformation would be expected. This is consistent with Holm's result and indicates force applied to the surfaces in contact may be transmitted by the contacting asperities to the bulk material between them. Equation (A-8) is then written

$$P = 0.6h\Pi n\alpha^2 \tag{A-9}$$

based on Holm's results. From this, it is seen that the actual contact area at normal pressures is very small because P is much smaller than h.

Constriction

Assuming only conduction through the touching contact spots of the interface, the thermal resistance (R_a) to the steady state heat transfer through a circular area, radius α, into a semi-infinite material with thermal conductivity, k, was determined by Carslaw and Jaeger[A18] to be $R_a = \frac{1}{4k\alpha}$. For two semi-infinite materials in contact in area $\Pi\alpha^2$, the thermal resistances are in series and addition gives:

$$R_a = \frac{1}{4k_F\alpha} + \frac{1}{4k_c\alpha} \tag{A-10}$$

So the thermal conductance through the a-spots per unit area is given approximately (since they are not actually infinite) by:

$$\frac{n}{R_a} = H_S = 4\alpha n \frac{k_F k_C}{k_F + k_C} \tag{A-11}$$

If we let $k_m = \frac{2k_F k_C}{k_F + k_C}$ (the harmonic mean of the conductivities), the approximate thermal conductance for this apparent contact surface is thus:

$$H_S = 2\alpha n k_m \tag{A-12}$$

Heat Transfer Through Solid-to-Solid Contacts

Combining Equations (A-9) and (A-12), we find the solid conductance can be written:

$$(A\text{-}13) \qquad H_S = \left(\frac{2}{0.6}\frac{\alpha P}{h\Pi\alpha^2}\right)(k_m) = 1.06\,\frac{k_m P}{\alpha h}$$

Further, Holm[A9] has found when the a-spots are of unequal size, the resistance should be increased by approximately 10%. Thus,

$$H_S \approx \frac{k_m P}{\alpha h}.$$

The replacement of α by a function dependent on surface roughness is the next step. Ross and Stoute present results from several investigators which indicate that α is essentially constant at moderate to high pressures. Assuming this, measurements of Ascoli and Germagnoli[A19] were used to obtain the empirical equation:

$$\alpha = A_1 \bar{R}^{-1/2}$$

where: $$\bar{R} = \left(\frac{R_1^2 + R_2^2}{2}\right)^{1/2}$$

R_1, R_2 = Arithmetic mean of the roughness heights of respective surfaces, cm, and

A_1 = An empirical constant, $cm^{1/2}$.

Thus, the final expression for constructive heat transfer through the a-spots is:

$$(A\text{-}14) \qquad H_S = \frac{k_m P}{A_1 \bar{R}^{-1/2} h}$$

For work with SIEX, the denominator of Equation (A-14) is further simplified. It is assumed Meyer's hardness, h, of the softer wall material,

in this case the cladding, is linearly proportional to the yield strength, y_c, of the material as noted in the analyses made for FMODEL.[A20] In addition, because no direct measurement of roughness was made for the test data used in this study, constant values of roughness are assumed and $\bar{R}^{(1/2)}$ can then be considered combined with A_1 to form a constant, A_2. The resulting equation is:

$$(A\text{-}15) \qquad H_S = \frac{k_m P}{A_1 \bar{R}^{1/2} h} = \frac{A_2 k_m P}{y_c}$$

The last assumption, of constant A_2 including $\bar{R}^{1/2}$, is the only logical choice at this time. Neither the HEDL P-19 and P-20 test fuels nor present commercially-produced FBR fuel have been characterized for surface roughness. However, almost all the test fuel was fabricated similarly to the commercial FBR fuel, and its response should be typical of that of the commercial fuel pins. The only test fuel not fabricated in this manner were fuel pellets sintered to size and used in four P-19 fuel pins[A21]; the other fuel pellets were centerless-ground to size. Review of the performance of these fuel pins showed no difference between their responses and the rest of the P-19 fuel pins. There remains, however, a slight possibility, as noted in Reference A27, that a difference in surface roughness between the P-19 and P-20 test fuels may be the reason for the lower Q'_m result, when compared to P-19, of the fresh P-20 pin with a 0.0055 inch (0.140 mm) diametral gap. For this and reasons noted later, it is recommended that in the future archive samples of the test pins be characterized for surface roughness and condition.

b. Heat Transfer Through Gas, H_G

The heat transfer through either open gaps or regions between the touching asperities of the a-spots is now considered. The conductivity through a gas gap, assuming perfect energy transfer at the walls and ignoring roughness, would be calculated from Equation (A-6) as:

$$(A\text{-}16) \qquad H_G = \frac{k_G}{X_G}$$

where: k_G = Thermal conductivity of the gas mixture, and
X_G = Distance between the fuel and cladding surfaces, taken from the furthest extreme of one surface mean roughness to the other.

At the small fuel-to-cladding gap distances (less than 0.005 inch or 0.13 mm) of interest here, consideration must be made for the incomplete exchange of energy of the gas molecules at each wall. This is done, as suggested by Kennard,[A20] using a calculated jump distance which equals the temperature drop caused by this effect at a wall, divided by the temperature gradient in the main portion of the gap. This, in effect, is the distance added to X_G in order that an effective gap size produces the correct total temperature drop with gas conductivity k_G. Equation (A-16) then becomes*

$$H_G = \frac{k_G}{X_G + g_F + g_C} \tag{A-17}$$

where: g_F, g_C = the jump distance at each wall of the gap.

Appendix B includes a description of the method used in this study to calculate $g_F + g_C$ based on a detailed review of available data from the literature made by the author.

Finally, consideration must be given to the effect of the surface roughness. When in contact, it is estimated that only about 10% of the apparent interface of contacting surfaces is involved with the a-spot contact. The remainder of the surface is involved with the lower conductivity regions occupied by the plenum gases. When in contact, $X_G = 0$ (see Figure A-2), and the distance, d_{CF}, between the effective surfaces is taken to be:

---

*To be strictly correct, this expression for an open gap should be for two concentric cylinders which results in the equation:

$$H_G = \frac{k_G}{r_C\left(\ln\frac{r_C}{r_F} + \frac{g_F}{r_F} + \frac{g_C}{r_C}\right)} \quad \text{where } r_F < r_C \text{ and } r_C - r_F = X_G.$$

However, the error introduced by using the plate form is extremely small (<0.5%) because $r_C \approx r_F$ and will be ignored to simplify the expression.

(A-18) $$d_{CF} = C_1(R_F + R_C) = Be^{D \cdot P}$$

where: R_F, R_C = The respective roughness of the surfaces,
C_1 = Empirical constant, and
P = The interface pressure.

The constants B and D are fitting parameters that are correlated in the main text of this report based on the experimental data. They are, to some extent, dependent on the waviness (Figure A-2) of the surface roughness. Again roughness has been removed from the expression since it was not measured for the data being analyzed and was assumed constant.

The final expression for conductance through the gas gap is:

(A-19) $$H_G = \frac{k_G}{C_1(R_F + R_C) + X_G + (g_F + g_C)}$$

$$= \frac{k_G}{(Be^{D \cdot P}) + X_G + (g_F + g_C)}$$

c. Thermal Conductance by Radiant Heat Transfer, H_r

The rate of heat exchanged between two surfaces by thermal radiation can be expressed as:

(A-20) $$q_r = A_F F_{F-C}(W_{bF} - W_{bC})$$

where: A_F = Area per unit length of the fuel surface, cm^2,
F_{F-C} = Exchange coefficient between the surfaces,
$W_{bF} = \sigma T_F^4$, $W_{bC} = \sigma T_C^4$ } The Stefan-Boltzmann law for black bodies with radiation into a gas, W/cm^2-s,

$\sigma = 5.67 \times 10^{-12} \frac{W}{cm^2\text{-}s\text{-}(°K)^4}$, Stefan-Boltzmann constant, and

T_F, T_C = Surface temperatures of the fuel and cladding ID, °C.

From a standard development in Chapman[A22] we find our case:

$$F_{F\text{-}C} = \frac{1}{\frac{1}{\varepsilon_F} + \frac{A_F}{A_C}\left(\frac{1}{\varepsilon_C} - 1\right)}$$

where: A_C = Area per unit length of the cladding surface, and

ε_F, ε_C = Emissivity of the fuel and cladding surfaces.

Since the H_r at the surface of the cladding is defined by (see Equation A-6):

$$H_r = \frac{q_r}{A_C(T_F - T_C)}$$

we have

(A-21)
$$H_r = \frac{A_F\,\sigma\left(T_F^4 - T_C^4\right)}{A_C\left[\frac{1}{\varepsilon_F} + \frac{A_F}{A_C}\left(\frac{1}{\varepsilon_C} - 1\right)\right](T_F - T_C)}$$

$$= \frac{r_F\,\sigma\left(T_F^2 + T_C^2\right)(T_F + T_C)}{r_C\left[\frac{1}{\varepsilon_F} + \frac{r_F}{r_C}\left(\frac{1}{\varepsilon_C} - 1\right)\right]},$$

since $A_F = 2r_F\pi(1)$, $A_C = 2r_C\pi(1)$.

d. Heat Transfer Due to Convection, H_{Con}

The effect of heat transport due to free convection in the fuel-to-cladding gap is negligible. This is because of the very small distance involved, less than 0.005 inch (0.13 mm). Dean[A7] notes for air at 500°F

(260°C) between plates that differ in temperature by 100°F (38°C), a distance of 0.4 inch (10.2 mm) is needed for incipient convection. A check of the magnitude of velocities that could be expected in the gap, based on an equation derived in Bird et al.,[A23] also confirms this conclusion (velocities of less than 0.01 in./s (0.25 mm/s) were calculated). Thus,

(A-22) $$H_{Con} = 0.$$

e. Total Fuel-to-Cladding Gap Conductance

Based on the Equations A-4, A-15, A-19, A-21, and A-22, the final equation for thermal conductance across the fuel-to-cladding gap is:

(A-23) $$H = \frac{A_2 k_m P}{y_c} + \frac{k_G}{X_G + (g_F + g_C) + Be^{P \cdot D}}$$

$$+ \frac{r_F \sigma (T_F^2 - T_C^2)(T_F - T_C)}{r_C \left[\frac{1}{\varepsilon_F} + \frac{r}{r_C}\left(\frac{1}{\varepsilon_C} - 1\right)\right]}$$

or

$$= \frac{k_m P}{A_1 \bar{R}^{1/2} h} + \frac{k_G}{C_1(R_F + R_C) + X_G + (g_F + g_C)}$$

$$+ \frac{r_F \sigma (T_F^2 + T_C^2)(T_F + T_C)}{r_C \left[\frac{1}{\varepsilon_F} + \frac{r_F}{r_C}\left(\frac{1}{\varepsilon_C} - 1\right)\right]}$$

5. HEAT TRANSFER IN THE FUEL

Heat transfer in the fuel is characterized using the steady state heat conduction equation to derive temperatures at any radius in the fuel. Thermal conductivity of the fuel material, as will be discussed under material properties, is assumed dependent on temperature and porosity remaining in the fuel material. Any consideration of fuel temperatures must account for the

phenomona of fuel restructuring which changes both the geometry and density of the fuel over a portion of the radius. So, while this is actually a material behavior mechanism, it is discussed in this appendix.

a. Fuel Temperature

The heat transfer in the fuel is based on the method of calculating fuel temperatures described by Merkx and Fox[A24] and was reviewed in the SIEX documentation. To find the temperature T at a radius r in the fuel the steady state heat conduction equation is used:

$$\nabla \cdot (k\nabla T) = -q_v$$

where: $k = k(T,\rho)$ thermal conductivity of the fuel (temperature and density dependent), and

q_v = Volumetric heat generation rate.

In cylindrical coordinates ∇T is:

$$\nabla T = \frac{\partial T}{\partial r}\,\bar{e}_r + \frac{1}{r}\,\frac{\partial T}{\partial \theta}\,\bar{e}_\theta + \frac{\partial T}{\partial Z}\,\bar{e}_Z$$

$$\nabla \cdot (k\nabla T) \quad \frac{1}{r}\,\frac{\partial\left(rk\,\frac{\partial T}{\partial r}\right)}{\partial r} + \frac{1}{r}\,\frac{\partial\left(\frac{k}{r}\,\frac{\partial T}{\partial \theta}\right)}{\partial \theta} + \frac{\partial\left(k\,\frac{\partial T}{\partial Z}\right)}{\partial Z}$$

We assume one dimensional radial heat flow so,

$$\frac{1}{r}\,\frac{\partial\left[rk(T)\,\frac{\partial T}{\partial r}\right]}{\partial r} = -q_v.$$

Rearranging for integration we obtain:

$$d\left[rk(T)\,\frac{dT}{dr}\right] = -rq_v dr. \qquad \text{(A-24)}$$

Let r_o and r_m be defined as in Figure A-3, multiply Equation (A-24) by the arbitrary r, and integrate from r_M to the radius r using the dummy variable β:

$$(A\text{-}25) \qquad rk(T)\frac{\partial T}{\partial r} = -\int_{r_M}^{r} \beta\, q_v(\beta)d\beta$$

Then dividing by r and integrating from r to r_F using new dummy variables ξ and γ we have:

$$\int_{T}^{T_o} k(\gamma)d\gamma = -\int_{r}^{r_F} \frac{1}{\xi}\int_{\xi_M}^{\xi} \beta\, q_v(\beta)d\beta d\xi.$$

For a uniform density fuel in a fast flux, heat generation can be considered uniform across the radius (i.e., negligible self-shielding). Therefore, we assume $q_v(\beta)$ is constant within an annular ring and thus can perform the integration of the last equation and obtain:

$$(A\text{-}26) \qquad \int_{T}^{T_o} k d\gamma = -\frac{q_v}{2}\int_{r}^{r_F} \frac{1}{\xi}\left(\xi^2 - \xi_M^2\right)d\xi$$

$$= -\frac{q_v}{2}\,\frac{r_F^2 - r^2}{2} - r_M^2 \ln\left(r_F/r\right).$$

Introducing variables S_r and S_o to denote the integral of fuel conductivity at the radii r and r_F respectively, the Equation (A-26) can be written:

$$(A\text{-}27) \qquad \left[\int k(\gamma)d\gamma\right]_{T_r} - \left[\int k(\gamma)d\gamma\right]_{T_o} = S_r - S_o = \frac{q_v}{2}\,\frac{r_F^2 - r^2}{2} - r_M \ln\left(\frac{r_F}{r}\right)$$

This equation is used to calculate the fuel temperatures. The right side can be computed as a function of volumetric heat generation rate, q_v, the radius, and surface temperature, T_o (to evaluate S_o). Once this is done, a numerical method can be used to find the corresponding T_r associated with the value S_r found. The SIEX code uses a "table look-up" procedure to accomplish this,

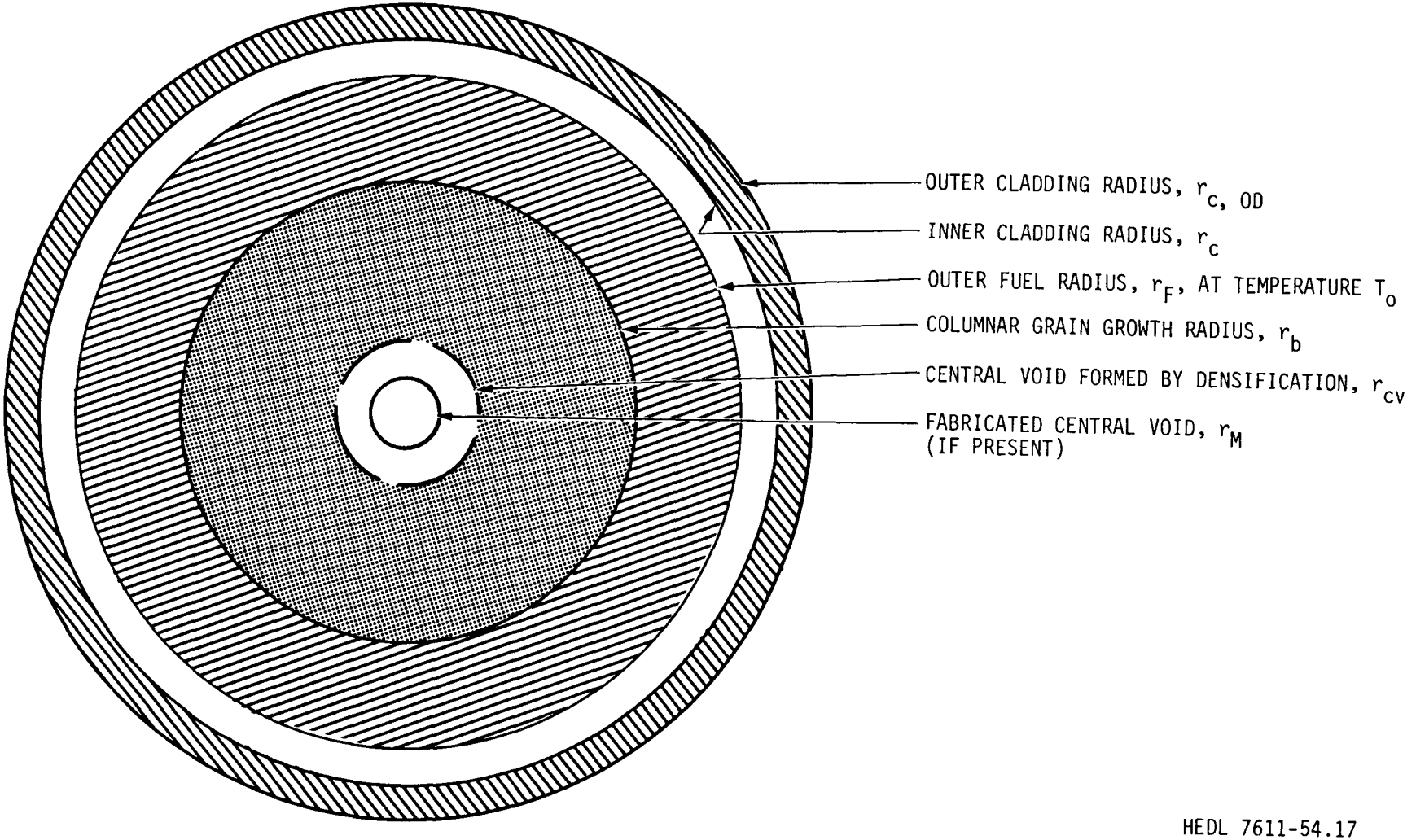

FIGURE A-3. Fuel and Cladding Heat Transfer Geometry.

i.e., a table of $\int k dT$ (or S_r's) are calculated for set, 392°F (200°C), intervals and the code then interpolates the value of T from the value of S_r, calculated by Equation (A-27) at radius r, using the table.

If fuel restructuring occurs (which in effect is a region of higher density fuel with a central void in it), as will be discussed in a following section, Equation (A-27) can be used to determine fuel temperatures in the sintered region by substituting (see Figure A-3):

$S_o \rightarrow S_B = S(T_b)$ where T_b is the temperature above which fuel restructuring occurs, and

$$q_v \rightarrow q_{vb} = q_v \frac{r_b^2 - r_M^2}{\left(r_b^2 - r_c^2\right)}$$ conservation of mass with formation of higher density grain region and central void in the fuel.

$r_F \rightarrow r_b$

$r_M \rightarrow r_{cv}$

Thus, Equation (A-27) is used up to the radius r_b, and then the modified version is used in the restructured zone.

b. Fuel Restructuring

A complete discussion of the heat transfer path in fast reactor fuel would not be complete without mention of fuel restructuring. The primary form, and the only one considered in this study, is the formation of columnar grains. During operation a radial temperature gradient is established across the fuel radius. Above a certain temperature isotherm porosity in the fuel migrates up the temperature gradient primarily in the form of lenticular voids. These sweeping voids form long "columnar" grains of higher density, at least 98% of theoretical density (TD). The voidage is deposited in the center of the fuel (Figure A-4) forming a central void of significant size even at the low fuel burnups considered here. The porosity which is moved is

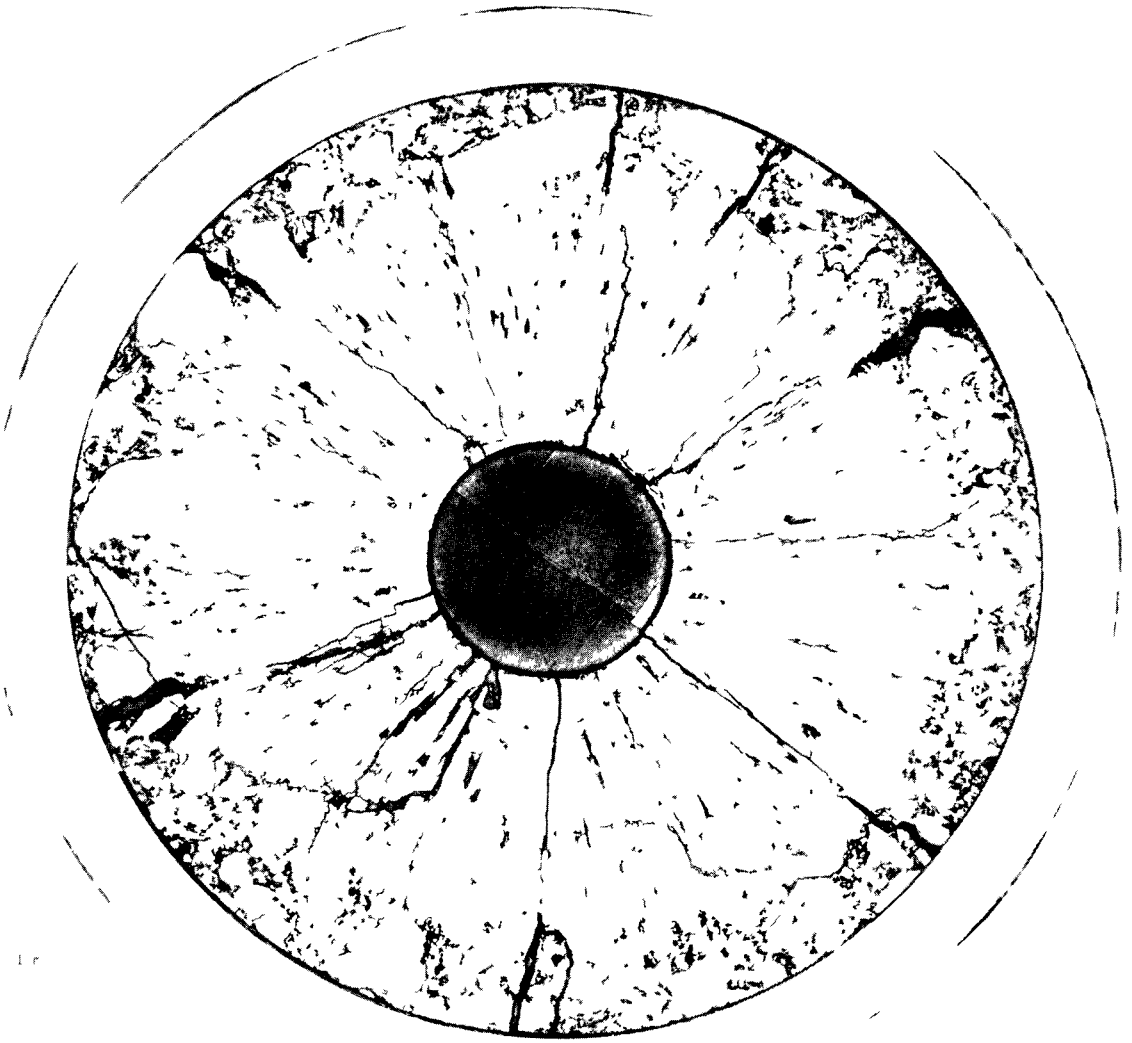

FIGURE A-4. Example of Transverse Fuel Ceramography.

primarily that left in the fuel during fabrication (fuel pellets are generally 90% TD), though generated fission gas can also be moved in this manner. The lenticular voids move by vapor transport mechanisms; for example, see Nichols.[A25]

The effect of columnar grain growth is to lower fuel centerline temperature by:

- Shortening the heat path; assuming a constant mass balance across the radius, the fuel from the area now occupied by the central void is considered moved and spread uniformly into the columnar grain region. Thus, the volumetric heat rate is increased in the columnar grain zone.

- Forming a higher density fuel zone which results in higher fuel thermal conductivity.

The effect on centerline temperature is significant (a typical decrease, for high power fuel originally of solid pellet configuration, would be 600°F or 316°C) especially with respect to Q'_m. The columnar grain typically can extend to 70% of the fuel radius with a central void to 20% of it.

Secondary mechanisms by which additional voidage, in this instance from the fabricated fuel-to-cladding gap, is moved to the central void have also been postulated[A26] by the author and co-scientists. These are needed to account for the majority of observed central void sizes being larger than can be accounted for by a mass balance with the observed columnar grain size. This movement of porosity is caused by the fuel cracking during operation, the ratcheting outward of the cracked pieces, and the cracks being healed in the columnar grain region by the pore migration mechanism. Thus the OD of the fuel pellet is moved closer to the cladding, and a portion of the original fuel-to-cladding gap is moved to the central void, shortening the radius of the maximum heat path and decreasing the gap heat transfer coefficient.

REFERENCES

A1 R. B. Bird, W. E. Stewart, and E. N. Lightfoot, Transport Phenomena, John Wiley and Sons, New York, NY, 1960.

A2 R. C. Martinelli, Trans. ASME 69, pp. 947-959 (1947).

A3 R. B. Baker, R. D. Leggett, and D. S. Dutt, "Interim Report: Effect of Burnup on Heat-Rating-to-Incipient Fuel Melting HEDL P-20," HEDL-TME 75-63.

A4 G. R. Horn and F. E. Panisko, "User's Guide for GAPCON: A Computer Program to Predict Fuel-to-Cladding Heat Transfer Coefficients in Oxide Fuel Pins," HEDL-TME 72-128, September 1972.

A5 A. M. Ross and R. D. Stoute, "Heat Transfer Coefficient Between UO_2 and Zircaloy 2," AECL-1552, June 1962.

A6 D. S. Dutt and R. B. Baker, "A Correlated Code for the Prediction of Liquid Metal Fast Breeder Reactor (LMFBR) Fuel Thermal Performance," HEDL-TME 74-55, June 1975.

A7 Richard A. Dean, "Thermal Contact Conductance," Thesis for Masters Degree Program, University of Pittsburgh, 1963.

A8 A. C. Rapeir, T. M. Jones, and J. E. McIntosh, "The Thermal Conductance of Uranium Dioxide/Stainless Steel Interfaces," Intern. J. Heat Mass Transfer, 6, p. 397, 1963.

A9 T. N. Cetinkale and M. Fishender, "Thermal Conductance of Metal Surfaces in Contact," Proc. of the Gen. Discussion on Heat Transfer, Institution of Mechanical Engineers and ASME, September 1951.

A10 M. G. Cooper, B. B. Mikic, and M. M. Yovanich, "Thermal Contact Conductance," Intern. J. Heat Mass. Transfer, 12, pp. 279-300, 1969.

A11 G. Jacobs and N. Todreas, "Thermal Contact Conductance in Reactor Fuel Elements," Nuclear Sci. and Engineer, 50, pp. 283-306, 1973.

A12 D. D. Lanning and C. R. Hann, "Review of Methods Applicable to the Calculation of Gap Conductance in Zircaloy-Clad UO_2 Fuel Rods," BNWL-1894, April 1975.

A13 S. McLain and J. H. Martens, Eds., Reactor Handbook, Vol. IV, 2nd Edition, p. 210, Interscience Publishers, New York.

A14 F. R. Campbell, R. Des Haies, "The Effect of Gas Pressure on Fuel/Sheath Heat Transfer," Trans. Amer. Nucl. Soc., Vol. 21, p. 380.

A15 D. S. Dutt, R. B. Baker, J. W. Weber and S. A. Chastain, "A Correlated Model for Prediction of the Performance of LMFBR Fuel," Trans. Amer. Nuc. Soc., Vol. 22, p. 228, November 1975.

A16 R. Holm, Electrical Contacts, Stockholm, Almquist and Wakrells, 1946, p. 398.

A17 A. J. W. Moore, "Deformation of Metals in Static and Slidding Contact," Proc. Roy. Soc., A, 195, pp. 231-246, 1948.

A18 H. S. Carslaw and J. C. Jaeger, Conductance of Heat in Solids, Oxford, 2nd Edition, 1959.

A19 Ascoli and E. Germagnoli, "On the Thermal Resistance Between Metal Surfaces in Contact," Energia Nucleare, 3, (2), pp. 113-118, 1956.

A20 E. H. Kennard, Kinetic Theory of Gases, New York, McGraw Hill, 1938.

A21 "Interim Status Report on Thermal Performance of LMFBR Oxide Fuel HEDL P-19," Compiled by R. D. Leggett, HEDL-TME 71-92, June 1971.

A22 A. J. Chapman, Heat Transfer, McMillan Co., New York, NY, pp. 617, 1967.

A23 R. B. Bird, W. E. Stewart, and E. N. Lightfoot, Transport Phenomena, John Wiley and Sons, New York, N.Y., 1960.

A24 K. R. Merkx and G. L. Fox, "SINTER - A Program for Calculating Radial Temperature Distributions in Oxide Fuel Pins Undergoing Sintering," BNWL-1241, 80, January 1970.

A25 F. A. Nichols, "Behavior of Gaseous Fission Products in Oxide Fuel Elements," Bettis Atomic Power Laboratory, Pittsburgh, PA, WAPD-TM-570, 1966.

A26 R. D. Leggett, R. B. Baker, D. S. Dutt and L. A. Pember, "Central Void Size in Irradiated Mixed Oxide Fuel Pins," Trans. Amer. Nucl. Soc., Vol. 17, p. 173, November 1973.

A27 R. B. Baker "Integral Heat Rate-to-Incipient Melting in UO_2-PuO_2 Fast Reactor Fuel," HEDL-TME 77-23, to be published.

A28 A. Calza-Bini, G. Cosoli, G. Filacchiani, M. Lanchi, "In-Pile Measurement of Fuel-Cladding Conductance for Pellet and Vipac Zircaloy-2 Sheathed Fuel Pins," Nuc. Tech. Vol. 25, January 1975.

APPENDIX B

CONTENTS

		Page
1.	JUMP DISTANCE AND ACCOMMODATION COEFFICIENTS FOR FUEL-TO-CLADDING HEAT TRANSFER	B-3
	a. Jump Distance	B-3
	b. Accommodation Coefficient	B-7
	c. Summary of Calculation of Jump Distance	B-10
2.	THERMAL CONDUCTIVITY OF GAS IN THE FUEL-TO-CLADDING GAP	B-11
	a. Thermal Conductivity of Each Gas Component	B-11
	b. Conductivity of Gas Mixture	B-13
3.	CLADDING YIELD STRENGTH	B-18
4.	FUEL AND CLADDING SURFACE ROUGHNESS	B-19
5.	EMISSIVITY OF THE FUEL AND CLADDING	B-20
6.	FUEL AND CLADDING THERMAL EXPANSION	B-20
7.	THERMAL CONDUCTIVITY OF THE PuO_2-UO_2 FUEL	B-21
8.	FUEL MELTING TEMPERATURE	B-26
	REFERENCES	B-27

FIGURES

B-1. Example Showing Temperature Jump Distances at a Gap. B-4

B-2. Comparison of Thermal Conductivity Values Predicted by Equation (B-12) and Measured from Experiment as Taken from Reference B-36 (All Corrected to 95% TD). B-23

B-3. Thermal Conductivity of Mixed-Oxide Fuel. B-24

TABLES

B-1. Comparison of Accommodation Coefficient Values. B-9

B-2. Values of a to be Used in Study. B-10

B-3. Gas Conductivity Coefficients. B-14

B-4. Comparison of Thermal Conductivity of Gas Mixtures. B-17

REVIEW OF SELECTED MATERIALS PROPERTIES

This appendix reviews those material properties that have a direct effect on the heat transfer calculations described in Appendix A. Where detailed review was made, a summary of the rationale used in the choice of the property will be made.

1. JUMP DISTANCE AND ACCOMMODATION COEFFICIENTS FOR FUEL-TO-CLADDING HEAT TRANSFER

In Appendix A, Section 4.b, the need for calculating temperature jump distances at each wall of the fuel-to-cladding gap was discussed briefly. The following summarizes a review made to define the best value of jump distance.

a. Jump Distance

The accommodation coefficient was originally proposed by Knudsen[B1] to account for observations he made of heat transfer across two surfaces in close proximity. He defined the accommodation coefficient "a" as the ratio between two temperature differences:

$$a = \frac{\tau_2 - \tau_0}{\tau_1 - \tau_0}$$

Here τ_0 denotes the temperature of the gas molecule impinging on the surface of a solid body at temperature τ_1; τ_2 then represents the temperature of the gas molecule after striking. Accommodation coefficient "a" then represents the incomplete energy exchange between the molecule and the solid. The temperatures actually stand for the mean energies of the molecules.

Kennard,[B2] in his work, defined a jump distance, g, as suggested by Poisson, by the temperature drop divided by the temperature gradient in the bulk of the gas gap (Figure B-1). Kennard obtained the following relationship between g and a:

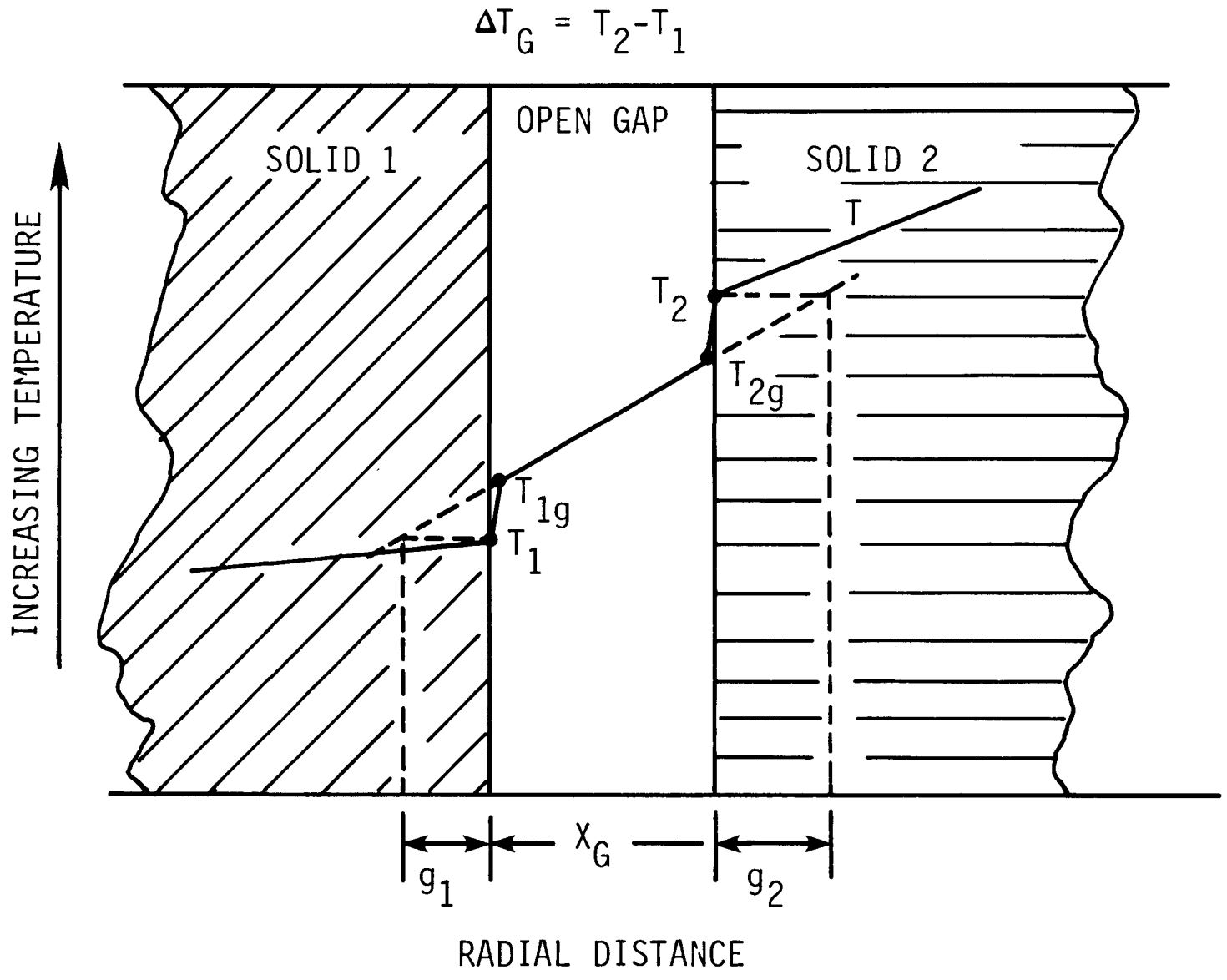

FIGURE B-1. Example Showing Temperature Jump Distances at a Gap.

HEDL 7611-54.16

$$g = \left(\frac{2 - a}{a}\right)\left(\frac{2}{1}\right)\left(\frac{k_G}{\mu C_V}\right)(\Omega)$$

or

$$g = \left(\frac{2 - a}{a}\right)\left(\frac{1}{1 + \gamma}\right)\left(\frac{k_G}{C_V P_G}\right)(2\pi RT)^{1/2}$$

where: C_p = Specific heat at constant pressure of the gas, cal/gm-°C,
C_V = Specific heat at constant volume of the gas, cal/gm-°C,
$\gamma = C_p/C_V$,
k_G = Mean gas conductivity, W/cm-°C,
μ = Absolute viscosity, gm/cm-s,
Ω = Mean free path of the gas molecules, cm,
R = Mean gas constant, cal/gm-°C,
T = Temperature of surface, °C, and
P_G = Pressure of the gas in the gap, dynes/cm^2.

The total jump distance across a gap between the fuel and cladding, assuming that "a" is different at each surface, is:

$$g_1 + g_2 = \left[\frac{2 - a_1}{a_1} k_G \sqrt{T_1} + \frac{2 - a_2}{a_2} k_G \sqrt{T_2}\right]\left[\frac{\sqrt{2\pi R}}{(1 + \gamma)C_V P_G}\right]$$

If we assume that T_1 and T_2 can be replaced by an average temperature, $\bar{T}$, and k_1 and k_2 by an average gas conductivity, $\bar{k}$, calculated at $\bar{T}$, as was assumed in the past for SIEX,[B3] then:

$$g_1 + g_2 = \left[\frac{2 - a_1}{a_1} + \frac{2 - a_2}{a_2}\right]\left[\bar{k}\sqrt{\bar{T}}\right]\left[\frac{\sqrt{2\pi R}}{(1 + \gamma)C_V P_G}\right]$$

or

$$= 2\left[\frac{a_1 + a_2 - a_1 a_2}{a_1 a_2}\right]\left[\frac{\bar{k}\sqrt{T 2\pi R}}{(1 + \gamma)C_V}\right]$$

in terms of the harmonic mean of the accommodation coefficients,

$\bar{a} = \dfrac{2a_1 a_2}{(a_1 + a_2)}$, then:

(B-1) $$g_1 + g_2 = 2\left[\frac{2}{\bar{a}} - 1\right]\left[\frac{\bar{k}\sqrt{2\pi R}}{(1+\gamma)C_V}\right].$$

Equation (B-1) can be evaluated using the following known values:

$(1 + \gamma)\gamma = 2.659$ assuming a monotomic gas*,

$\bar{W} = \sum_{i=1}^{n} f_i W_i$, the average atomic weight of the "n" gases in the fuel-to-cladding gap, gm/mol,

f_i = mole fraction of each gas,

W_i = atomic weight of each gas,

$C_V = \frac{\sum_{j=1}^{n} f_{wj}\tilde{C}_{vj}}{\bar{W}}$, specific heat at a constant volume for the gas mixture in the gap based on Kennard,[B2]

$f_{wj} = \frac{f_j W_j}{\bar{W}}$, weight fraction of each gas, and

$\tilde{C}_{vj} = 2.988$, specific heat at a constant volume for each gas, $\left(\frac{\text{cal}}{\text{mol-°C}}\right)$.

Thus, $$C_V = \frac{2.988 \sum_{i=1}^{n} \frac{f_i W_i}{\bar{W}}}{\bar{W}} = 2.988/\bar{W}.$$

Similarly, $R = 1.99/\bar{W}$.

Thus combining we have:

(B-2) $$\frac{2\sqrt{2\pi R}}{(1+\gamma)C_V} = \frac{2\sqrt{(6.283)\left(\frac{1.99 \text{ cal/mol-°K}}{\bar{W} \text{ gm/mol}}\right)\left(4.186 \times 10^7 \frac{\text{erg}}{\text{cal}}\right)}}{(2.659)\left(\frac{2.988 \text{ cal/mol-°K}}{\bar{W} \text{ gm/mol}}\right)\left(4.186 \times 10^7 \frac{\text{erg}}{\text{cal}}\right)}$$

$$= 1.376 \times 10^{-4} (\bar{W})^{1/2}\left(\frac{\text{gm-°K}}{\text{erg}}\right)^{1/2}$$

*While some nitrogen (N_2) is present, the added complexity of adjusting does not appear warranted considering the accuracy of the other variables.

Recalling 1 erg = 1 cm - dyne = 1 $\frac{gm - cm^2}{s^2}$; assuming $\bar{k}$ is in W/cm-°K, noting that a Watt-second = 10^7 ergs and substituting Equation (B-2) into (B-1) gives:

$$g_1 + g_2 = \left[\frac{2}{\bar{a}} - 1\right]\left[\frac{(\bar{T}\bar{W})^{1/2}}{P}\right]\left[1.376 \times 10^{-4}\right]\left[10^7\right]$$

$$= \left[\frac{2 - \bar{a}}{\bar{a}}\right]\left[\frac{\bar{k}(\bar{T}\bar{W})^{1/2}}{P_G}\right]\left[1376\right], \text{ cm}$$

b. Accommodation Coefficient

Assuming the classical methods and only elastic collisions between gas and metal molecules, Jeans[B46] found:

(B-3) $$a = 1 - \left(\frac{M_G - M_W}{M_G + M_W}\right)^2 = \frac{4M_GM_W}{\left(M_G + M_W\right)^2}$$

where: M_G = Atomic mass of the gas, gm/mol, and
M_W = Molecular mass of the wall, gm/mol.

This, as noted by Jeans, does not give good agreement with the data in the case of small gaps. For this reason, the collision probability with other atoms, particularly oxygen, needed to be considered. Assuming a monotomic gas, the probability of collision of a gas atom with the plutonium (or uranium) and oxygen atoms can be approximated as being proportional to the cross section of each and to the number present. As stated by Giuliani and Mustacchi,[B4] this cross section can be estimated proportional to the 2/3 power of the atomic weight of each atom. This follows from the radius of an atom being proportional to the cube root of the atom's mass and the cross section, in turn, being proportional to the square of the radius.

Thus, Equation (B-3) above for a molecular solid and monotomic gas (assuming the wall molecule is composed of N_1 atoms of atomic mass M_1 plus N_2 atoms of mass M_2, etc.) is:

$$a = C_a \sum_{i=1}^{m} \frac{4M_G M_i}{(M_G + M_i)^2} \frac{N_i M_i^{2/3}}{\sum_{j=1}^{\ell} N_j M_j^{2/3}}$$

where: C_a = Constant of proportionality to be determined, and
M_G = The atomic mass of the gas,

summing limits m = ℓ = the number of types of atoms in the wall molecule. So,

(B-4) $$a = C_a \frac{4M_G}{\sum_{j=1}^{\ell} N_j M_j^{2/3}} \sum_{i=1}^{m} \frac{N_i M_i^{5/3}}{(M_G + M_i)}$$

Giuliani and Mustacchi[B4] performed experiments with Al-UC surfaces and assumed a UO_2 and Al_2O_3 surface existed. They found reasonably good agreement between the shape of the experimental and theoretical curves, "a" versus M_G, (C_a = 1) but observed as much as 30% discrepancy in absolute values. Values were slightly under-predicted up to a gas atomic mass of 6 and constantly over-predicted for the remainder of atomic mass values up to 200. The over-prediction was a fairly constant 30%. Based on this and another study with two Al surfaces, they concluded the equation should be corrected by downward 30% (C_a = 0.7). They also found no detectable temperature dependence between 450 K and 750 K.

Ullman et al.[B5] have measured "a" for Xe and He gas on surfaces of 316 stainless steel and UO_2. They measured a definite temperature dependence for their data between 500 K and 1200 K. These data are not global values but were measured at a particular incidents and reflection angles which were expected to be qualitatively applicable to global energy exchange. As seen in Table B-1, using the middle of their temperature range and comparing it to the results of Equation (B-4) with C_a = 1, He was in agreement but for Xe the difference was on the order of that observed by Giulacani and Mastacchi. No attempt was made to clean the surfaces of the UO_2 or 316 stainless steel used in this work.

TABLE B-I

COMPARISON OF ACCOMMODATION COEFFICIENT VALUES

	Equation 1,[a] (C_a = 1)			Reference B5 (800 K)	
	a_{Fuel}	a_{Clad}	$\bar{a}$	a_{Fuel}	a_{Clad}
He	0.21	0.25	0.23	∿0.21	∿0.20(∿0.20)[b]
Xe	0.79	0.84	0.81	∿0.61	∿0.50(∿0.61)
Kr	0.71	0.96	0.82	--	--
N_2	0.52	0.89	0.65	--	--
Ar	0.57	0.97	0.72	--	--

[a] Assume cladding Fe and fuel UO_2.

[b] Values in "( )" for $\theta_i = 60°$, $\theta_r = 30°$ all other $\theta_i = \theta_r = 45°$.

Godesar, et al.,[B6] in his brief review of the method used in COMETHE-II to calculate jump distance, presented a graph of "a" versus gas atomic weight. While an explanation of the meaning of the material pairs of each curve was not given, they appeared similar to the mean of values calculated by Equation (B-4).

Prior work with SIEX[B3] was based on these values of Godesar, et al.[B6] While the temperature dependence of "a" appeared real, based on Ullman, et al.[B5] and work by Trilling,[B7] it was believed not enough data were available at that time to warrant adding the complexity to the models. Also, as pointed out by Dushman[B8] and Dean,[B9] the condition of the surfaces has a direct effect on "a"; the rougher the surface the higher "a" becomes. Thus it appeared that the values from Equation (B-4) (letting C_a = 1 when M_G is less 6 and C_a = 0.75 for masses greater than 6), should give sufficiently accurate values. This was true especially when the uncertainty of the surface conditions of the fuel and cladding in-reactor were considered. Assuming walls responded similarly to UO_2 and Fe, Table B-II summarizes the values of "a" pertinent to this study.

TABLE B-II

VALUES OF a TO BE USED IN STUDY

	a_{Fuel}	a_{Clad}	$\bar{a}$
He	0.21	0.25	0.23
Xe	0.59	0.63	0.61
Kr	0.53	0.72	0.62
N_2	0.39	0.67	0.49
Ar	0.42	0.73	0.54

Finally, since the gas in the fuel-to-cladding gap was made up of a mixture of at least five gases, the accommodation coefficient of the mixture had to be considered. We assumed the expression used by Mikami et al.[B10] and W-ARD[B4] to be valid:

(B-5) $$a_{mixture} = \frac{\sum_j f_j a_j / (\sqrt{W_j})}{\sum_j f_j / (\sqrt{W_j})}$$

where: a_j = Accommodation coefficient for each gas,
W_j = Atomic weight of each gas, and
f_j = Concentration of this gas.

Sums should be taken over the five gases present.

c. Summary of Calculation of Jump Distance

For the analysis of HEDL P-19 and P-20 then, we proposed:

1) To use the corrected version of Equation (B-4), $C_a = 1$ when $M_G < 6$ and $C_a = 0.75$ when $M_G > 6$, to find the accommodation coefficient, a_{ij}, at each surface of the gap ($i = 1, 2$) and for each component of the plenum gas ($j = 1$-5),

2) To use Equation (B-5) to find the accommodation coefficient, a_i, for the gas mixture at each surface of the gap, and

3) To find the harmonic mean $\bar{a}$ [$\bar{a} = 2a_1a_2/(a_1 + a_2)$] and use this result in Equation (B-1) to find the total jump distance $(g_1 + g_2)$ for the fuel-to-cladding gap (see Table B-II).

2. THERMAL CONDUCTIVITY OF GAS IN THE FUEL-TO-CLADDING GAP

The thermal conductivity of the gas, k_G, present in the fuel-to-cladding gap, was very important to the calculation of heat transfer through this region, as was noted in Appendix A. A significant amount of heat was transferred through the gas even when there was solid-to-solid contact between the fuel and cladding.

a. Thermal Conductivity of Each Gas Component

Two possible methods of representing individual gas values were considered. The first was calculation of values from theoretically-based equations such as the Chapman-Enskog formula recommended by Bird et al.[B11]:

(B-6) $$k = 1.9891 \times 10^{-4} \frac{\sqrt{T/M}}{\sigma_L^2 \Omega_k}$$ monotomic

where: k = Gas thermal conductivity, $\frac{cal}{cm\text{-}s\text{-}K}$,
T = Temperature of gas, K,
M = Molecular weight, gm,
σ_L = Characteristic diameter (different from molecular diameter) from Lennard-Jones potential function, Å,
Ω_k = Collision integral, dependent on the dimensionless temperature K T/ε, and

where: K = Boltzman's constant, and
ε = Characteristic energy in interaction from Lennard-Jones potential function.

For gases which were not monotomic, thermal conductivity could be calculated from[B11]:

(B-7) $$k = (C_p + \frac{5}{4} R)\mu$$

where: C_p = Heat capacity at constant pressure, $\frac{cal}{gm\text{-}K}$,

R = Gas constant, $\frac{cal}{gm\text{-}K}$.

(B-7a) μ = viscosity, $\frac{gm}{cm\text{-}s}$

$$= \frac{2.67 \times 10^{-5}(MT)^{1/2}}{\sigma_L^2 \Omega_k}$$

[While Equation (B-7a) was derived from monotomic gases, it has been found in good agreement for polyatomic gases as well.]

Predictions from these equations have been found to be in good agreement[B11] with measured gas thermal conductivity data. Equations similar to these have been used directly by Horn and Panisko,[B12] Lloyd, et al.,[B13] and Hann and Lanning[B14] in their work in the area of gap conductance.

The second method for handling conductivity is to develop an expression which is simply a mathematical fit of the available measured thermal conductivity data for these gases. This was done in the past in the development of both SIEX[B3] and FMODEL[B15] computer codes. It was this second method which was chosen to be used in the present analysis and calibration effort. This method was consistent with the past formulation of the SIEX code, which will be used exclusively in this work, and it should lead to values of conductivity which are at least as accurate as values produced by the first method, as long as sufficient data is available.

Available references with conductivity data on the five gases in question were reviewed. It was decided to use the results of the "Thermophysical

Properties Research Center Data Book,"[B16] as a primary source. These data have been reviewed in several reports. Reference B17, a National Bureau of Standards report, includes the results from the Data Book for He, Ar, and N_2. Reference B18, a paper presented at Fourth Symposium on Thermophysical Properties, is a "capsule summary" by Liley, of the material presented in the Data Book on the thermal conductivity of 46 gases. The latter data source was used, in part, in the past to derive the gas thermal conductivity expression used in the SIEX code.

The range of temperatures of interest to fuel-to-cladding gap conductance is 0.0 to 2500°C. Data from the above described source was used for He, Ar, and N_2; however, Xe and Kr data from this source was only available to about 450°C (842°F). For this reason, additional sources of data were reviewed and used for Xe and Kr. These included work by Dymond,[B19] Massey,[B20] Saxena,[B21] and Collins and Menard.[B22] These extended the data base for the two gases to at least 2100°C.

A quadratic expression of temperature was mathematically fit to the data. The resulting coefficients found are shown Table B-III.

All data was at atmospheric (14.7 psi or 1.01×10^6 dynes/cm^2) pressure. Gas pressure in fuel pins typically range up to 800 psi (5.52×10^7 dynes/cm^2) at end-of-life (80,000 MWd/MTM). Figure 8.2-2 of Bird et al.,[B11] which represents reduced thermal conductivity as a function of reduced pressure, was used to evaluate the effect of pressure on gas conductivity in the ranges of interest. The conductivity correction for several extremes for individual gases was calculated, and it was concluded that no correction of the correlations for pressure was needed.

b. Conductivity of Gas Mixture

The thermal conductivity of the mixture of five gases was needed to calculate the temperature drop through the open portion fuel-to-cladding

TABLE B-III

GAS CONDUCTIVITY COEFFICIENTS

$$k = \gamma_1 + \gamma_2 T + \gamma_3 T^2$$

$$k \rightarrow \frac{W}{cm\text{-}^\circ C}$$

$$T \rightarrow {}^\circ C$$

Coefficient	Helium (He)	Xenon (Xe)	Kripton (Kr)	Nitrogen (N_2)	Argon (Ar)
γ_1	1.43×10^{-3}	5.15×10^{-5}	9.05×10^{-5}	2.72×10^{-4}	1.83×10^{-4}
γ_2	3.17×10^{-6}	1.69×10^{-7}	2.47×10^{-7}	4.81×10^{-7}	3.58×10^{-7}
γ_3	-2.24×10^{-10}	-3.50×10^{-11}	-4.89×10^{-11}	9.68×10^{-12}	-2.32×10^{-11}

gaps. Data on high temperature mixtures of He-Xe-Kr gases was scarce and apparently did not exist for all five gases combined.

Two forms of equations were considered for calculating the thermal conductivity of gas mixtures from individual gas conductivity values. The first was proposed to Brokaw[B23] as an empirical and simple method for calculating conductivity of gas mixtures:

(B-8) $$k_M = \underline{b}\ k_{SM} + (1 - \underline{b})\ k_{RM}$$

where: $$k_{SM} = \sum_{i=1}^{n} X_i k_i \quad \text{(simple mixing)}$$

$$k_{RM} = \frac{1}{\sum_{i=1}^{n} \frac{X_i}{K_i}} \quad \text{(reciprocal mixing)}$$

K = Thermal conductivity,
X = Mole fraction, and
$\underline{b}$ = Dimensionless factor, and

Subscripts: i = Components of mixture (1 to 5 in this case), and
M = Mixture.

Brokaw presented this equation primarily with binary gas mixture data. From analysis of these data, it was found $\underline{b}$ varied between 0.3 to 0.8, and increased with increasing fraction of the light constituent of the gas mixture (e.g., He). The agreement with the data was found to be good using $\underline{b}$ as a function of the light constituent. It was further stated that Equation (B-8) could be applied to multicomponent mixtures as long as the variation of $\underline{b}$ was known. However, it was noted little data was (and is) available, and as a rough approximation $\underline{b}$ = 0.5. This led to the equation:

(B-9) $$k_M = 0.5\ (k_{SM} + k_{RM})$$

$$k_M = 0.5 \left(\sum_{j=1}^{n} X_j k_j + \frac{1}{\sum_{i=1}^{n} \frac{X_i}{k_i}} \right)$$

This equation was also referenced in Massy's[B20] review, and used in the past in SIEX. The present review, however, showed it appeared to lead to significant errors when the light constituent was not 50 to 70% of the mixture. The comparisons of data to Equation (B-9) predictions cited by Brokaw[B23] for some ternary mixtures fall in this favorable range of percentage of light constituent and show good agreement, but as shown in Table B-IV, using data from Ubisch,[B24] the errors from this form are significant. However, the errors show the same trend noted by Brokaw for binary gas mixtures.

A fit of Brokaw's correction curve for binary mixtures is:

(B-10) $$\underline{b} = 0.45\ X_1^2 + 0.3X_1 + 0.32$$

where: X_1 = Mole fraction of helium.

When this expression was used for $\underline{b}$ with Equation (B-9), the agreement of predicted and measured values, as noted in Table B-IV, greatly improved.

The second equation form for calculating the conductivity of the gas mixture was a theoretically-based one recommended by Bird et al.[B11] for gases at low density, credited to Mason and Saxena:[B25]

(B-11) $$k_M = \sum_{i=1}^{n} \frac{X_i K_i}{\sum_{j=1}^{n} X_j \Phi_{ij}}$$

$$\Phi_{ij} = \frac{1}{\sqrt{8}} \left(1 + \frac{M_i}{M_j}\right)^{-1/2} \left[1 + \left(\frac{\mu_i}{\mu_j}\right)^{1/2} \left(\frac{\mu_j}{\mu_i}\right)^{1/4}\right]^2$$

[Terms are defined in previous Equations (B-6) and (B-7).]

TABLE B-IV

COMPARISON OF THERMAL CONDUCTIVITY OF GAS MIXTURES

Fraction in Gas Mixture				Measured[B24] Conductivity	Calculated Conductivity					
He	Xe	Kr	Ar	W/cm-°C	Eq. B-9 W/cm-°C	% Error	Eqs. B-8, B-10 W/cm-°C	% Error	Eq. B-11 W/cm-°C	% Error
0.2190	0.6950	0.0860	0.0	0.360×10^{-4}	0.470×10^{-4}	30.5	0.379×10^{-4}	5.3	0.381×10^{-4}	5.8
0.8650	0.0290	0.1060	0.0	2.143	1.805	-15.8	2.108	-1.6	2.208	3.0
0.4800	0.4580	0.0820	0.0	0.787	0.888	12.8	0.810	2.9	0.819	4.1
0.8690	0.1210	0.0160	0.0	2.126	1.706	-19.8	2.053	-3.4	2.098	-1.3
0.2450	0.1620	0.5930	0.0	0.477	0.560	17.4	0.466	-2.3	0.498	4.4
0.5190	0.1030	0.3780	0.0	0.942	1.007	-6.9	0.951	0.95	1.015	7.7
0.2480	0.6330	0.1190	0.0	0.409	0.518	26.7	0.420	2.7	0.425	3.9
0.2270	0.3790	0.3940	0.0	0.417	0.509	22.1	0.418	0.2	0.436	4.6
0.2400	0.0	0.7600	0.0	0.507	0.572	12.8	0.482	-4.9	0.522	3.0
0.8800	0.0	0.1200	0.0	2.306	1.911	-17.6	2.211	-4.1	2.317	0.5
0.2020	0.7980	0.0	0.0	0.322	0.437	35.7	0.351	9.0	0.348	8.1
0.4180	0.5820	0.0	0.0	0.624	0.776	24.4	0.677	8.5	0.675	8.2
0.7870	0.2130	0.0	0.0	1.651	1.464	-11.6	1.693	2.2	1.710	3.2
0.4900	0.0	0.5100	0.0	0.942	0.981	4.1	0.912	-3.2	0.991	5.2
0.2900	0.0	0.0	0.7100	0.749	0.807	7.7	0.720	-3.0	0.781	4.3
0.4590	0.0	0.0	0.5410	1.088	1.092	0.4	1.022	-6.1	1.109	1.9
0.8940	0.0	0.0	0.1060	2.470	2.470	-10.4	2.429	-1.7	2.482	0.5

Viscosity, μ, can be calculated from Equation (B-7a). Values for σ_L and ε/K for each pure gas are given in Bird et al.[B11] and Hirschfelder et al.[B26] Also tabulated in these references is Ω_K as a function KT/ε. This table was mathematically fit to the function:

$$\Omega_k = 0.639 + \frac{1.086}{0.135 + \left(K\frac{T}{\varepsilon}\right)^{0.838}} - 0.000482\left(K\frac{T}{\varepsilon}\right)$$

for inclusion in the SIEX prediction code.

Table B-IV shows a comparison of applicable experimental results (at 968°F or 520°C) from Ubisch[B24] for some of the gases of interest to this study. Also shown are the calculated values from Equations (B-8), (B-9) with (B-10), and (B-11), using the data fits, Table B-III, of thermal conductivity previously described for the pure gases. As can be seen, the Brokaw equation with b defined by Equation (B-10) and the theoretically based Equation (B-11) are about comparable in agreement with the experimental data though the theoretical equation consistently tends to over-predict measured values.

For the present analysis, it was decided to use the equation which is theoretical based, Equation (B-11). More confidence could be implied to the theoretically-based equation in extrapolating to the mixtures of the five gases of interest, where there was no actual data to verify the form of b for the Brokaw equation.

3. CLADDING YIELD STRENGTH

The model for solid-to-solid heat conductance in Appendix A, Section 4.A required the use of the yield strength of the softer wall material. This was substituted for Meyer's hardness since the values should be proportional, and yield values were more readily available. A review of the yield strength of the mixed-oxide fuel (about 100 ksi at 1000°F or 6.90×10^6 dynes/cm^2 at 537.8°C) and the 316 20% CW SS cladding (about 70 ksi at 1000°F or 4.83×10^6 dynes/cm^2 at 537.8°C) showed the cladding to be the softer material.

The yield strength data from Reference B27 was used to obtain the following expression for the 316 SS cladding material:

$$y_C = 4.82 \times 10^9 - 1.08 \times 10^7 \, (T - 555°C), \, \frac{\text{dynes}}{\text{cm}^2}$$

4. FUEL AND CLADDING SURFACE ROUGHNESS

Surface roughness of the fuel and cladding was a value used in the basic fuel-to-cladding heat transfer equations found in Appendix A, Sections 4.A and 4.B. Because roughness, as previously noted, was not measured on the experimental fuel or cladding used in the HEDL P-19 and P-20 tests and was not being measured on production fast reactor fuel pins, these were combined into a constant A_2 and B in Equations (3a) and (3b) in the main text [Equations (A-15) and (A-19) of Appendix A]. However, for comparisons, typical values of roughness found by other investigators will be suggested here.

Summarizing all available data for unirradiated studies, work by Jacob and Todreas[B28] showed the following ranges:

Cladding Roughness, R_C, 3 to 465 μinch.
(8×10^{-6} to 118×10^{-5} cm)

Oxide Fuel Roughness, R_F, 8 to 685 μinch.
(20×10^{-6} to 174×10^{-5} cm)

For consistent comparison with past work at HEDL the following typical roughness values were assumed;

$$R_C = 3.30 \times 10^{-4} \text{ cm}$$
$$R_F = 1.78 \times 10^{-4} \text{ cm}$$

so, $\bar{R} = 2.65 \times 10^{-4}$ cm, $(\bar{R}^{1/2} = 0.0163)$.

5. EMISSIVITY OF THE FUEL AND CLADDING

Two sources[B29][B30] were reviewed for fuel emissivity values. These studies were made on UO_2, which should apply directly to the PuO_2-UO_2 fuel of concern here. Emissivity, like the accommodation coefficients, is very dependent on surface conditions which have not been characterized in-reactor where fission products may accumulate. For this reason, and because of an uncertainty that appeared to exist in the temperature dependence, a single value, $\varepsilon_F = 0.80$, was used as the hemispherical total emissivity of the fuel. This value was taken from Belle's[B29] compilation which was for a spectral wave length of 6500 angstroms and a temperature of about 1050°C (1900°F). This value was in the middle of the range of values, 0.7 to 0.9, found by Held and Wilder.[B30]

There was little data available on the oxidized surface of the stainless steel cladding. For the cladding surface we again assume a single value, $\varepsilon_C = 0.9$, for the total hemispherical emissivity based on data in Reference B31.

6. FUEL AND CLADDING THERMAL EXPANSION

The size of the fuel-to-cladding gap during the test was critical to the mode of heat transfer in the gap. The differential thermal expansion of the fuel and cladding was one of two mechanisms considered to close this gap, and thus the assumptions made about the expressions used were very important.

For fuel thermal expansion we used the expression recommended by Bard et al.[B32] which was based on UO_2 data of Conway, Fincel, and Hein.[B33]

$$\alpha_F = 6.8 \times 10^{-6} + (2.9 \times 10^{-9})T, \ (°C)^{-1}.$$

No dependence on the oxygen-to-metal ratio was considered here because of the uncertainty in its effect. Also, no consideration was given to the volumetric increase that was observed (about 10%) when fuel melting occurs.

It was believed any stress caused by the amounts of melting observed in the tests would be relieved by movement of the molten fuel axially in the central void and thus would have no radial effect.

The thermal expansion of the 316 20% CW SS cladding was based on the ASME Boiler and Pressure Vessel Code[B34] and Braun[B33] (temperatures from 302°F to 1202°F or 150°C to 650°C):

$$\alpha_c = 16.55 \times 10^{-6} + (3.68 \times 10^{-9})T, \ (°C)^{-1}.$$

7. THERMAL CONDUCTIVITY OF THE PuO_2-UO_2 FUEL

After review and evaluation of the thermal conductivity data and recommendations on the $0.25PuO_2$-$0.75UO_2$ fuel, it was decided to use an expression proposed by Brancheria et al.[B35]:

$$k_F = D_1\left[\frac{1}{2.88 + 0.0252T_a} + \left(5.83 \times 10^{-13}\right)T_a^3\right] \tag{B-12}$$

where:

$$D_1 = \begin{cases} 21.\rho - 10 - 10\rho^2 = \dfrac{2.1\rho - 1 - \rho^2}{0.1}, \text{ when } 0.85 \leq \rho \leq 0.95 \\ \dfrac{3\rho - 1}{2} = 1.5\rho - 0.5, \text{ when } 0.95 \leq \rho_f \leq 1.0 \end{cases}$$

or

$$= \begin{cases} \dfrac{2 - 3P_f}{2} = 1 - 1.5P_f, \text{ when } 0.05 \leq P_f \leq 0.0 \\ \dfrac{0.1 - 0.1P_f - P_f^2}{0.1} = 1 - P_f - 10P_f^2, \text{ when } 0.15 \leq P_f \leq 0.05 \end{cases}$$

P_f = Fraction porosity,
ρ = Fraction of theoretical density,
T_a = Temperature, K, and
k_F = Thermal conductivity, W/cm-K.

Data on thermal conductivity of PuO_2-UO_2 were very limited at the time of this study. The data were all from unirradiated, unrestructured fuel and only one study included data for temperatures above 1700°C (most fresh fuel in these tests had centerline temperatures above melting, 2760°C). The primary source for the review was the extensive survey made by Washington.[B36] Other sources,[B35,B37,B38] including those used for SIEX in the past, were also considered. Equation (B-12) represents the available data well (see Figure B-2). It has been used in past versions of SIEX and resulted in very reasonable models for fuel restructuring and gap behavior after code calibration.

A brief summary follows of the dependences of thermal conductivity, k_F, of the fuel to help clarify the difficulties involved in characterizing this property. Thermal conductivity of the ceramic fuel is dependent on:

- Temperature
- Porosity
  - Concentration
  - Form
  - Gas composition within
- Oxygen to metal ratio (O/M) in the fuel
- Restraint
- Pu content.

The first two dependencies were primary. Conductivity of unirradiated fuel apparently was also significantly dependent on O/M; however, in-reactor the effect of this dependence was uncertain. The remaining two dependencies were secondary because of lack of effect or lack of data to quantify the effect.

The temperature dependence noted in Figure B-3 for Equation (B-12) agreed well with the available data between 500°C and 1700°C described by Washington.[B36] Nearly all fuel conductivity expressions for PuO_2-UO_2 derived in the literature used the same temperature dependence form used in Equation B-12, which accounted for the upturn observed in the UO_2 data

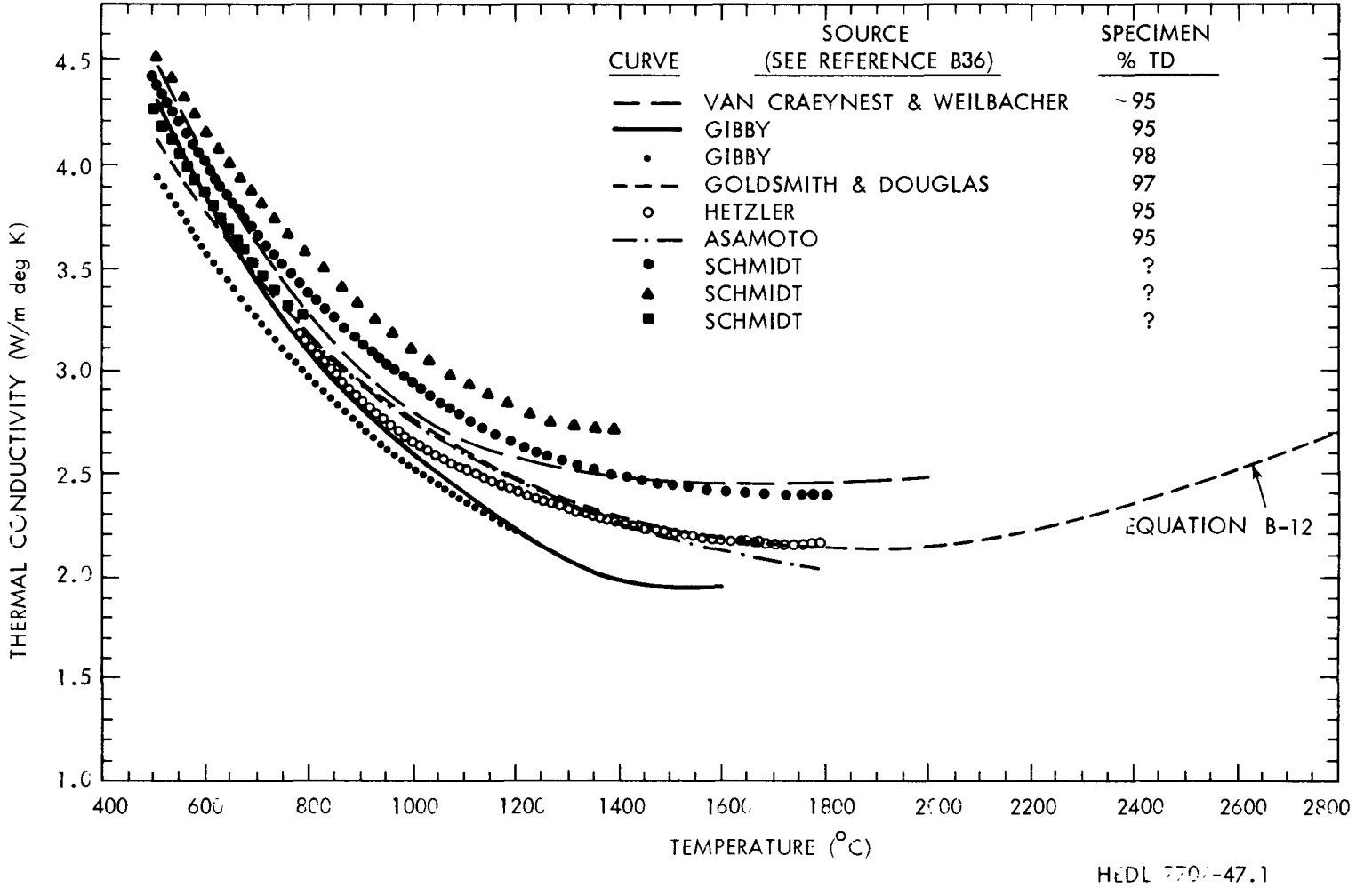

FIGURE B-2. Comparison of Thermal Conductivity Values Predicted by Equation (B-12) and Measured from Experiment as Taken from Reference B36 (All Corrected to 95% TD).

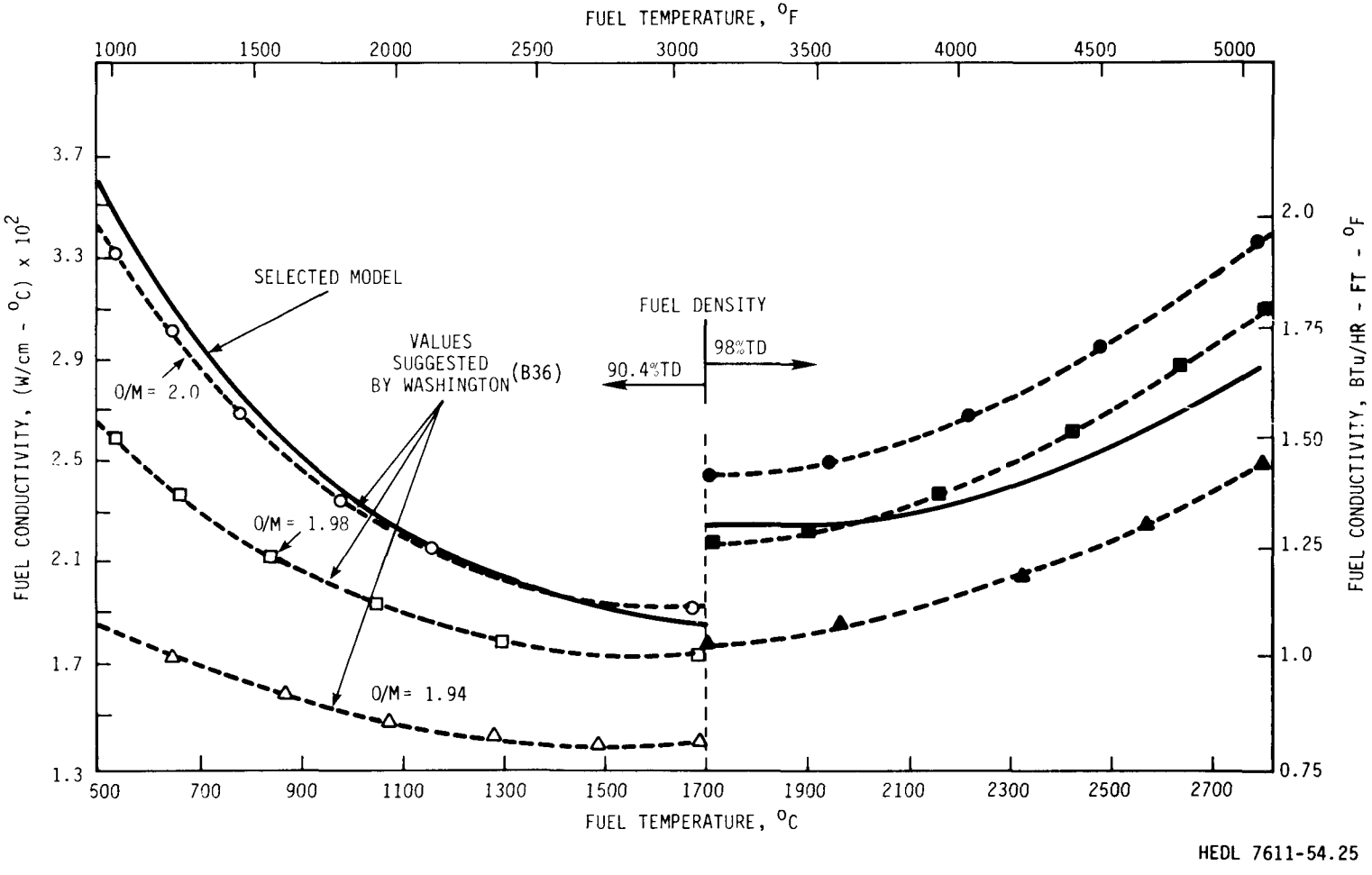

FIGURE B-3. Thermal Conductivity of Mixed-Oxide Fuel.

at high temperatures. Since there was little direct information for PuO_2-UO_2 fuel above 1700°C, there was a large uncertainty in the expressions above this point.

There are a number of different forms of equations being currently used to account for the effects of porosity on thermal conductivity. Equation (B-12) used a reduced Maxwell equation [see "D_1" in Equation (B-12)]. A further assumption[B39] was made in the equation -- that there was a greater effect of porosity when the pore volume was greater than 5% -- implying the pore morphology was not spherical. Below 5% this Equation (B-12) assumed the equivalent to a Eucken relationship for dilute concentrations of spherical pores. This was reasonable because in this study, and in present FBR applications, densities greater than 95% are in columnar grain zones while those less than this are unrestructured fuel. The unrestructured P-19 and P-20 fuel had nonspherical pores (except for one P-20 pin) because a high pressure pre-slugging fabrication method was used.

It should be noted that the thermal conductivity of the columnar grain zone may indeed be higher than that directly calculated from the unrestructured fuel porosity form. This would follow because the region is made up of high density radial stringers with porosity, probably spherical, along the edges. This region bears little resemblence to the unrestructured pore/fuel system.

The effect of O/M ratio in the fuel on fuel conductivity (PuO_2-UO_2) has been found to be significant in out-of-reactor tests (see Figure B-3). However, in-reactor the O/M of the fuel varies across the radius from the fabricated values. The trend is for O/M to increase at the fuel OD and decrease toward the center. Because of the lack of an accepted O/M model and the lack of confirming in-reactor work, the O/M variable will not be considered in this study. It should, however, be noted that Equation (B-12) was derived on the assumption of O/M being equal to 1.98 in the fabricated fuel.

Data from the study described in Appendix J of Reference B40, where fuel conductivity was derived from specimens from one fuel pellet from each fuel

batch used in P-19, were not used in the present study. All the fuel (except for two pins) in P-19 and P-20 was fabricated by a high pressure pre-slugging technique[B41] which resulted in interconnected porosity. The majority of the data used for Equation (B-12) was from fuel fabricated with techniques that result in closed porosity. The results of the study[B40] on P-19 fuel showed there was as much as 30% lower k_F for it compared to the closed porosity fuel. It was decided not to use these data, however, because:

1) It was believed that not enough values were measured to draw a statistically valid conclusion, considering the randomness of the pre-slugged fuel structure.[B41]

2) Studies by the author, using a Hybrid computer version of SINTER,[B42] showed a negative gap conductance was needed for some P-19 data to match the melting observed when using the measured k_F values. This would indicate too low a fuel conductivity.

3) An in-reactor Q'_m study made by Gibby and Lawrence,[B39] for the two types of fuel showing a similar difference (about 30%) in k_F, resulted in a calculated difference of only 3 to 6% in Q'_m. This appeared to be within the uncertainty for normalizing the test data from the two batches of fuel.

Thus, Equation (B-12) was chosen to represent data from the literature and did not include the limited data on the two fuel pellets from P-19.

8. FUEL MELTING TEMPERATURE

Review of the solidus melting temperature for $25\%PuO_2$-$75\%UO_2$ led to choosing the value 2760°C (5000°F). This was based on work by Aitken and Evans[B43,B44] who used the same technique as Lyon and Baily[B45] but with improved pyrometric equipment. No adjustment was assumed for burnup[B44]. Also, though there may be some O/M dependence, it is not clear at this time what it is because of limited data.

REFERENCES

B1 M. Knudsen, The Kinetic Theory of Gases, New York, John Wiley and Sons, Inc., 1946.

B2 E. H. Kennard, Kinetic Theory of Gases, New York, McGraw Hill, 1938.

B3 D. S. Dutt and R. B. Baker, "A Correlated Code for the Prediction of Liquid Metal Fast Breeder Reactor (LMFBR) Fuel Thermal Performance," HEDL-TME 74-55, June 1975.

B4 S. Giuliani and C. Mustacchi, "Heat Transfer in a Fuel Element Gas Gap," European Atomic Energy Community, Joint Nuclear Research Center, Ispra, Italy, 1964, EUR-521-E, UC-80.

B5 A. Ullman, R. Acharya, and D. R. Olander, "Thermal Accommodation Coefficients of Inert Gases on Stainless Steel and UO_2," Journal of Nuclear Materials 51, (1974), pp. 277-279.

B6 R. Godesar et al., "COMETHE-II-A Computer Code for Predicting the Mechanical and Thermal Behavior of a Fuel Pin," Nuclear App. and Techn., Vol. 9, August 1970.

B7 Leon Trilling, "The Interaction of Monotomic Inert Gas Molecules with a Continuous Elastic Solid," Surface Science, 21 (1970), p. 337-365.

B8 S. Dushman, Scientific Foundations of Vacuum Technique, John Wiley and Sons, Inc., New York, 1958.

B9 Richard A. Dean, "Thermal Contact Conductance," Thesis for Masters' Degree Program, University of Pittsburgh, 1963.

B10 H. Mikami, Y. Endo, and Y. Takahima, "Heat Transfer from a Sphere to Rarefied Gas Mixtures," Int. J. Heat Transfer, Vol. 9, pp. 1435-1448, Pargamon Press, 1966.

B11 R. B. Bird, W. E. Stewart, and E. N. Lightfoot, Transport Phenomena, John Wiley and Sons, New York, N.Y., 1960.

B12 G. R. Horn and F. E. Panisko, "User's Guide for GAPCON: A Computer Program to Predict Fuel-to-Cladding Heat Transfer Coefficients in Oxide Fuel Pins," HEDL-TME 72-128, September 1972.

B13 W. R. Lloyd, D. P. Wilkins, and P. R. Hill, "Heat Transfer in Multicomponent Monotomic Gases in Low, Intermediate and High Pressure Regime," IEEE Thermoionic Conversion Specialist Conference, 7th, Framingham, Mass., 1968.

B14 D. D. Lanning and C. R. Hann, "Review of Methods Applicable to the Calculation of Gap Conductance in Zircaloy-Clad UO_2 Fuel Rods," BNWL-1894, April 1975.

B15 C. M. Cox, F. J. Homan, and R. L. Diamond, "LMFBR Fuel Cycle Progress Report," ORNL-TM-3759, February 1972.

B16 Purdue University Thermophysical Properties Research Center Data Book, Vol. 2, Chapter 1, December 1966.

B17 R. W. Powell, C. Y. Ho, and P. E. Liley, Thermal Conductivity of Selected Materials, National Standard Reference Data Series - National Bureau of Standards - 8, (Category 5 - Thermodynamic and Transport Properties), November 25, 1966.

B18 P. E. Liley, "Thermal Conductivity of 46 Gases at Atmospheric Pressure," Proc. Fourth Symposium on Thermophysical Properties, College Park, MD, J. R. Mogyski, Ed., ASME, April 1968.

B19 J. H. Dymond, High Temperature Transport Coefficients for Rare Gases Neon to Xenon, J. Phys. B: Atom. Molec. Phys., Vol. 4, 1971.

B20 G. V. Massey, "The Thermal Properties of Gases for Use in Reactor Heat-Transfer Calculations," United Kingdom Atomic Energy Authority Development and Engineering Group, Downery, Carthness, Scotland, 1960, (DEG Report 14D).

B21 B. K. Saxena and S. C. Saxena, "Thermal Conductivity of Krypton and Xenon in the Temperature Range 350-1500 K," Journal of Chemistry Physics, Vol. 51, No. 8, October 1969.

B22 D. J. Collins and W. A. Menard, "Measurement of the Thermal Conductivity of Noble Gases in the Temperature Range 1500 to 5000 Degrees Kelvin," Journal of Heat Transfer, 88c, pp. 52-5.

B23 R. S. Brokaw, "Estimating Thermal Conductivity for Non-Polar Mixtures: Simple Empirical Method," Ind. Eng. Chem. 47 (11), pp. 2390-2400, 1955.

B24 H. Ubisch, "The Thermal Conductivity of Mixtures of Rare Gases at 29°C and 520°C," Arkiv Fysik, 16, 7, p. 93, 1959.

B25 E. A. Mason and S. C. Saxena, The Physics of Fluids, Vol. 1, pp. 361-369, 1958.

B26 J. O. Hirchfelder, C. F. Curtiss, and R. B. Bird, Molecular Theory of Gases and Liquids, Wiley, New York, 1954.

B27 M. M. Paxton, "Mechanical Properties of Prototype FTR Cladding-20% CW 316 Stainless Steel Tubing," App. A & B, HEDL-TME 71-59, April 1971.

B28 G. Jacobs and N. Todreas, "Thermal Contact Conductance in Reactor Fuel Elements," Nuclear Sci. and Engineer, 50, pp. 283-306, 1973.

B29 J. Belle, "Uranium Dioxide: Properties and Nuclear Applications," Naval Reactors, Division of Reactor Development, USAEC, U.S. Government Printing Office, 1961.

B30 Peter C. Held and D. K. Wilder, "High Temperature Hemispherical Spectral Emittance of Uranium Oxides at 0.65 and 0.70 μm," J. Am. Cer. Soc., 52, pp. 182-186, 1969.

B31 Handbook of Chemistry and Physics, 57th Edition, Chemical Rubber Publishing Company, Cleveland, Ohio, 1976, p. 3041.

B32 F. E. Bard, B. C. Gneiting, and C. M. Cox, "A Thermoelastic Material Properties Correlation for Uranium/Plutonium Mixed Oxides," HEDL-TME 74-12, February 1974.

B33 C. F. Braun, "Piping Design Guide for LMFBR Sodium Piping," SAN-781-1, February 1, 1971.

B34 ASME Boiler and Pressure Vessel Code, Section III, "Nuclear Power Plant Components," 1971 Edition.

B35 A. Biancheria et al., "Oxide Fuel Element Development Quarterly Progress Report," September 30, 1969, WARD-4135-1, Westinghouse Advanced Reactor Division.

B36 A. B. G. Washington, "Preferred Values for the Thermal Conductivity of Sintered Ceramic Fuel for Fast Reactor Use," UKAEA Reactor Group, Risley, TRG-Report-2236, September 1973.

B37 H. Kleykamp, "Variation in the Thermal Conductivity of an Oxide Fuel Element During Burnup," Karlsruhe Nuclear Research Center, Germany, KFK-1245 (EURFNR-816), July 1970.

B38 R. A. Laskiewicz et al., "Thermal Conductivity of Uranium-Plutonium Oxide," GEAP-13733, September 1971.

B39 L. A. Lawrence and R. L. Gibby, "Effects of Pore Structure on the Melting Heat Rating of Oxide Fuels," HEDL-TME 72-81, May 1972.

B40 "Interim Status Report on Thermal Performance of LMFBR Oxide Fuel HEDL P-19," Compiled by R. D. Leggett, HEDL-TME 71-92, June 1971.

B41 R. B. Baker, R. D. Leggett, and D. S. Dutt, "Interim Report: Effect of Burnup on Heat-Rating-to-Incipient Fuel Melting HEDL P-20," HEDL-TME 75-63.

B42 K. R. Kerkx and G. L. Fox, "SINTER - A Program for Calculating Radial Temperature Distributions in Oxide Fuel Pins Undergoing Sintering," BNWL-1241, January 1970.

B43 E. A. Aitken and S. K. Evans, "A Thermodynamic Data Program Involving Plutonium and Urania at High Temperatures," GEAP-5672, October 1968.

B44 J. K. Krankota and C. N. Craig, "The Melting Point of Plutonia-Urania Mixed Oxides Irradiated to High Burnup," GEAP-13515, July 1969.

B45 W. L. Lyon and W. E. Baily, "The Solid-Liquid Phase Diagram for the UO_2-PuO_2 System," GEAP-4878, December 1965.

B46 J. H. Jeans, Kinetic Theory of Gases, Cambridge University Press, 1940.

APPENDIX C

CONTENTS

		Page
1.	RESIDUAL FUEL-TO-CLADDING GAPS	C-5
2.	FUEL THERMAL EXPANSION MODEL	C-7
3.	FUEL ABSORBED GAS RELEASE	C-9
4.	FISSION GAS RELEASE	C-9
5.	FUEL RESTRUCTURING IN THE COLUMNAR GRAIN REGION	C-10
	REFERENCES	C-11

FIGURES

C-1. Data Interaction and Usage for SIEX Correlations. C-4

C-2. Residual Post-Irradiation Fuel-to-Cladding Gap Correlation. C-8

TABLES

C-I. Fitting Coefficients for Residual Fuel-to-Cladding Gap Model. C-7

REVIEW OF FUEL BEHAVIOR RELATED TO GAP CONDUCTANCE

The basic concern of this report is the fuel-to-cladding heat transfer. However, for FBR fuel pins a fully independent heat transfer code must include models for phenomena beyond basic material properties of Appendix B. These include:

- Fuel-to-cladding gap closure due to fuel cracking and swelling,
- The release during irradiation of gases absorbed in the fuel during fabrication (H, N_2, and Ar),
- The release of fission gases (Xe and Kr), and
- The restructuring of the fuel.

It was beyond the scope of this study to develop detailed models necessary for these items because a data base much larger and more varied than that from the two tests of concern here was available for developing these. This has been done in the past at HEDL with the SIEX code.[C1]

For development of the constants concerned with gap conductance, which are calibrated in the text, only one of these models was used -- that for the fuel-to-cladding gap closure. The remaining values needed for gas release and fuel restructuring were input directly based on measured data from the pins. This followed as the second step in the method, Figure C-1, developed previously for calibration of SIEX and allowed the most meaningful model development.

In the following paragraphs some simplified models are suggested, where possible, based on just the data from HEDL P-19 and P-20. Comments will be made on trends and observations relating to what future models should consider based on these two tests.

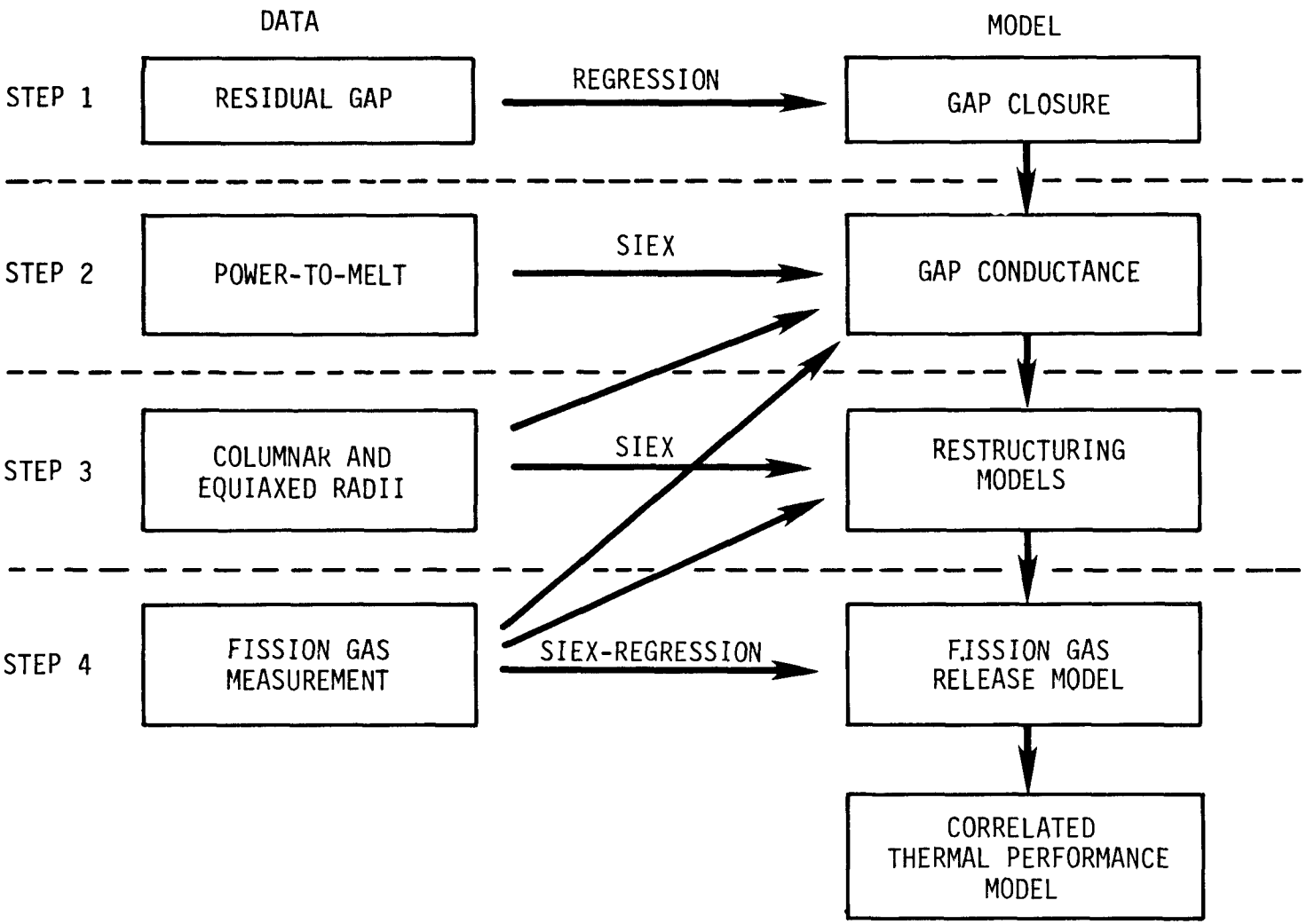

HEDL 7611-54.14

FIGURE C-1. Data Interaction and Usage for SIEX Correlations.

1. RESIDUAL FUEL-TO-CLADDING GAPS

Measurements of all residual fuel-to-cladding gaps (gaps observed at room temperature in transverse ceramography sections from the irradiated pins) were made in manner similar to that used in prior work[C2] (see Tables E-IV and E-V, and Appendix C of Reference C3). For the purpose of calibrating gap conductance constants, it was judged a model based only on HEDL P-19 and P-20 data should be used.

A series of computer plots of the gap closure data and fabrication and operating parameters which could affect fuel-to-cladding gap closure were made. These parameters included:

- Local power,
- Local fuel pellet density,
- Local fuel burnup,
- Local fuel-to-cladding gap size,
- Local radius of melting,
- Cladding ID size, and
- Irradiation history.

It was noted that the actual driving forces for closure of the fuel-to-cladding gap were probably fuel temperature, fuel temperature gradiant, fuel burnup (fission products), and power cycles. A method for direct calculation of fuel temperatures and correlation of this data set of over 120 measurements was not available and would be complex; hence, the development of a simplified model similar to the one used[C2] in the past with the SIEX code. Here parameters related to the actual driving forces were considered (i.e., local pin power instead of fuel temperature).

Using the data plots as a guide, and starting with the general SIEX gap closure equation used in the past, a series of correlations using the REEP[C4] regression analysis computer code were made. Two equations were selected to represent the data: one for pins whose irradiation history included the 15% overpower (P-19 and Phase III of P-20), and the other for pins which operated

only under steady-state conditions (pins described in Appendix C of Reference C3). The final equation form for both was the same -- only the fitting coefficients were changed:

$$(C\text{-}1) \qquad G_p = G\left\{1 - \tau\left[1 - \exp\left(-\Theta_3 \cdot N_c\right)\right] - \left[\Theta_4 - \tau\right]\left[1 - \exp\left(-\Theta_5 \cdot Bu\right)\right]\right\} + Q_2'\Theta_6/G$$

where: $\tau = \Theta_1 \cdot Q_1' \cdot (Q_1' - \Theta_2)$,

Q_1' = Time averaged local linear heat rate, kW/ft (for fresh fuel $Q_1' = Q_2'$),

Q_2' = Maximum local linear heat rate, kW/ft,

Bu = Local burnup, MWd/kgM,

N_c = Number of full power cycles,

G_p = Post-irradiation diametral gap, mil,

G = Fabricated diametral gap, mil, and

Θ's = Fitting coefficients (see Table C-I for 15% overpower values).

Here, τ was an estimate of thermal stress in the fuel. The first negative term in Equation (C-1) represented gap closure due to fuel cracking. The second negative term represented a thermal stress dependent swelling such as would be related to collection of fission gas in the fuel matrix. The final term, inversely dependent on original gap size, partially compensated for plastic strain of the fuel caused by differential thermal expansion of the fuel and cladding.

No consistent dependence could be identified with the variables of pellet density, cladding ID size, and melt extent. Figure C-2 gives an indication of the "goodness of fit" of the model-equation derived for the overpower case. Included in Table C-I is also the standard deviation of this model from the data. Considering the possible random variations in observed gap sizes because of random fuel cracking, this was considered a very good representation of the data.

TABLE C-I

FITTING COEFFICIENTS FOR RESIDUAL FUEL-TO-CLADDING GAP MODEL
(FOR PINS THAT EXPERIENCED OVERPOWER CONDITIONS)

Number of Data Points	Standard Deviation	θ_1	θ_2	θ_3	θ_4	θ_5	θ_6
77	0.66	0.00672	12.5	0.919	0.890	7.11	0.239

2. FUEL THERMAL EXPANSION MODEL

In the past, the thermal expansion (fraction of expansion $\Delta d/d$) of the fuel has been calculated in SIEX on a radial average basis. Thus,

$$\frac{\Delta d}{d} = \frac{\int \Delta d/d \; r \; dr}{\int r \; dr} .$$

Previous calibration efforts with SIEX using this method were never able to correlate both the measured residual fuel-to-cladding gap sizes from the fresh fuel pins and the apparent closure of the hot fuel-to-cladding gap in pins with fabricated diametral gap sizes less than 0.005 inch (0.127 mm). This resulted in the inability to use the measured residual gap data for the fresh fuel pins.

Evidence of the fuel thermally expanding more than can be accounted for by this method for fresh fuel in HEDL P-19 and P-20 resulted in the adoption of a revised model. It was assumed here that the fuel had cracked and could expand radially similar to a solid rod; therefore,

$$\Delta d = \int \Delta d/d \; dr \qquad \text{(C-2)}$$

This resulted in the amount of thermal expansion (Δd) expected based on evidence of when the fuel was coming into contact with the cladding, and allowed the measured residual gap data to be used. It was noted this model

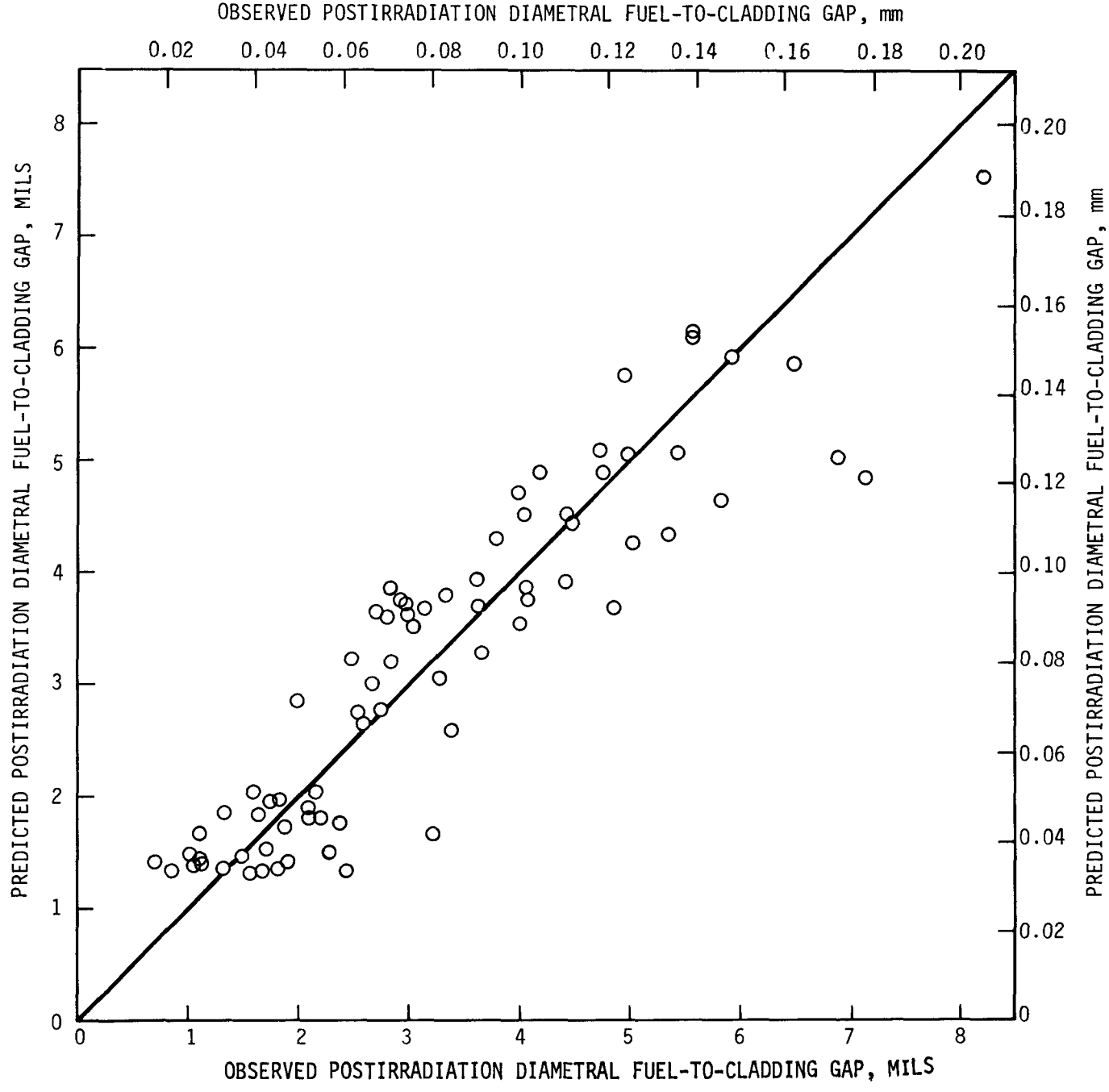

FIGURE C-2. Residual Post-irradiation Fuel-to-Cladding Gap Correlation.

HEDL 7611-54.6

was probably an oversimplification of the complete mechanism (due to crack healing, etc.); however, it appeared reasonable to use until more data became available.

3. FUEL ABSORBED GAS RELEASE

The data from HEDL P-19 and P-20 on measured gas concentrations of N_2 and Ar in the plenum were directly input for calibration of gap conductance. These were typically N_2 = 0.018 and Ar = 0.035 cc at STP for the fresh pins.

For other prediction purposes using SIEX-M1, these low levels of N_2 and Ar gas are suggested except when a gross concentration of either of the two gases are present in the fabricated fuel. There is suspicion that high concentrations of these gases, which have much lower thermal conductivity than He, result in higher fuel temperatures. This would result from either the gas in the fuel matrix or in the fuel-to-cladding gap.

4. FISSION GAS RELEASE

For calibration of the gap conductance model, fission gas release from the fuel was based on the measured gas release found for each pin plenum during destructive examination. The HEDL P-19 data is discussed in Reference C7; the trend of the P-20 data is shown in Reference C3.

In the past, a good fit to general data has been made with fission gas release models[C5] dependent on burnup and the sizes of fuel grain structure regions (i.e., columnar grain, equiaxed grain and unrestructured fuel); however, P-20 results indicated this would be reasonable only up to about 3000 MWd/MTM for fuel operating at high power. Beyond this, the P-20 data showed an obvious switch in trend that was taken to indicate there was a strong temperature dependence (note discussion in Appendix C of Reference C3 on fuel temperatures with burnup). Based on this, it was postulated that the gas release model should be dependent not only on fuel burnup and fuel grain region sizes but also temperature.

5. FUEL RESTRUCTURING IN THE COLUMNAR GRAIN REGION

The columnar grain region size and apparent columnar density (based on a mass balance within the columnar grain region and the central void size) observed to form near the axial extents of melting were used to analyze the data for the gap conductance work. These data are tabulated in Reference C3. A simple columnar grain region model can use a columnar grain isotherm, T_{CG}, (above which the grains form) and a columnar grain density, ρ_{CG}. A value for T_{CG} based on HEDL P-19 and P-20 fresh fuel was:

(C-3) $$T_{CG} = 2190°C.$$

At burnups above those of the fresh fuel (60 to 90 MWd/MTM or about 0.01 at.%) a model is needed that is also dependent on temperature gradient (or local power) and perhaps other parameters.

The apparent columnar grain density was dependent on several mechanisms as noted in Appendix A. Accounting only for densification of material originally present, past work with SIEX has used a constant value of ρ_{CG} of 98% TD. However, some temperature gradient dependence was apparent based on the work with the fresh P-19 and P-20 data -- with the small gap pins having an apparently lower columnar density than the larger gap pins. At higher burnups than the fresh fuel, observed central voids cannot be explained by just the movement of porosity from fabrication to the central void. A model[C6] accounting for other mechanisms must be used and will be developed for SIEX in the future. Based on ceramography of the fuel, the columnar grain region never appeared to densify beyond about 98.5% TD.

For comparing SIEX-M1 predictions to normalized data points after the gap conductance model was calibrated, average restructuring for a fabricated gap size, observed in representative fuel ceramography, was reproduced as nearly as possible by adjusting columnar grain temperatures, T_{CG}, and columnar grain densities. Thus no fuel restructuring modeling uncertainty was imposed on the comparisons.

REFERENCES

C1 D. S. Dutt and R. B. Baker, "A Correlated Code for the Prediction of Liquid Metal Fast Breeder Reactor (LMFBR) Fuel Thermal Performance," HEDL-TME 74-55, June 1975.

C2 D. S. Dutt, R. B. Baker, and S. A. Chastain, "Modeling of Postirradiation Fuel-Cladding Gap in Mixed Oxide Fuels," HEDL-TME 74-19, April 1974.

C3 R. B. Baker, "Integral Heat Rate-to-Incipient Melting of PuO_2-UO_2 Fast Reactor Fuel," HEDL-TME 77-23, to be published.

C4 David F. Shanno, "REEP-Nonlinear Estimation Package," IBM Share Program Library, January 27, 1967.

C5 D. S. Dutt, D. C. Bullington, R. B. Baker, and L. A. Pember, "A Correlated Fission Gas Release Model for Fast Reactor Fuels," Trans. Amer. Nucl. Soc., Vol. 15, No. 1, June 1972.

C6 R. D. Leggett, R. B. Baker, D. S. Dutt, and L. A. Pember, "Central Void Size in Irradiated Mixed-Oxide Fuel Pins," Trans. Amer. Nucl. Soc., Vol. 17, page 173, November 1973.

C7 "Interim Status Report on Thermal Performance of LMFBR Oxide Fuel, HEDL P-19," Compiled by R. D. Leggett, HEDL-TME 71-92, June 1971.

APPENDIX D

NOMENCLATURE

Symbol	Description	Unit
A	Average surface area at fuel-to-cladding gap.	cm^2
A_C, A_F	Surface area of cladding and fuel, respectively, at the fuel-to-cladding gap.	cm^2
A_1	Empirical constant relating α to surface roughness (H_S model).	$cm^{1/2}$
A_2	Empirical constant equal to $(A_1\bar{R}^{1/2})^{-1}$.	cm^{-1}
a	Accommodation coefficient.	--
a_{ij}	Accommodation coefficient for each surface (i = 1, 2) for each component (j = 1, 2, 3, 4, 5) making up the gas in the fuel-to-cladding gap.	--
$\bar{a}$	Harmonic mean of accommodation coefficients at each surface $(\bar{a} = \frac{2a_1a_2}{a_1 + a_2})$.	--
B	Fitting parameter relating roughness to d_{CF} $[d_{CF} = Be^{DP} = C_1(R_C + R_F)]$.	cm
Bu	Local fuel burnup (residual gap model).	MWd/kgM
b	Dimensionless constant in the Brokaw gas mixture equation.	--
C_1	Empirical constant relating surface roughness to d_{CF}.	--
C_a	Constant of proportionality in accommodation coefficient model.	--
C_p, C_v	Specific heat, at a constant pressure and volume, respectively, of the gas in the gap.	Cal/gm-K
C_p, N_a	Specific heat of sodium at a constant pressure.	Cal/gm-K
$\tilde{C}_{vj}$	Specific heat at a constant volume for each gas component (j = 1 to 5) of the gas in the fuel-to-cladding gap (per mol).	Cal/mol-K

Symbol	Description	Unit
D	Fitting parameters associated with the decrease of d_{CF} with interface pressure.	cm^2/dyne
D_e	Coolant equivalent diameter.	cm
d_{CF}	Effective distance between fuel and cladding surfaces involved in heat transfer through the gas when surfaces are in contact.	cm
d, Δd	Diameter and change of a diameter in fuel due to thermal expansion.	cm
F	Function dependent on surface roughness and waviness (H_S model).	--
G	Fabricated diametral fuel-to-cladding gap.	mil (cm)
G_p	Postirradiation diametral fuel-to-cladding gap at room temperature.	mil (cm)
g	Jump distance.	cm
g_c, g_F	Jump distance at the cladding and fuel surfaces, respectively.	W/cm^2-°C
H	Unit thermal conductance through fuel-to-cladding gap (gap conductance or gap coefficient).	W/cm^2-°C
H_{Con}	Unit thermal conductance at fuel-to-cladding gap due to convection.	W/cm^2-°C
H_{eq}	Equivalent film coefficient, H_F, which accounts for test pins being encapsulated.	W/cm^2-°C
H_F	Film coefficient between sodium coolant and cladding outside surface.	W/cm^2-°C
H_G	Unit thermal conductance through gas in fuel-to-cladding gap.	W/cm^2-°C
H_S	Unit thermal conductance through solid-to-solid contact at fuel-to-cladding gap.	W/cm^2-°C
H_R	Unit thermal conductance due to radiant heat transfer between fuel and cladding.	W/cm^2-°C
h	Meyers' hardness of cladding.	dynes/cm^2 (psi)

Symbol	Description	Unit
K	Boltzman constant.	erg/K
k	Thermal conductivity.	W/cm-°C
$\bar{k}$	Average thermal conductivity of gas in the fuel-to-cladding gap.	W/cm-°C
k_C	Cladding thermal conductivity at inner surface.	W/cm-°C
k_F	Fuel thermal conductivity at outer surface.	W/cm-°C
k_G	Thermal conductivity of gas in fuel-to-cladding gap.	W/cm-°C
k_M	Thermal conductivity of gas mixture.	W/cm-°C
k_m	Harmonic mean of thermal conductivities of the fuel and cladding at the interface, ($k_m = \frac{2k_1k_2}{k_1 + k_2}$).	W/cm-°C
k_{SM}	Thermal conductivity of gas mixture by simple mixing.	W/cm-°C
k_{RM}	Thermal conductivity of gas mixture by reciprocal mixing.	W/cm-°C
M_F	Mass flow rate of sodium coolant.	gm/s
M_G	Atomic mass of gas in fuel-to-cladding gap.	gm/mol
M_i	Atomic mass of i^{th} type atom making up a wall molecule.	gm/mol
M_W	Molecular mass of wall molecules.	gm/mol
N	Exponent which may be pressure dependent (H_S model).	--
N_C	Number of full power reactor cycles.	--
N_i	Number of atoms of atomic mass M_i making up wall molecule.	--
Nu	Nusselt number (coolant - pin system).	--
n	Number of contact spots between fuel and cladding per unit area.	--

Symbol	Description	Unit
O/M	Stoichiometry of the fuel.	--
P	Apparent interface pressure between fuel and cladding.	$dynes/cm^2$
P_f	Fraction of porosity in the fuel.	--
P_G	Pressure of gas in fuel-to-cladding gap.	$dynes/cm^2$
Pr	Prandtle number (coolant-pin system).	--
Q'	Linear heat rate or linear power.	kW/ft (W/cm)
Q'_i	Linear heat rate or linear power at a specific axial location.	kW/ft (W/cm)
Q'_m	Linear heat rate-to-incipient fuel melting (power-to-melt).	kW/ft (W/cm)
Q'_1, Q'_2	Time-averaged local linear heat rate (1) and maximum local linear heat rate (2), respectively.	kW/ft
q	Heat flow rate.	W (Btu/hr)
q_v, q_{vb}	Volumetric heat generation in the unrestructured fuel (v) and the restructured fuel (vb), respectively.	W/cm^3
q_G, q_s, q_r, q_{Con}	Heat flow rate through the gas, the contact points, radiant heat transfer, and convective heat transfer, respectively, at the fuel-to-cladding gap.	W (Btu/hr)
R	Mean gas constant.	Cal/gm-K
$\bar{R}$	$(\frac{R_F^2 + R_C^2}{2})^{1/2}$.	cm
R_a	Thermal resistance through one contact a-spot between fuel and cladding per unit area.	cm^2-°C/W
R_c, R_F	Arithmetic mean of surface roughness of the cladding and the fuel, respectively.	cm
Re	Reynolds number (coolant-pin system).	--
r	Radius in the fuel.	cm

Symbol	Description	Unit
r_b	Radius of columnar grain region OD.	cm
r_c	Radius of cladding inner surface.	cm
r_c, OD	Radius of cladding outer surface.	cm
r_{cv}	Radius of central void in the fuel.	cm
r_F	Radius of fuel outer surface.	cm
r_M	Fabricated central void radius.	cm
S_r, S_o	Integral of fuel conductivity at the radius r (at temperature T_r) and r_F (at temperature T_o), respectively, with respect to T.	W/cm
T	Temperature.	°C
$\bar{T}$	Average temperature of gas in the fuel-to-cladding gap.	°C
T_a	Absolute temperature.	K
T_C	Temperature of cladding ID.	°C
T_{CG}	Isotherm above which columnar grains form.	°C
T_F	Temperature at the fuel outside surface.	°C
T_I	Sodium coolant temperature.	°C
T_{In}	Sodium coolant inlet temperature.	°C
T_M	Melting temperature of fuel.	°C
T_o	Temperature at the fuel outside surface.	°C
T_r	Temperature at arbitrary radius in fuel.	°C
ΔT_C	Temperature drop through cladding.	°C
ΔT_F	Temperature drop through unrestructured fuel region.	°C
ΔT_{Fl}	Temperature drop between the coolant and the cladding.	°C

Symbol	Description	Unit
ΔT_G	Temperature drop between fuel and cladding.	°C
Δ_{RF}	Temperature drop through restructured fuel region.	°C
W_{bC}, W_{bF}	Emissive power of a black body at the temperature of the cladding and fuel, respectively.	W/cm^2
$\bar{W}$	Average atomic weight of gas in the fuel-to-cladding gap.	gm/mol
X	Thickness of material.	cm
X_G	Hot radial fuel-to-cladding gap size.	cm
x_i	Axial distance along fuel column.	cm
X_i	Mole fraction of each component (i = 1,2, 3, 4, 5) of gas making up the gas mixture in the fuel-to-cladding gap.	--
y_C	Yield strength of cladding.	$dynes/cm^2$ (psi)
α	Average radius of surface contact spots between fuel and cladding.	cm
α_C, α_F	Thermal expansion of the cladding and fuel, respectively.	$°C^{-1}$
ε	Characteristic energy in interaction of gas molecules from Lennard Jones potential function.	W-s
ε_C, ε_F	Emissivity of the cladding and fuel surfaces, respectively.	--
γ	$\frac{C_p}{C_v}$.	--
γ_1, γ_2, γ_3	Fitting coefficients for pure gas models.	--
μ	Absolute viscosity of the gas.	gm/cm-s
Ω	Mean free path of gas molecules.	cm
Ω_k	Collision integral dependent on the dimensionless temperature KT/ε.	--

Symbol	Description	Unit
ρ	Fraction of fuel theoretical density (TD) in fabricated fuel.	--
ρ_{CG}	Fraction of fuel theoretical density (TD) in columnar grain zone.	--
σ	Stefan Boltzman constant.	W/cm^2-K^4
σ_L	Characteristic diameter from Lennard-Jones potential function.	cm
τ_0, τ_1	Temperature of gas molecule on surface of a solid body at temperature, τ.	°C
τ_2	Temperature of gas molecule after striking solid body.	°C
θ_i, θ_r	Angle of incident (i) and reflection (r).	°
θ_j(j=1 to 6)	Fitting coefficients for residual fuel-to-cladding gap model.	--

DISTRIBUTION

UC-79 (206)

DOE HDQ (2)

Program Division Director

DOE-RL (2)

Manager
Chief Patent Attorney

FFTF-PO (5)

R. L. Ferguson

HEDL (56)

R. L. Baars	W/E-10
R. B. Baker (2)	W/E-1
R. A. Bennett	W/FED
S. A. Chastain	W/A-72
T. T. Claudson	W/C-15
C. M. Cox (2)	W/C-5
G. E. Culley	W/E8
D. S. Dutt (2)	W/E-1
E. A. Evans	W/C-16
G. L. Fox	W/E-10
R. L. Gibby	W/C14
B. C. Gneiting (2)	W/E10
J. W. Hales	W/E-1
J. E. Hanson (2)	W/E-4
E. N. Heck (2)	W/E-3
J. M. Henderson	W/E-8
T. Hikido	W/E-9
D. M. Hoyt	W/E-1
R. J. Jackson (2)	W/E-7
J. W. Jost	W/E-1
R. A. Karnesky	W/E-1
G. A. Last	W/E-2
L. A Lawrence	W/E-1
R. D. Leggett (2)	W/E-1
R. B. McCord	W/C19
J. Muraoka	W/F-119
M. B. Parker	W/E-3
L. A. Pember	W/A-72
R. E. Peterson	W/FED109
E. H. Randklev	W/E-10
J. D. Rector	W/E-7
W. E. Roake	W/E-2
R. B. Rothrock	W/FED
L. D. Scott	W/E-1
W. F. Sheely	W/C-44
D. P. Schively	W/FED-119
F. R. Shober	W/E-6
I. Z. Stone	W/E-1
J. P. Taylor (2)	W/E-7
J. E. Tobin	W/E-1
D. F. Washburn	W/E-10
E. T. Weber	W/A-63
J. W. Weber	W/E-1

Central Records and Files (10)
Publications Services (2)